MODEL UPDATING AND DAMAGE DETECTION OF FRAME STRUCTURES USING OUTPUT-ONLY MEASUREMENTS

HOOMAN MONAJEMI

THESIS SUBMITTED IN FULFILLMENT OF THE REQUIREMENTS FOR THE DEGREE OF DOCTOR OF PHILOSOPHY

FACULTY OF ENGINEERING
UNIVERSITY OF MALAYA
KUALA LUMPUR

2018

UNIVERSITI MALAYA

ORIGINAL LITERARY WORK DECLARATION

Name of Candidate: **Hooman Monajemi**

Registration/Matric No: **KHA090069**

Name of Degree: **Doctor of Philosophy**

Title of Thesis: **Model Updating and Damage Detection of Frame Structures using Output-Only Measurements**

Field of Study: **Civil / Structural Engineering**

I do solemnly and sincerely declare that:

(1) I am the sole author/writer of this Work;
(2) This Work is original;
(3) Any use of any work in which copyright exists was done by way of fair dealing and for permitted purposes and any excerpt or extract from, or reference to or reproduction of any copyright work has been disclosed expressly and sufficiently and the title of the Work and its authorship have been acknowledged in this Work;
(4) I do not have any actual knowledge nor do I ought reasonably to know that the making of this work constitutes an infringement of any copyright work;
(5) I hereby assign all and every rights in the copyright to this Work to the University of Malaya ("UM"), who henceforth shall be owner of the copyright in this Work and that any reproduction or use in any form or by any means whatsoever is prohibited without the written consent of UM having been first had and obtained;
(6) I am fully aware that if in the course of making this Work I have infringed any copyright whether intentionally or otherwise, I may be subject to legal action or any other action as may be determined by UM.

Candidate's Signature Date

Subscribed and solemnly declared before,

Witness's Signature Date

Name:
Designation:

MODEL UPDATING AND DAMAGE DETECTION OF FRAME STRUCTURES USING OUTPUT-ONLY MEASUREMENTS

ABSTRACT

Modal based damage detection and localization is one of the most efficient non-destructive health assessment methods in civil structures. It is based on the fact that damage in the structure alters structural and consequently modal properties of the system. There are many ways of employing modal properties for damage detection, including reconstructing flexibility matrix using modal data i.e. modal flexibility matrix. Among various structural systems, utilizing this method in frame structures is relatively more difficult. The main reason is their complex geometry and subsequently complex flexibility matrix. The second concern is that mass normalized mode shapes are required to reconstruct flexibility matrix and they are not so easy to obtain, especially in operational modal testing. The third issue is incomplete measurements. In frame structures like jacket platforms for example, it is not possible to measure all degrees of freedom and it is important to find a solution to detect damages on unmeasured part of the structure. This study aims to address these concerns and other issues that are related to damage detection of frame structures using operational modal analysis (OMA). A scaled model of a steel frame structure was constructed and tested in the laboratory. The model was excited using two shakers that were mounted on top of the structure. Although the input forces were available, but they were just used to validate the results of operational modal analysis. Since input forces were assumed to be unavailable in OMA, an alternative scaling method based on change in mass was used to normalize mode shapes. Among various flexibility based detection methods, damage locating vectors were found to be one of the most suitable methods considering the complex geometry of the frame structure and were used as the primary detection method in this

study. The method was tested by a number of damage scenarios and the results were showing that damage locating vectors (DLV) is always certain on indicating the undamaged members, but it sometimes fails to indicate the damaged member(s) with an acceptable certainty. To solve this problem, a second damage indicator was suggested based on cross model cross mode (CMCM) model updating method. The advantage of using this indicator was that it has the opposite type of error compare to DLV and so combining these two methods resulted on a more certain damage indicator. Cross model cross mode model updating was also used to address the problem of incomplete measurements by updating a finite element model of the frame structures in respect to the experimental data. Then each unmeasured member was damaged in updated FE model which provided a range of frequencies for each damage case. Comparing the calculated frequencies with the frequencies obtained from the experiment and also using the extra information provided by the measured DOFs, it was possible to approximate the location of the damaged member.

MODEL UPDATING AND DAMAGE DETECTION OF FRAME STRUCTURES USING OUTPUT-ONLY MEASUREMENTS

ABSTRAK

Dalam kejuruteraan awam kaedah yang paling efisyen dalam pengesanan kerosakan stuktur adalah kaedah *non-destructive health assessment*. Ia adalah berdasarkan kepada fakta bahawa kerosakan dalam struktur mengubah sifat-sifat struktur. Terdapat banyak cara untuk menggunakan modal analisis untuk mengesan kerosakan stuktur termasuk membina semula fleksibiliti matriks menggunakan data modal. Sebab utama kaedah ini dipilih kerana ia boleh menyelesaikan masalah geometri yang kompleks, berkebolehan membina jisim bentuk mod normal yang dikehendaki dan melengkapkan data yang tidak lengkap terutama stuktur berangka. Kajian ini bertujuan untuk menangani masalah yang berkaitan dengan pengesanan kerosakan struktur menggunakan OMA. Model berskala struktur kerangka keluli berskala makmal telah dibina dan diuji di makmal dengan menggunakan dua penggoncang yang dipasang di atas struktur. Oleh sebab input tidak tersedia di OMA, kaedah *scaling* alternatif berdasarkan perubahan dalam jisim digunakan untuk menormalkan bentuk mod. Di antara pelbagai kaedah pengesanan fleksibiliti, *damage locating vectors* kerosakan adalah kaedah yang paling sesuai kerana kaedah geometri kompleks struktur kerangka telah digunakan dalam kaedah pengesanan stuktur di awal kajian. Kaedah ini telah diuji oleh beberapa kes kerosakan dan keputusan menunjukkan bahawa DLV sentiasa menumpu pada bahagian-bahagian yang tidak rosak, tetapi juga gagal untuk mengesan bahagian yang rosak dengan tepat. Untuk menyelesaikan masalah ini, kaedah *cross model cross mode* (CMCM) telah digunakan. Kaedah ini mempunyai jenis yang bertentangan dengan ralat bandingkan dengan DLV dan menggabungkan kedua-dua kaedah untuk menghasilkan pengesan kerosakan yang lebih tepat. CMCM juga digunakan untuk menangani masalah

data tidak lengkap dengan mengemaskini model unsur terhingga struktur rangka berkenaan dengan data eksperimen. Kemudian setiap stuktur dalam model FE dikemaskini untuk menyediakan julat frekuensi bagi setiap kes kerosakan. Dengan membandingkan frekuensi yang telah dikira dengan frekuensi yang diperolehi daripada eksperimen dan DOFS yang telah diukur, ia dapat mengesan kerosakan pada stuktur kajian.

ACKNOWLEDGEMENTS

I would like to extend thanks to many people who contributed to the work presented in this thesis.

Special mention goes to my supervisors, Prof. Dr. Hashim Abdul Razak and Prof. Dr. Zubaidah Ismail. My study has been an amazing experience and I thank them not only for their tremendous academic and financial supports, but also for supporting me mentally and emotionally.

I should also thank members and technicians of Civil Engineering Department of University of Malaya for their full support during the experimental works. I would like to thank University of Malaya Research Grant (UMRG) RG092-10AET and Fundamental Research Grant (FRGS) FP055-2010A for the financial support throughout my studies.

I met my lovely wife when I was waiting for examiners' reports. Her support during the correction of the thesis was so effective that I deeply regret not knowing her sooner.

I should specially thank my sister for her remarkable helps and supports despite her very busy schedule as a PhD student.

Last but not the least I should thank my parents whom without them, I couldn't peruse my studies. Although not in the same field, but my father's advises and suggestions were always like a beacon in those moments which I couldn't see what is ahead of me.

TABLE OF CONTENT

LIST OF FIGURES

LIST OF TABLES

LIST OF SYMBOLS

C	Damping matrix
f	Force
G	Flexibility matrix
K	Stiffness matrix
E	Young's Modulus
M	Mass matrix
t	Time
L	Load vector
S_x	Standard deviation
R, r	Pearson's correlation ratio
g	Acceleration of gravity
A	Surface area
L	Length
I	Moment of inertia
T	Period (s)
f	Frequency (Hz)
ω	Frequency (Rad)
λ	Eigenvalue (ω^2)
γ	Modal participation
ϕ	Arbitrarily scaled mode shape vector
ψ	Mode shape vector scaled to unity
Φ	Mass normalized mode shape vectors
α_n	Stiffness correction factors of the n^{th} member
β_n	Mass correction factors of the n^{th} member
α	Mode shape scaling factor
$\{u\}$	Displacement vector
σ	Stress
ζ	Damping ratio

LIST OF ABBREVIATIONS

BFD	Basic Frequency Domain
CMCM	Cross Model Cross Mode
DDLV	Dynamic Damage Locating Vector
DLV	Damage Locating Vectors
DOF	Degree of Freedom
EFDD	Enhanced Frequency Domain Decomposition
EMA	Experimental Modal Analysis
FDD	Frequency Domain Decomposition
FEM	Finite Element Modeling
FFT	Fast Fourier Transform
FRF	Frequency Response Function
IRF	Impulse Response Function
nsi	Normalized Stress Index
ODS	Operational Deflection Shape
OMA	Operational Modal Analysis
PLS	Partial Least Squares
SDDLV	Stochastic Dynamic Damage Locating Vector
SDLV	Stochastic Damage Locating Vector
SDOF	Single Degree of Freedom
SVD	Singular Value Decomposition
UMM	Unit Modal Mass
WSI	Weighted Stress Index

LIST OF APPENDICES

CHAPTER 1: INTRODUCTION

1.1 Overview

Non-destructive structural examination and damage detection methods can be classified as local damage detection and global damage detection. Local damage detection methods e.g. visual inspection, CT scanning, ultrasonic, etc, are mainly used to detect local damages in some specific regions of the structure. The results of these methods are fairly accurate. However to perform them, the existence of damage and its estimated location must be known; otherwise a whole structure inspection is necessary. This illuminates the weakness of these methods for the large and complicated structures in closed or invisible environments e.g. almost all civil structures. Therefore in such structures, using global damage detection methods are the only option, either to precisely locate the damaged section of the structure or to identify the existence of damage and its approximate location for further inspections.

One of the global damage identification and detection approaches, and in fact the most reported one, is modal based damage detection. The basic principle of this approach is simple. The modal parameters of a structure e.g. natural frequencies, mode shapes, modal strains energy etc, are consequences of structural characteristic i.e. mass, damping and stiffness. Once some damages appear in the structure, it changes some of the structural parameters, usually stiffness, which accordingly affects the modal behaviour of the structure. Therefore major changes in vibration characteristics or modal parameters of the structure may be understood as existence of damage.

Modal based damage detection approach have been developed for the past few decades (Salawu, 1997). Over these years, a large number of methods and techniques have been introduced, studied and developed in different aspects. Vibration based damage

detection procedure includes two main elements. The first is modal parameter estimation techniques. Like nearly all engineering or scientific topics, this area was greatly benefited by the escalation technology. The second element of a vibration based damage detection process is identification and detection methods that employ estimated modal parameters to detect and locate damage. It is important to mention that although these two elements can be seen individually, to use them in a damage detection strategy they are influenced by each other and need to be studied together.

Modal parameter estimation methods are divided into two main categories i.e. Experimental Modal Analysis (EMA) and Operational Modal Analysis (OMA). Experimental modal analysis uses both input and output measurements i.e. excitation and response to estimate modal parameters whereas operational modal analysis relies only on output measurements. That is why OMA often referred to as output-only modal analysis. In EMA, artificial excitation is normally used to measure Frequency Response Function (FRF) or Impulse Response Functions (IRF). Conducting EMA is normally possible in the lab environments only and it is very difficult and often impossible to be used in the field and for large civil structures. That is why in the field of civil engineering, the final applications of modal based damage detection methods are limited to Operational Modal Analysis.

The second element of modal based damage detection is the methods and techniques that are used to employ the modal parameters of the structure to identify and locate damages. Several approaches are reported and developed in the past few decades. Some of these methods are using frequency changes to identify damage. Some methods use mode shapes or its derivatives like mode shape curvature or strain mode shape. Another group of damage identification methods are based on dynamically measured flexibility of the structure etc. Any of these methods have some advantages and disadvantages that

make them suitable for a particular case. However, one of the most important parameters that are governing this is the modal estimation techniques that were used to estimate modal parameters. For example, EMA obtains more accurate mode shapes and is able to scale them more precisely than OMA. On the other hand, complete measurements are not always possible in the field and so complete mode shapes are not always available in OMA. That is why in general, frequency based damage detection methods are the better option for OMA and using methods based on mode shapes or modal flexibility is rather challenging in real structures. This study aims to address few of these challenges.

1.2 Problem Statement

This study has several problems that need to be addressed in order to achieve its objectives. However, they can be summarized into two:

1. Damage detection based on operational modal analysis is one of the two main problems of this study. Since input force is not available, a lots of valuable information including mass are missing. In general, there are two strategies to encounter this problem. One is developing a damage detection method that does not require those missing information as input data e.g. frequency based methods. The second solution is to obtain those missing information by other means and methods. This study chooses the second strategy.

2. The second main problem of this study is the issue of incomplete measurement. In a jacket platform, it is not very practical to put sensors under water. So a section of the structure that has the maximum risk of damaged cannot be measured. This study proposed a strategy to solve this problem in an easy and cheap way.

1.3 Objectives

The objectives of this study are as follow:

i. To evaluate the consistency of modal identification and damage detection methods employing operational modal analysis on a lab-scale frame structure

ii. To examine the factors that are contributing to reliability and consistency of mode shape scaling method based on mass modification in a frame-like structure.

iii. To evaluate the reliability of using damage locating vectors to locate damage using output only modal analysis.

iv. To propose an easy and reliable detection method that is able to detect damages which are located in unmeasured region of the structure.

1.4 Scope of the Study

This study focuses on modal testing and damage detection of a jacket-like frame structure. The original test set up was to model and test the frame with and without braces, however only the results of frame without braces are presented in this thesis. All the objectives of this study are based on the results of output-only modal testing. Frequency response function (FRF) based modal identification is not the concern of this study and is used only to validate the results. One of the important assumptions of this study is that the intact and damaged structures are both linear systems. In other word, damage does not have any nonlinear effect on the structure and its response can still be modelled using linear equations of motion.

1.5 Outline of Thesis

This thesis contains six chapters. The next chapter reviews the work that had been carried out by various researchers on the theme studied in this work and gives a brief introduction to the different topics discussed in this thesis. The third chapter presents all the theories that are used in various aspects of this thesis, either directly or as the background theory of the package that are employed. Chapter 4 presents the proposed methods that are employed in this thesis. The chapter consists of the methods of numerical modelling and analyses, experimental methods and also the methods of applying mass normalization, model updating and damage detection approaches to the particular problem of this study. Chapter 5 comprises the results and discussion of the work carried out in this research and finally chapter 6 contains conclusions and recommendations.

CHAPTER 2: LITERATURE REVIEW

2.1 Overview

Structural health monitoring and vibration based damage detection has been the subject of many studies in the past few decades. From the early years which these methods were very basic, many researchers devoted their career to advance this engineering topic. Today, vibration based damage detection and localization techniques are based on variety of approaches e.g. flexibility based methods, modal strain energy based methods, model updating based methods, damage locating vectors, statistical approaches etc. This chapter aims to review some of these researches, mainly those which are directly or indirectly related to the topic of this study.

2.2 Frequency based Methods

Frequency-based detection methods use changes of natural frequencies caused by damage as the basic feature to indicate and locate them. In fact, the observation that natural frequency of a structure changes by introducing damage (lost of stiffness) was the first motivation for vibration based damage detection methods (Salawu, 1997). There are a large number of studies in the past few decades on frequency based damage identification methods. The earliest studies on this subjects can be found in a review paper presented by (Salawu, 1997). The most important advantage of frequency based methods is that natural frequencies can be easily measured using a few sensors and access to the entire structure is not required. However, the method has few limitations that have been addresses in the literature. One of the first known limitations of these methods is that natural frequencies are not very sensitive to the local errors. So to use these methods either the measurements must be very precise or the damage must be severe. Otherwise, the frequency shift is difficult to measure. Although based on an

statistical study, (S. W. Doebling, Farrar, & Goodman, 1997) suggested that among modal variables, modal frequencies have the least statistical variation from random error sources.

Another limitation of frequency based methods is that frequencies are more of a global property of the structure and they might not contain the local information of damage. However this issue can be addressed by measuring higher natural frequencies which requires more advance technologies (Salawu, 1997). Frequency based methods can be divided into two categories i.e. forward problems and inverse problems.

The forward problems are based on determining frequency shifts caused by known damage cases and comparing them with the measured frequencies to predict the damage location. The known frequency shifts are usually obtained numerically e.g. using FE modelling and analysis. One of the earliest studies on using forward problems for damage detection is dated back to three decades ago (Cawley & Adams, 1979). Their method was based on an error term that relates the measured frequency shifts of a pair of modes to a set of numerical data that produces frequency shifts caused by stiffness reduction. (M. I. Friswell, Penny, & Wilson, 1994) presume a highly accurate model of the structure and use this model to calculate frequency shifts of undamaged structure as well as postulated damage scenarios. They then calculate the ratio of frequency shift for all the modes and damage scenarios. They compared the measured frequency shifts with these data by fitting a power-law relation to them. A fit that is a line with unity slope is the identification of correct damage scenario. A similar form of study is presented by (Juneja, Haftka, & Cudney, 1997) which is based on matching the response of the damaged structure to a database of structural responses.

There are another groups of studies based on explicit frequency shifts that fit in this category. (Hasan, 1995) derived an explicit frequency shift expression for a beam on an elastic foundation, showing that frequency shift does not have an explicit dependence in this condition. (Hu & Liang, 1993; Morassi & Rollo, 2001) derived an explicit frequency shift expression for a cracked beam vibrating in bending using a perturbation approach. (Kasper, Swanson, & Reichard, 2008) applied the expressions of explicit wave-number shift and frequency shift to a cracked uniform beam, with both shallow and deep cracks. However their expression is based on high frequency approximation and inapplicable for fundamental frequencies.

Inverse methods on the other hand, are based on an initial model of the structure e.g. FEM which is combined with measured data to improve the model. The measurements are often in form of modal parameters which are extracted from acceleration and force data, although frequency response function (FRF) can also be used (M. I. Friswell, 2007).

The application of inverse problems on damage detection is dated back to early 70s (Lifshitz & Rotem, 1969). These inverse methods are not necessarily categorized as model updating methods. For example (Stubbs & Osegueda, 1990a, 1990b) presented a damage detection method based on the sensitivity of modal frequency changes. They computed an error function for the i^{th} mode and j^{th} structural member and any member with minimum error is detected as damaged member. A good number of early publication in this subject are presented in (Salawu, 1997).

(Messina, Williams, & Contursi, 1998) proposed a detection method based on the sensitivity of the frequency of each mode to damage in each location. It uses the statistical correlation between the numerically estimated frequency shifts and the actual

measured frequency shifts. They wrote the analytical frequency shifts as a function of the damage extent vector. Damage extent vector which maximizes the multiple damage location assurance is indicating the damage state.

(Liang, Choy, & Hu, 1991) and (Nandwana & Maiti, 1997) and (Chaudhari & Maiti, 2000) used a rotational spring to represent crack in Euler-Bernoulli type beams. They obtained plots of the spring's stiffness with the spring's location for any of the three bending natural modes through the characteristic equation. The crack's location and stiffness was identifying by the intersection of the three curves. (Patil & Maiti, 2003) extended this method to beams with varying boundary conditions. Further studies on damage detection using inverse problem with the scope of beams are carried out by (J-T Kim & Stubbs, 2003; Maity & Tripathy, 2005; Morassi & Rollo, 2001; Zhong, Oyadiji, & Ding, 2008).

2.3 Frame Structures

(Jeong-Tae Kim & Stubbs, 1995) presented an algorithm to detect and locate damage in jacket offshore platforms in unsupervised condition. It means only post-damage modal parameters are available. To do this, they estimated a baseline modal parameters of jacket-type offshore platforms. Based on that they formulated a theory of damage localization and severity estimation. To verify their method, they use a numerical example of a jacket-type offshore structure with limited modal information.

(Farrar & Jauregui, 1998a, 1998b) used five damage identification algorithms and applied them to the I-40 bridge in an experimental study. The five algorithms they used were change in flexibility, change in stiffness, change in uniform load surface curvature, damage index and mode shape curvature methods. They concluded that standard modal properties i.e. natural frequencies and mode shapes were relatively less capable of

detecting damage. In compare, damage index method which uses the second derivatives of mode shapes and also the mode shape curvature method are more capable of detecting and locating damage. However, they indicated that all these mode shape based methods are still suffering from a few well-known confounding actors i.e. the difficulty of accurately identifying mode shapes, the need for complete measurements which requires a big number of sensors etc. More importantly, they stated that compared to a basic modal parameter like natural frequency, mode shapes have a larger statistical variability.

(Z. Shi, Law, & Zhang, 2002; Z. Shi, Law, & Zhang, 2000) demonstrated a method to detect and locate damage by using the elemental energy quotient difference and modal strain energy change. Their method also quantifies the damage using sensitivity analysis as well as using an algorithm based on change in modal strain energy. (Mangal, Idichandy, & Ganapathy, 2001) used vibration responses due to impulse and relaxation on a laboratory model of a jacket platform. They concluded that both impulse and relaxation responses are useful for monitoring the jacket structure and that their results can be used as the basis for automated and on-line monitoring of offshore jacket platforms using neural networks.

(Nichols, 2003) conducted an experimental study to realize the use of ambient excitation in detecting damage in offshore structure. He excited two models of an articulated offshore structure and estimated the prediction error. The results demonstrated that the prediction error was increasing when damage was introduced to the structure. They use this technique mostly to predict the presence of damage.

(Yang, Li, & Hu, 2004) used a damage localization method based on decomposing the modal strain energy to locate damage in an offshore platform. Their method required

only a few numbers of identified mode shapes from intact and damaged structure. They demonstrated their method by successfully localizing damaged member of a template offshore structure. (X. Shi, Matsui, Li, & Gong, 2007) use partial measurements of offshore jacket platforms in unsupervised condition to identify and localize damage. The advantage of their method is that it is robust against identification error of baseline structure.

(Cheng & Wang, 2008) demonstrated a method that uses time-domain data under random loading to detecting damage in offshore platforms. They suggested that only a few number of accelerometers can be used to efficiently detect the damage and increasing the number of sensors only improves the damage detection's success rate.

(X. Shi, Li, Yang, & Gong, 2008) proposed a method to evaluate location and severity of damage in jacket platforms. They used incomplete measurements of modal parameters of a scaled platform that was excited from the ground using white noise. They demonstrated that their damage detection algorithm is robust against the errors of baseline FEM model in compare to the real structure when the principal errors is formed by difference of modal frequencies.

(Cavalieri, Imbimbo, Betti, & Brügger, 2009) conducted an experiment for dynamic identification and the damage assessment of a steel frame under ground motion. They used both OKID-ERA/DC time domain approach and EFDD frequency domain approach for modal identification. They evaluated a number of damage detection algorithms and concluded that *MSECR* and the rdi_2 indices are mode reliable on positioning the damaged member.

One of the issues that are frequently reported in the literature is the insensitivity of global modes to local damages. In large frame structures, higher modes are more

localized than lower modes since they represent local member vibration characteristics. Mode localization is a dynamic phenomenon associated with weakly-coupled periodic Structures which is caused by small imperfections which perturb the periodicity (Yi, Zhou, Kunnath, & Xu, 2008). So higher modes are generally more significant in identifying local structural damages. The identification and employment of higher local modes in engineering structures for damage detection or other purposes are reported in the work of many researchers (Bouzit & Pierre, 1995; Cox & Agnes, 1999; Mester & Benaroya, 1994; Qi, Xun, Xiaozhai, Dong, & Chang, 2005).

In case of frame structures in particular (Yi, et al., 2008) use sensitive higher modes in physical structural parameter identification of local members. They used hammer-impact and stable sinusoidal sweep to excite local vibrations of a column in a four story reinforced concrete frame structure. They used poly-reference least-squares complex frequency domain method to identify modal parameters. Their study shows that higher modes posses localized characteristics while lower modes represent the global dynamic properties of the entire frame stricture. They concluded that higher modes are concentrate in several 'modal' regions of the FRF diagram called pass-bands. The order of the pass-band is similar to the order of the vibration mode shape of a single member's half sine wave.

(Ulriksen et. al. 2017 a) presented a damage detection method using shape input distribution. Their method is based on a shaping inputs with fixed spatial distribution. Then they use a theoretical model such that these inputs suppress certain steady-state vibration quantities. Damage is localized when the vibration signature induced by the shaped inputs in the damaged state corresponds to that in the reference state. They employed this method to localize damage in a model of offshore platform (Ulriksen et. al. 2017 b). They applied harmonic inputs to interrogate the structural domain with

respect to a 1% mass perturbation, acting in all translational DOF in a single node below the sea level. The method was able to locate damage, although with a poor accuracy which can be improved by employing more sensors to increase resolution.

2.4 Mass Normalization

In modal analysis, displacement mode shapes are vectors that are containing relative displacement of all measured DOFs in respect to each other. So in general form, the size of these vectors are arbitrary and based on the application, they might need to be scaled to a specific size. The simplest form of scaling a mode shape is to set the maximum value of displacement to unity. Another form of scaling is to set the length of the vector to unity. However, the most important mode shape scaling is when mode shapes are scaled with respect to the mass matrix i.e. mass normalization.

Mass normalized mode shapes are usually determined through an experimental modal analysis (EMA) where the excitation force is measured and frequency response function (FRF) can be obtained (Ewins, 1984; Heylen & Sas, 2006). However, one of the challenges in structural health monitoring is that in real civil structures, which are in fact the actual application of damage detection methods, it is not possible to measure the input force. In Most cases, modal analysis procedure of civil structures is what is called operational modal analysis. In this case the excitation forces are ambient forces which cannot be measured and the modal analysis relies solely on measuring the outputs i.e. output-only modal analysis (Heylen & Sas, 2006; Zhang & Brincker, 2005).

Early methods of normalizing operational mode shapes were using the results of finite element simulations to scale the mode shapes (Pandey & Biswas, 1994). (Gao & Randall, 1996a, 1996b) proposed a method to determine frequency response function from response measurements only, which consequently could mass normalize mode

shapes using measurement data. However, one of the most reported and effective methods of mass normalization of operational mode shapes are called sensitivity based methods. These methods are based on frequency shifts caused by a structural modification (Kranjc, Slavič, & Boltežar, 2013).

A civil structure can be modified in different ways. For example, (Coppotelli, 2009) used stiffness change as structural modification to obtain FRF using operational data. (Parloo, Verboven, Guillaume, & Van Overmeire, 2002) proposed a sensitivity based mass normalization method in which the structure is modified by adding mass. This method was later employed, improved and updated by (Hout & Avitabile, 2004, López Aenlle, Brincker, & Fernández Canteli, 2005; López Aenlle, Brincker, Fernández Canteli, & Villa García, 2005). (Khatibi, Ashory, & Malekjafarian, 2009) suggested that the first mode of the structure is not very sensitive to change in mass and cannot be properly normalized using mass modification method. They proposed a combination of mass and stiffness modification method to address this problem. (Hout & Avitabile, 2004) used different mass change ratios to normalize opertional mode shapes, varying between 1 to 5%. They suggested that mass change ratio of 5% gives the optimum results as it changes modal frequencies considerabley without changing the mode shapes significantly. They also suggested that the position and distribution of additional mass influences the reliabilityof the results.

2.5 Model Updating

Numerical modeling in engineering is a way to simulate the behavior of real systems. In structural engineering, this is normally done using finite element modeling and analysis. The most important concern of any simulation is the level of similarity to the real system. In other word, how much of the properties of the real system are replicated in the model. In any simulation, there are always some unknown or uncertain properties

that can only be modelled using certain assumptions. These assumptions are often detracting the accuracy of the model. To resolve the inaccuracy caused by uncertainty, model updating methods has been developed to adjust unknown system properties based on other behaviors of the system. One of the most suitable behaviors of structural systems that can be used to update FE simulations are its modal and vibrations parameters. Modal properties not only provide comprehensive information of the global and local behaviour of the structure, but they are relatively easy to extract experimentally from an actual structure (M. Friswell & Mottershead, 1995; Mottershead & Friswell, 1993).

One of the many applications of model updating in civil and structural engineering is structural health monitoring and damage detection. The basic idea behind this application is that damage in the structure is usually equivalent to loose of stiffness. So if the stiffness of a member or components of the structure need to be updated from undamaged to damaged state, this can be translated as presence of damage (Brownjohn, De Stefano, Xu, Wenzel, & Aktan, 2011; Deraemaeker & Worden, 2012; Scott W Doebling, Farrar, & Prime, 1998; Scott W Doebling, Farrar, Prime, & Shevitz, 1996).

Model updating problems are inverse problems. As oppose to "forward problems" which output of the models are estimated by structural parameters, in "inverse problems" outputs are used to estimate or modify structural parameters (Simoen, De Roeck, & Lombaert, 2015). In regard to uncertainty, model updating methods are used to improve the uncertainty problem of structural properties while they themselves are influenced by uncertainty of modal data. These two types of uncertainly are referred to as "uncertainty related to the prediction model" and "uncertainty related to the experimental data" respectively.

Uncertainty related to the prediction model is discussed by many authors such as (Der Kiureghian & Ditlevsen, 2009; Kennedy & O'Hagan, 2001; Walker et al., 2003). Based on their discussions, (Simoen, et al., 2015) summarized this type of uncertainty into three groups. First is model parameter uncertainty or model input uncertainty or variable uncertainty. This type of uncertainty is caused by uncertainty of the input parameters such as material or physical properties, load characteristics or geometry. The second is model structure uncertainty, also referred to as model framework or model form uncertainty. This type of uncertainty is caused by the lack of knowledge or understanding of the true system which forces the designer to make assumptions and do simplifications. The third is model code uncertainty or numerical uncertainty or technical model uncertainty. This uncertainty arises from errors in the computer implementation i.e. software or hardware errors.

The second type of uncertainty is uncertainty related to the experimental data. The results of modal analysis are always subjected to uncertainties. This causes unreliability and inaccurateness in prediction, detection and localization of damage in the structure. Uncertainties in modal parameters are having two sources. The first source is the natural variability of structural parameters which causes the same inconsistency and randomness in modal parameters. These types of uncertainties cannot be eliminated. The second type of uncertainties of modal parameters are related to the modal analysis itself i.e. modal identification methods, accuracy of sensors and measurements, measurement noises etc. It is possible to reduce this type of uncertainty by increasing the accuracy of measurements and modal identification methods (Xu, Qian, Chen, & Song, 2015). A frequently used method of incorporating these uncertainties in damage detection is based on probabilistic approaches (Huang, Gardoni, & Hurlebaus, 2012; Papadopoulos & Garcia, 1998; Xia & Hao, 2003; Yeo, Shin, Lee, & Chang, 2000).

They describe uncertainties as random variables characterized by mean values and standard deviations.

Model updating methods can be categorized into two groups i.e. direct matrix methods and indirect physical property adjustment methods. In direct matrix methods, updating changes are made to the mass and stiffness matrices directly. Since the whole mass and stiffness matrices are updated at once, these methods are generally non-iterative methods. The advantage of these types of methods is that since they are non-iterative, they do not require a lot of computational effort. However, their disadvantage is that although they can generate a modified model through structural matrices, but the physical property of individual structural members cannot be obtained. On the other hand there are indirect physical property adjustment methods that are correcting individual members in order to update the whole structure. Using these methods, it is possible to physically realize the updated structure. However since these methods are iterative, they demand more computational effort (S. Wang, Li, & Li, 2015).

(Hu & Li, 2007) developed a model updating method called Cross Model Cross Mode. CMCM model updating method is capable of updating the stiffness, mass and damping matrices simultaneously. This method has the advantages of both groups of updating method. It is a non-iterative method, yet its modification is based on the original physical form of the structure and so the updated model can still be physically realized. CMCM updating method was used and verified in the numerical studies presented by (Hu, Li, & Wang, 2007; Li, Wang, & Hu, 2008). In 2015, (S. Wang, et al., 2015) conducted an experimental verification of the method by applying it on a laboratory model of an offshore jacket platform.

2.6 Damage Detection

Damage detection based on change in modal flexibility matrix was first used by (Pandey & Biswas, 1994). They demonstrated that the flexibility matrix can be accurately estimated from a few of the lower modes which are easy to measure. However since flexibility matrix is global, using even an accurately measured flexibility matrix to locate damage in complex structures like trusses and frames is not so straight forward. In 2002, Bernal proposed a method called "Damage Locating Vectors" that employs flexibility change matrix to locate damaged member (Bernal, 2002). This method which is also known as DLV is based on calculating sets of load vectors that when are applied to the structure (either intact or damaged) cause zero stress in the damage member/region. In this method, DLVs are the null space of flexibility matrix which can be calculated using singular value decomposition of flexibility changes.

In 2004, Bernal and Gunes evaluated DLV method by using it in a benchmark study developed by the IASC-ASCE SHM Task Group. In this study, they computed a state-space realization of the system from the measured signals and then extracted flexibility matrices from the matrices of the realization. They described that by measuring at least three DOFs at each level and using DLV method, it is possible to define inter-story stiffness and centre of stiffness positions from the modal data and use them to determine the level, location, and extent of the damage without the need for an explicit model (Bernal & Gunes, 2004).

(Gao, 2005) and later (Gao, Spencer Jr, & Bernal, 2007) presented experimental verification of DLV method using a 5.6m long three dimensional truss structure. They used the same approach discussed in (Bernal & Gunes, 2004) to estimate flexibility matrices using small number of sensors. They concluded that despite of the small effect of damage on the modal properties, DLV is able to correctly locate the damage member

using only limited number of sensors and truncated modes. However, they reported a significant number of false positive detections which was caused by using small number of sensors. They solved this issue by conducting the modal testing in few stages. In the first stage, the approximate location of damage is identified and in second stage, a dense distribution of sensors in that region identifies the exact location of damage.

DLV method is based on flexibility matrices of intact and damaged structure which are extracted from mass normalized mode shapes. So DLV works best when the information of input excitation is available. Although it is not easy, often impossible, to excite a real structure and measure the input forces. This limits the application of DLV. One way of dealing with this problem is to use a method to scale mode shapes in output only modal testing. There are numerous studies regarding mode shape identification and scaling using output-only modal data. (Brincker & Andersen, 2003; Brincker, Rodrigues, & Andersen, 2004; Hout & Avitabile, 2004; López Aenlle, Brincker, & Fernández Canteli, 2005; B.-T. Wang, 2001). By employing mass normalized mode shapes obtained from output-only modal data, DLV can be used to detect damage in a structure under ambient excitation (Gao, 2005; Gao & Spencer, 2002).

In 2006, an enhanced version of DLV was proposed by Bernal called "Stochastic Damage Locating Vector" method. SDLV method is the extension of DLV when the input is unknown (Bernal, 2006). So by employing this method, damage locating vector can be directly used for real structures under ambient excitation. SDLV was later tested experimentally by (An, Ou, Li, & Spencer, 2014) using an 8 m long steel truss structure.

In 2007, Bernal proposed a generalization of DLV approach called Dynamic Damage Locating Vector or (DDLV) (Bernal, 2007a). Change in flexibility matrices which the original DLV method is based on, only contains the information of the static response of

the system. So if a particular damage case does not change the static response of the system, it remains undetectable. However, in a system identification procedure, information of the dynamic behaviour of the system is also obtained. DDLV approach make use of these extra information to provide a more robust and effective damage localization (Bernal, 2007a; Maddalo & Bernal, 2011). Later that year, Bernal proposed an improved version of DDLV called Stochastic Dynamic Damage Locating Vector or (SDDLV). The proposed method is based on the fact that what is actually needed in the DDLV is not necessarily change of flexibility matrix itself, but a basis for its null space (Bernal, 2007b).

In latest techniques of vibration based damage detection, modal identification is not required for damage localization (Sekjær et. al. 2017). (Bernal & Kunwar, 2016) presented a method that operating with two frequency domain subspaces which one of them are obtained by Fourier transformation of output measurements and the other from a model of the reference state together with a postulated damage distribution. This is somehow similar to detection methods based on model updating, except that only the damage distribution enters the formulation. The advantage of their method is that the time histories of the excitation are not used in their technique.

2.7 Summary

This Chapter contains a review of previous studies related to the subject of this research. The contents of this Chapter can be categorises into three i.e. mass normalization, model updating and damage detection.

In case of mass normalization, this review emphasises on the methods based on operational modal analysis. Most of the studies in this group were just theoretical and they have rarely been experimentally tested. So a numerical/experimental set up is

proposed in this study to examine one of the methods i.e. mass change method and to eventually use its findings for damage detection.

Model updating is the other reviewed topic. The forward vs. inverse problems, various types of prediction model uncertainty and also direct matrix vs. indirect physical property adjustment updating methods were reviewed in this Chapter. Among them, an indirect method called Cross Model Cross Mode is selected and modified to update the finite element model in this study.

The main part of this Chapter is the review of various damage detection methods. The main focus is on a particular method called “Damage Locating Vectors”. various theoretical, numerical and experimental studies on this method were founded in the literature and a number of them were reviewed in this Chapter. The main focus of this study is on the issue of false positive in incomplete measurements. This issue is reported in some articles and their solution is sensor redistribution. This solution is not applicable if the incomplete measurement is due to inaccessibility to parts of the structure and so an alternative method is proposed in this study to overcome this problem.

CHAPTER 3: THEORETICAL BACKGROUND

3.1 Modal Identification

3.1.1 Frequency Response Function

Here, the background theory of frequency response function, which is used in ICATS software is described. (Avitabile, 2001; Boot, van de Molengraft, & Nuij, 2003; Heylen & Sas, 2006; Ibsen & Liingaard, 2006; Irvine, 2000; Schwarz & Richardson, 1999)

The general and famous mathematical representation of a dynamic system is shown in Equation 3.1

$$M\ddot{x}(t) + C\dot{x}(t) + Kx(t) = f(t) \tag{3.1}$$

were M is mass matrix, C is damping matrix , K is stiffness matrix and f is excitation force.

By setting $f(t)=0$, the solution of the Equation can be assumed as $x(t) = Xe^{st}$. Substituting its derivatives into Equation 3.1 gives:

$$(Ms^2 + Cs + K)Xe^{st} = 0 \tag{3.2}$$

The non-trivial solution of this Equation is:

$$Ms^2 + Cs + K = 0 \tag{3.3}$$

Equation 3.3 is called *Characteristic Equation of the System* and s is complex-valued frequency variable or Laplace variable.

Roots of Equation 3.3 are λ_1 and λ_2 :

$$\lambda_{1,2} = \frac{-C}{2M} \pm \sqrt{\left(\frac{C}{2M}\right)^2 - \left(\frac{K}{M}\right)} \tag{3.4}$$

So the general solution of Equation 3.3 is:

$$x(t) = Ae^{\lambda_1 t} + Be^{\lambda_2 t} \tag{3.5}$$

where *A* and *B* are initial condition constants.

For under-damped systems with damping ratio less than one ($\zeta < 1$), the roots of Equation 3.5 (λ_1 and λ_2) are always complex conjugates of each other:

$$\lambda_{1\&2} = \sigma_1 \pm j\omega \tag{3.6}$$

where σ_1 is damping factor and ω is the damped natural frequency. The other way of solving Equation 3.3 is by writing it in frequency domain. It converts the second order differential equation to an algebraic equation. Using Fourier transform, Equation 3.3 converts to:

$$(-M\omega^2 + jC\omega + K)X(\omega) = F(\omega) \tag{3.7}$$

The reverse of the term $(-M\omega^2 + jC\omega + K)$ in Equation 3.7 is is called frequency response function $H(\omega)$. The frequency response function relates the Fourier transform of the system's input and response and can be written as:

$$H(\omega) = \frac{1}{-M\omega^2 + jC\omega + K} = \frac{1/M}{-\omega^2 + j\left(\frac{C}{M}\right)\omega + \frac{K}{M}} \tag{3.8}$$

The characteristic values of the denominator of Equation 3.8 are called the complex poles of the system or otherwise known as modal frequencies.

The frequency response function can also be expressed as the function of the complex roots:

$$H(\omega) = \frac{1/M}{(j\omega-\lambda_1)(j\omega-\lambda_2)} = \frac{A_1}{(j\omega-\lambda_1)} + \frac{A_2}{(j\omega-\lambda_2)} \quad (3.9)$$

For a multi degree of freedom system, frequency response function can be written as:

$$[H(\omega)] = \sum_{r=1}^{N}\left(\frac{A_r}{j\omega-\lambda_r} + \frac{A_r^*}{j\omega-\lambda_r^*}\right) \quad (3.10)$$

where:

ω = Frequency variable

r = Modal vector number

λ_r = System pole

N = Number of modal frequencies

3.1.2 Frequency Domain Decomposition

One of the earliest response only modal identification methods is called Basic Frequency Domain (BFD). This approach is based on simple signal processing using Discrete Fourier Transform. This method estimates well separated modes from the power spectral density matrix (Bendat & Piersol, 1980). The classical method is fairy reliable on estimating natural frequencies and mode shapes of the well separated modes. However, it typically fails to detect close modes or in case it does, the results are heavily biased. The other problem of this method is that it estimates frequencies only within the frequency resolution and it cannot estimate damping.

Frequency Domain Decomposition (FDD), established by Brincker and others (Brincker, Zhang, & Andersen, 2000; Brincker, Zhang, & Andersen, 2001), is an

extension to the classical frequency domain approach. The core of this method is decomposing the spectral matrix into a set of auto spectral density functions using Singular Value Decomposition (SVD). Each of the auto spectral density functions are corresponding to a single degree of freedom system. The exact results obtain by this method if the structure is lightly damped, the loading is white noise and the geometries of the two close modes are orthogonal. If some of these conditions are not satisfied, then decomposition into SDOF system is approximate, however the results are still significantly more accurate than classical approach (Brincker, et al., 2001).

Referring to (Brincker, et al., 2001), the relationship between unknown inputs $x(t)$ and measured response $y(t)$ can be expressed as:

$$G_{yy}(j\omega) = \overline{H}(j\omega)G_{xx}(j\omega)H(j\omega)^T \tag{3.11}$$

where $G_{xx}(j\omega)$ is the $r \times r$ Power Spectral Density matrix of the input, $G_{yy}(j\omega)$ is the $m \times m$ Power Spectral Density matrix of the responses and r and m are the number of inputs and responses respectively. $H(j\omega)$ is the $m \times r$ Frequency Response Function matrix and "—" denote complex conjunction. The FRF can be written in pole - residue form of:

$$H(j\omega) = \sum_{k=1}^{n} \frac{R_k}{j\omega - \lambda_k} + \frac{\overline{R}_k}{j\omega - \overline{\lambda}_k} \tag{3.12}$$

where n is the number of modes, λ_k is the pole and R_k is the residue which is expressed as:

$$R_k = \phi_k \gamma_k^T \tag{3.13}$$

where ϕ_k and γ_k are modes shape vector and modal participation vector respectively. If the input force is a white noise, its power spectral density is a constant matrix i.e. $G_{xx}(j\omega) = C$. With this assumption, Equation 3.11 becomes:

$$G_{yy}(j\omega) = \sum_{k=1}^{n}\sum_{s=1}^{n}\left[\frac{R_k}{j\omega-\lambda_k}+\frac{\overline{R}_k}{j\omega-\overline{\lambda}_k}\right]C\left[\frac{R_s}{j\omega-\lambda_s}+\frac{\overline{R}_s}{j\omega-\overline{\lambda}_s}\right]^H \tag{3.14}$$

where H denotes transposed complex conjugate. Multiplying two partial fraction factors while using the Heaviside partial fraction theorem, the output power spectral density can be reduced to a pole - residue form:

$$G_{yy}(j\omega) = \sum_{k=1}^{n}\frac{A_k}{j\omega-\lambda_k}+\frac{\overline{A}_k}{j\omega-\overline{\lambda}_k}+\frac{B_k}{-j\omega-\lambda_k}+\frac{\overline{B}_k}{-j\omega-\overline{\lambda}_k} \tag{3.15}$$

where A_k is the k^{th} residue matrix of the output power spectral density which is given by:

$$A_k = R_k C\left(\sum_{s=1}^{n}\frac{\overline{R}_s^T}{-\lambda_k-\overline{\lambda}_s}+\frac{R_s^T}{-\lambda_k-\lambda_s}\right) \tag{3.16}$$

The contribution of the k^{th} mode to the residue is given by:

$$A_k = \frac{R_k C\overline{R}_k^T}{2\alpha_k} \tag{3.17}$$

where α_k is negative of the real part of the pole $\lambda_k=-\alpha_k+j\omega_k$. In case of light damping, this term become dominating and so the residue becomes proportional to the mode shape vector:

$$A_k \propto R_k C\overline{R}_k^T = \phi_k\gamma_k^T C\gamma_k\phi_k^T = d_k\phi_k\phi_k^T \tag{3.18}$$

where d_k is a scalar constant. At a certain frequency ω, only one or two modes are contributing significantly which can be denoted by $Sub(\omega)$. So in case of lightly damped structure, the response spectral density can be written as:

$$G_{yy}(j\omega) = \sum_{k \in Sub(\omega)} \frac{d_k \phi_k \phi_k^T}{j\omega - \lambda_k} + \frac{\bar{d}_k \bar{\phi}_k \bar{\phi}_k^T}{j\omega - \bar{\lambda}_k} \tag{3.19}$$

To identify modes using frequency domain decomposition (FDD) method, first power spectral density must be estimated. Then the estimated output power spectral density is decomposed by taking the SVD of the matrix:

$$\hat{G}_{yy}(j\omega_i) = U_i S_i U_i^H \tag{3.20}$$

where ω_i denotes discrete frequencies, $U_i = [u_{i1}, u_{i2}, ..., u_{im}]$ is a unity matrix holding the singular values u_{ij}, and S_i is a diagonal matrix holding the scalar singular values s_{ij}. Near a peak corresponding to the k^{th} mode in the spectrum, this mode or a possible close mode is dominating. If only the k^{th} mode is dominating, there is only one term in Equation 3.19. In this case, the first singular vector u_{ij} is an estimation of the mode shape:

$$\hat{\phi} = u_{i1} \tag{3.21}$$

Referring to Equation 3.19, the corresponding singular value is the auto power spectral density function of the corresponding SDOF system. This function is identified around the peak by comparing the mode shape estimate $\hat{\phi}$ with the singular vectors for the frequency lines around the peak. If the singular vector has high modal assurance criterion (MAC) value with $\hat{\phi}$, the corresponding singular value belongs to the SDOF density function. It should be noted that modal assurance criterion index is a measure

of degree of linearity between estimates of a modal vector. It makes it an effective index for quantifying the correspondence between two sets of mode shapes. MAC value of 0 represents two completely independent mode shapes while the value of 1 indicates two identical mode shapes.

Normal FDD technique can only estimate modal frequencies and mode shapes. In order to estimate damping ratio, those singular value data near the peak which their corresponding singular vectors are having high enough MAC value, are transferred back to time domain via inverse FFT. From the free decay time domain function, which is also the auto correlation function of the SDOF system, the natural frequency and the damping ratio are found by estimating crossing times and logarithmic decrement. This extension to FDD is called Enhanced Frequency Domain Decomposition (EFDD) (Jacobsen, Andersen, & Brincker, 2006).

For the first step, all extremes r_k on the correlation function are found for both peaks and valleys. The logarithmic decrement δ is then given by

$$\delta = \frac{2}{k}\ln\left(\frac{r_0}{|r_k|}\right) \tag{3.22}$$

where r_0 is the initial value of the correlation function and r_k is the k^{th} extreme. Therefore, the initial value of the correlation function and the logarithmic decrement can be found by linear regression on kδ and $2\ln(|r_k|)$. Finally, the damping ratio is given by:

$$\varsigma = \frac{\delta}{\sqrt{\delta^2 + 4\pi^2}} \tag{3.23}$$

By adopting a similar procedure, the frequency is found by making a linear regression on the crossing times and the times corresponding to the extremes, considering that the relationship between damped and undammed natural frequencies is:

$$f = \frac{f_d}{\sqrt{1-\varsigma^2}} \tag{3.24}$$

3.2 CMCM Model Updating

Cross Model Cross Mode is a model updating method, developed by (Hu & Li, 2007) and is going to be used to update the finite element model of this study. More details on this method in compare to other updating methods can be found in CHAPTER 2:. In this section, the theory of CMCM updating method is presented based on (Hu & Li, 2007; Hu, et al., 2007).

Let's Imagine M and K are the mass and stiffness matrices that are obtained using unmodified finite element model and M^* and K^* are the mass and stiffness matrices of the actual model. The aim is to update M and K using modal properties including a number of modal frequencies and mode shapes of both FE and actual models. Lets λ_i and ϕ_i be the i_{th} modal frequencies and arbitrarily scaled mode shapes, associated with M and K, which can be expressed in form of:

$$\lambda_i M\phi_i = K\phi_i \tag{3.25}$$

Now let's assume that the stiffness and mass matrices of the actual i.e. experimental model, K^* and M^* are modifications of K and M respectively which can be expressed as:

$$K^* = K + \sum_{n=1}^{N_e} \alpha_n K_n \tag{3.26}$$

$$M^* = M + \sum_{n=1}^{N_e} \beta_n M_n \tag{3.27}$$

where K_n and M_n are the stiffness and mass matrices, corresponding to the n^{th} member. N_e is the number of elements and α_n and β_n are stiffness and mass correction factors respectively. In a simple form, each element is assumed to be updated by only one parameter. For example α_n is correcting Young's Modulus to update stiffness matrix and β_n is correcting mass density to update mass matrix. Although in many cases, the stiffness matrix of each element is more complex and cannot be updated using only one correction parameter. For example in beam elements, change in geometry might results on stiffness change in only one direction and to address that, α_n need to have more than one correction term.

Similar to Equation 3.25, the j^{th} eigenvalue and eigenvector associated with M^* and K^* is expressed as:

$$\lambda_j^* M^* \phi_j^* = K^* \phi_j^* \tag{3.28}$$

Pre-multiplying Equation 3.25 by $(\phi_j^*)^T$ and Equation 3.28 by $(\phi_i)^T$ yields:

$$\lambda_i (\phi_j^*)^T M \phi_i = (\phi_j^*)^T K \phi_i \tag{3.29}$$

$$\lambda_j^* (\phi_i)^T M^* \phi_j^* = (\phi_i)^T K^* \phi_j^* \tag{3.30}$$

Since M and K are symmetric matrices, their transposes are equal to themselves. So the left side of Equations 3.29 and 3.30 can be written as:

$$((\phi_j^*)^T M \phi_i)^T = (\phi_i)^T M \phi_j^* \tag{3.31}$$

$$((\phi_j^*)^T K \phi_i)^T = (\phi_i)^T K \phi_j^* \tag{3.32}$$

Furthermore, the transpose of a scalar matrix is equal to itself. For example $((\phi_j^*)^T M\phi_i)^T = (\phi_j^*)^T M\phi_i$. Considering this, Equations 3.31 and 3.32 can be expressed as:

$$(\phi_j^*)^T M\phi_i = (\phi_i)^T M\phi_j^* \tag{3.33}$$

$$(\phi_j^*)^T K\phi_i = (\phi_i)^T K\phi_j^* \tag{3.34}$$

Dividing Equation. 3.30 by Equation 3.29, and using the scalar identities of Equations 3.33 and 3.34, one obtains:

$$\frac{(\phi_i)^T K^*\phi_j^*}{(\phi_i)^T K\phi_j^*} = \frac{\lambda_j^*}{\lambda_i}\frac{(\phi_i)^T M^*\phi_j^*}{(\phi_i)^T M\phi_j^*} \tag{3.35}$$

Substituting Equations 3.26 and 3.27 into Equation 3.35 yields:

$$1 + \sum_{n=1}^{N_e} \alpha_n C_{n,ij} = \frac{\lambda_j^*}{\lambda_i}\left(1 + \sum_{n=1}^{N_e} \beta_n D_{n,ij}\right) \tag{3.36}$$

where

$$C_{n,ij} = \frac{(\phi_i)^T K_n\phi_j^*}{(\phi_i)^T K\phi_j^*} \tag{3.37}$$

$$D_{n,ij} = \frac{(\phi_i)^T M_n\phi_j^*}{(\phi_i)^T M\phi_j^*} \tag{3.38}$$

To summarize this equation, lets replace *ij* with a new index *m* and also introduce $b_m = \frac{\lambda_j^*}{\lambda_i}$, so Equation 3.36 becomes:

$$1 + \sum_{n=1}^{N_e} \alpha_n C_{n,m} = b_m\left(1 + \sum_{n=1}^{N_e} \beta_n D_{n,m}\right) \tag{3.39}$$

Rearranging Equation 3.39, one obtains:

$$\sum_{n=1}^{N_e} \alpha_n C_{n,m} - b_m \sum_{n=1}^{N_e} \beta_n D_{n,m} = b_m - 1 \quad (3.40)$$

By introducing $E_{n,m} = -b_m D_{n,m}$ and $f_m = b_m - 1$, Equation 3.40 can be expressed as:

$$\sum_{n=1}^{N_e} \alpha_n C_{n,m} + \sum_{n=1}^{N_e} \beta_n E_{n,m} = f_m \quad (3.41)$$

When the number of available modes from the finite-element model and corresponding real structure are N_i and N_j respectively, a total number of $N_m = N_i \times N_j$ equations can be formed from Equation 3.41 which can be written in matrix form:

$$C\alpha + E\beta = f \quad (3.42)$$

In Equation 3.42, C and E are matrices with dimension of $N_m \times N_e$, α and β are column vectors of size N_e and f is a column vector of size N_m.

3.3 Mass Normalization

Output-only modal testing, sometimes refers to as operational modal analysis, is a modal testing method based on the ambient excitation which are in most cases unknown. There are many advantages to this method as oppose to experimental modal testing.

First of all, this method is applicable for a wider range of structures. Although acquiring the precise and useful information of input force is usually feasible for scaled laboratory structures, but it should never be forgotten that the reason for those tests are to use their findings in real case scenarios. It is safe to say that in most cases, it is either not possible

to apply input forces to full scale structures or it is not possible to effectively measure them.

Furthermore, exciting the structure for modal testing purpose, assuming that it is effectively possible, might influence the operating conditions of the structure. Output-only technology provides better and more reliable results in cases where the actual conditions of the system are essential for the structural response.

Output-only technology is a lot cheaper than EMA. It is possible to consider permanent sensors for important structures and record the measurements over a long period of time for further use. It also gives other possible applications like vibration level estimation since the actual response of the system is stored.

Despite of all these advantages, this technology still has many problems remain entirely or partly unsolved. One of the important problems which is going to be discussed here is the problem of mode shape scaling.

To answer this, it is important to first discuses mode shape versus operating deflection shape. Mode shapes and operational deflection shapes are a lot similar to each other in the first glance, but in fact there are not the same. Modeshapes are independent from the forces that are acting on the system. They only depend on material properties and boundary conditions and also geometrical properties. Mode shapes do not have unique values and units, although mode shapes themselves are unique and can be defined as the motion of one DOF relative to other DOFs.

Operational deflection shape in other hand is depending on the excitation forces applied to a system. They do have units, usually displacement or displacement per force. In a nutshell, ODSs are actually demonstrating that how much the structure is really moving

at a particular time or frequency. Unlike mode shapes that can only be defined for stationary linear systems, ODSs can also be defined for non stationary and/or nonlinear conditions and even for structures that do not resonate. So the question is how are they related? Modes are more of a mathematical concept. They are solutions to differential equations of motion which express the stationary linear vibration of a structure. This is from an analytical perspective. Although experimentally, modal testing is in fact done by measuring operational deflection shapes and interpreting them to define mode shapes. For example for sine testing where a sinusoidal input force applies to the system near to one of its resonant frequencies, the mode shape is ODS itself. In case of lightly damped structures where the modes are not coupled together, the ODS near a resonant frequency is dominated by a single mode shape. These are some assumption behind all normal mode testing. Using these assumptions and interpretations, considering that the excitation forces are measured, mode shapes can be obtained by curve fitting frequency response function. In case the information of input forces is no available, further assumptions are required.

A description of a mode consists of three quantities; eigenvalue, eigenvector and modal mass. Eigenvectors are vectors which their entries are representing the motion at each degree of freedom. Eigenvectors are describing a shape and not the value of vibratory motion, so they do not have a specific length. They are often referred to as mode shapes. Each eigenvector comes with a complex number called eigenvalue which hold the frequency at which the mode shape is being excited. Modal mass is the physical scaling factor between force and resulting motion. Unlike modal frequency and mode shape, modal mass cannot be derived from experimental operating deflection shape.

When modes are defined numerically, since mass and stiffness matrices are available the calculated mode shapes have orthogonal property. It means since the computed

modal vectors are derived directly from mass and stiffness matrices, they are scaled in a way that they can diagonalize these two matrices by pre and post multiplication as shown in Equation 3.43. In this Equation, mass matrix is being pre and post multiplied by mode shapes and the result is a diagonal matrix which refers to as modal mass matrix.

$$[\emptyset]^T[M][\emptyset] = [m] \tag{3.43}$$

If the lengths of eigenvectors are regulated in a way that the modal masses are all equal to one, such operation is called unit modal mass scaling. In this case the eigenvectors or mode shapes are referred to as mass normalized mode shapes. Mode shape scaling and particularly mass normalization is a common practice when the modal properties are needed for structural response simulation, structural modification or damage identification and detection applications.

When the mass matrix is available, in FE analysis for instance, the mode shapes can be simply scaled using the mass matrix. However this is not the case for nearly all experimental measurements. In a real case, the only available information is the structure's responses to the unmeasured or at best measured exciting forces. So there are other techniques to scale the calculated mode shapes which some are going to be discussed here.

3.3.1 FRF based Mass Normalization

Frequency response is the measure of the output spectrum of the structure in response to the input force. Considering the theoretical form of FRFs (Equation 3.10), it is represented in rational fraction form with two matrix polynomial function as numerator and denominator. The denominator parts of the FRF $(j\omega - \lambda_r)$ and $(j\omega - \lambda_r^*)$ are called

the characteristic equation. The process of curve fitting the FRF to find damping and frequency is in fact solving the roots of the characteristic equation, λ_r.

The numerator part of the Equation 3.10 is called residue. Assuming that p and q are the output and input measured degrees of freedom and r is modal vector number, residue can be written as follow:

$$A_{pqr} = Q_r \Psi_{pr} \Psi_{qr} \tag{3.44}$$

where Q is modal scaling factor and Ψ is modal coefficient.

Analytically, modal scaling factor, Q, is the relationship between the normalized modal vectors and the absolute scaling of the mass matrix. Experimentally, modal scaling factor is the relationship between normalized modal vectors and the absolute scaling of the residue information. This definition of modal scaling factor offers a solution to the mode shape scaling problem in experimental modal analysis.

For undamped or proportionally damped systems, modal scaling factor is normally presented as modal mass:

$$M_r = \frac{1}{Q_r \omega_r} = \frac{\Psi_{pr} \Psi_{qr}}{A_{pqr} \omega_r} \tag{3.45}$$

To scale mode shapes to unit modal mass, Equation 3.44 must be written for q^{th} column:

$$\begin{Bmatrix} A_{1qr} \\ A_{2qr} \\ \vdots \\ A_{qqr} \\ \vdots \\ A_{nqr} \end{Bmatrix} = Q_r \Psi_{qr} \begin{Bmatrix} \Psi_{1r} \\ \Psi_{2r} \\ \vdots \\ \Psi_{qr} \\ \vdots \\ \Psi_{nr} \end{Bmatrix} \tag{3.46}$$

where *r*=number of modes and *n*=number of DOFs.

It must be noticed that in this Equation, residues have unique values and reflect physical properties of the structure, but the mode shapes are not unique in value and can be arbitrarily scaled. The scaling constant Q_r must always be set in a way that Equation 3.46 remains valid. The value of Q_r can be chosen prior to the mode shape scaling or the mode shapes can be scaled first and then Q_r be calculated to satisfy Equation 3.46. In order to scale mode shapes to unit modal mass (UMM), next step is to set the modal mass in Equation 3.45 to one, therefore:

$$Q_r = \frac{1}{\omega_r} \tag{3.47}$$

Substituting Equation 3.47 into Equation 3.46 gives:

$$\underbrace{\begin{Bmatrix} \Psi_{1r} \\ \Psi_{2r} \\ \vdots \\ \Psi_{nr} \end{Bmatrix}}_{UMM} = \frac{1}{Q_r \Psi_{qr}} \begin{Bmatrix} A_{1qr} \\ A_{2qr} \\ \vdots \\ A_{nqr} \end{Bmatrix} = \sqrt{\frac{\omega_r}{A_{qqr}}} \begin{Bmatrix} A_{1qr} \\ A_{2qr} \\ \vdots \\ A_{nqr} \end{Bmatrix} \tag{3.48}$$

3.3.2 Mass Normalization using Mass Change Method

The most vital assumption of the previous scaling method is that the input force must be measured. Although in most cases, the input force is unknown or hard to measure. Scaling mode shapes when the input data is not available is in fact the ultimate challenge. There are a couple of methods and suggestions in the literature to solve this problem (Bernal & Gunes, 2002; Brincker & Andersen, 2003; López Aenlle, Brincker, & Fernández Canteli, 2005; López Aenlle, Brincker, Fernández Canteli, et al., 2005; Parloo, et al., 2002). A description of their mass normalization method is described in this section.

Imagine a structure with mass matrix of *M* and stiffness matrix of *K*. Operational modal testing of the structures determines modal frequencies (ω) and arbitrary scaled mode shape (φ) of the structure. Let's (Ψ) be the mode shape (φ) that is scaled to unity i.e. $\Psi.\Psi^T$=1 . From equation of motion;

$$M\Psi_1\omega_1^2 = K\Psi_1 \tag{3.49}$$

Now let's assume some changes in the mass matrix on DOFs where the mode shape is measured. This alters both modal frequencies and mode shapes and Equation 3.49 can be written as:

$$(M + \Delta M)\Psi_2\omega_2^2 = K\Psi_2 \tag{3.50}$$

where ΔM is the mass change matrix and ω_2 and Ψ_2 are the new modal frequencies and mode shapes. Subtracting Equations 3.49 and 3.50 gives:

$$M(\Psi_1\omega_1^2 - \Psi_2\omega_2^2) = \Delta M\Psi_2\omega_2^2 + K(\Psi_2 - \Psi_1) \tag{3.51}$$

Now let's assume that the change in mass does not significantly change the mode shapes, which means $\Psi_1 \cong \Psi_2$. Frequency shifts due to mass changes can be written in form of Equation 3.52:

$$\omega_1^2 - \omega_2^2 = 2\omega\Delta\omega \tag{3.52}$$

where $\omega = \frac{(\omega_1+\omega_2)}{2}$ and $\Delta\omega = \omega_1 - \omega_2$

So from Equations 3.51 and 3.52;

$$2M\Psi\frac{\Delta\omega}{\omega} = \Delta M\Psi \tag{3.53}$$

Among various scaling factors, there is one particular scaling factor that scales the mode shape Ψ to Φ so that it satisfies Equation 3.54:

$$\Phi^T M \Phi = 1 \tag{3.54}$$

where M is mass matrix and Φ is mass normalized mode shape. The desired scaling factor, α, is the factor that relates Ψ and Φ;

$$\Phi = \alpha \Psi \tag{3.55}$$

From Equation 3.53 to 3.55 one can obtain:

$$2\frac{\Delta\omega}{\omega} = \alpha^2 \Psi^T \Delta M \Psi \tag{3.56}$$

So the scaling factor can be obtained using Equation 3.57

$$\alpha = \sqrt{\frac{2\Delta\omega}{\omega \Psi^T \Delta M \Psi}} \tag{3.57}$$

This method is one of the simplest scaling methods based on mass change. Although the scaling factor is not so precise, but it is fast and handy and can be used for most cases. There is another scaling method in this group that is able to calculate the scaling factor more precisely. Again, let's α be the scaling factor that relates the scaled to unity mode shape Ψ to mass normalized mode shape Φ (Equation 3.55). Pre and past multiplication of this Equation to mass matrix gives:

$$\Phi^T M \Phi = (\alpha \Psi)^T M (\alpha \Psi) \tag{3.58}$$

Considering Equation 3.54, the scaling factor in its general form is:

$$\alpha = \frac{1}{\sqrt{\Psi^T M \Psi}} \tag{3.59}$$

So the scaling factor for normal structure and structure with change in mass are as follows:

$$\alpha_1 = \frac{1}{\sqrt{\Psi_1^T M \Psi_1}} \tag{3.60}$$

$$\alpha_2 = \frac{1}{\sqrt{\Psi_2^T (M+\Delta M) \Psi_2}} \tag{3.61}$$

Again, let's assume that the change in mass does not significantly change the mode shapes, which means $\Psi_1 \cong \Psi_2$. Then Equation 3.61 can be written as:

$$\alpha_2 = \frac{1}{\sqrt{\Psi_1^T M \Psi_1 + \Psi_1^T \Delta M \Psi_1}} = \frac{1}{\sqrt{\frac{1}{\alpha_1^2} + \Psi_1^T \Delta M \Psi_1}} \tag{3.62}$$

Equation 3.62 shows that when a mass change applies to the structure, it decreases the scaling factor and in the other hand limit of Equation 3.62 when *ΔM* approaching *"0"* is:

$$lim_{\Delta M \to 0} \left(\frac{1}{\sqrt{\frac{1}{\alpha_1^2} + \Psi_1^T \Delta M \Psi_1}} \right) = \alpha_1^2 \tag{3.63}$$

If β is mass change factor so that $\Delta M_1 = \beta_1(\Delta m)$, $\Delta M_2 = \beta_2(\Delta m)$ and $\Delta M_n = \beta_n(\Delta m)$, then the scaling factor can be calculated by drawing α versus β diagram and extrapolating it toward β=0.

3.4 Damage Locating Vectors

3.4.1 Modal Flexibility

Equation 3.64 is a second order differential equation, describing the undamped free vibration of a structure. In this equation $[M]$ represents mass matrix, $[K]$ is the stiffness matrix and $\{u\}$ is the displacement vector.

$$[M]\{\ddot{u}\} + [K]\{u\} = 0 \tag{3.64}$$

Equation 3.65 is the eigen solution of this system were $[\Lambda]$ and $[\Phi]$ are the eigenvalue and eigenvector matrices respectively. Eigenvalue matrix is the diagonal matrix of the squared natural frequencies of the structure, ω_i^2. Eigenvector matrix holds mass normalized eigenvectors of the structure as rows. Eigenvectors are mass normalized if their matrix satisfies Equation 3.66;

$$[\Phi]^T[K][\Phi] = [\Lambda] \tag{3.65}$$

$$[\Phi]^T[M][\Phi] = [I] \tag{3.66}$$

So considering Equation 3.65, the stiffness matrix can be calculated using Equation 3.67;

$$[K] = [\Phi]^{-T}[\Lambda][\Phi]^{-1} \tag{3.67}$$

Since flexibility matrix is the inverse of stiffness matrix, $[G] = [K]^{-1}$ the flexibility matrix can be calculated using Equation 3.68;

$$[G] = [\Phi][\Lambda]^{-1}[\Phi]^T \tag{3.68}$$

Let's assume that n is the number of degrees of freedom and m is the number of estimated modes were $m < n$. Therefore m eigenvectors with n entries are available and so Φ is an $n \times m$ matrix. Since only m modes are available, eigenvalue is an $m \times m$ diagonal matrix. So regardless of the number of available modes, the result of Equations 3.67 and 3.68 are always $n \times n$ matrices.

Equations 3.67 and 3.68 are presenting the mathematical relationship between eigenvalue, eigenvector, stiffness and flexibility matrices in their general form. Although an important point must be considered when using them with actual data. Stiffness and flexibility matrices are inverse of each other, only if they are full rank. In this case, being full rank means all the modes are participating in them i.e. $m=n$. However, since in this case the number of modes is less than the number of DOFs, none of the two matrices are full rank. The important point in using Equations 3.67 and 3.68 is that if $m=n$, both equations are valid and their results are accurate. However in case which few numbers of modes are available, the results of at least one of the two equations are biased. Equation 3.67 is able to estimate stiffness matrix, if a few number of higher modes are available. In other word, stiffness matrix converges using the modes with higher eigenvalues. On the other hand, flexibility matrix can be estimated using a few numbers of lower modes. In practice, it is not possible to extract higher modes of a system. It is usually not possible to acquire higher modes using modal analysis, hens it is not possible to estimate stiffness matrix using modal testing.

3.4.2 Damage Locating Vectors

One of the most distinguished damage detection methods based on change in flexibility is called *Damage Locating Vectors*. Damage locating vectors (DLV) is in fact one of the best methods that uses dynamically measured flexibility matrix to locate damage. This method, introduced by (Bernal, 2002), has the ability to accurately locate single and

multiple damage cases in the structure, regardless of its geometry. Damage locating vectors are a set of vectors with a particular property. They cause identical deformations when they are applied to undamaged and damaged state of the structure. As a result, when DLVs are applied to undamaged structure, they induce zero (or relatively small) stress in damage member(s). So using these load vectors and doing linear static analysis of the undamaged structure under these loading and extracting the characterizing stress of all members, the damaged member can be easily spotted as it has zero or relatively small stress compare to other members.

Damage locating vectors defines as the null space of the change in flexibility (Bernal, 2002). However, precise flexibility changes are not the only parameters that can be used to compute DLVs. (Bernal, 2006) stated that even though flexibility cannot be extracted exclusively from output signals in case of operational or ambient vibration, the vectors in the null space can be estimated from output signals without having explicit flexibility matrices. Damage locating vectors can also be extracted from the null space of change in the transfer matrix (Bernal, 2007a, 2010).

Consider a structure that is as linear in damaged state that it is in undamaged state. Also consider determining damaged and undamaged flexibility matrices at m sensor locations (G_D and G_U) in which $m \leq n$, the number of DOFs. For an ideal situation where the flexibility matrices are exact, assume that there are a number of load vectors l, defined in sensor coordinates, which results in identical deformations at undamaged and the damaged states (Bernal, 2002) :

$$(G_D)L = (G_U)L \tag{3.69}$$

If all the load vectors that satisfy this requirement are written in a matrix L, then:

$$(G_D - G_U)L = \Delta G.L = 0 \tag{3.70}$$

There are two conditions that Equation 3.70 can be satisfied. Either G_D - G_U =0 or L is a basis for the null space. The first possibility implies when there is no damage on the structure i.e. $G_D = G_U$ or that the damage is in a part of the structure where the stresses are zero for any loading in sensor coordinates. However, less assume that G_D - $G_U \neq 0$ and there is damage(s) in the system. In this case, the vectors assigned to the null space of ΔG (matrix L) can be found by calculating singular value decomposition (SVD) of flexibility shifts (Bernal, 2002).

$$\Delta G = USV^T = [U]\begin{bmatrix} S_r & 0 \\ 0 & 0 \end{bmatrix}\begin{bmatrix} V^T \\ L^T \end{bmatrix} \tag{3.71}$$

In Equation 3.71, the matrix S is a diagonal matrix, containing singular values and matrix V is an orthogonal matrix, containing vectors of row space and null space (L).

To employ load vectors of matrix V to locate damaged members, the first step is to apply them to the undamaged structure and to their corresponding sensor locations which causes stress in the members. To distinguish large and small stresses, the independent internal stresses in every element must be reduced to a single value that is called the characterizing stress, σ. Unlike "stress" which is a generalized term pointing to actual stress or a stress resultant, the characterizing stress is defined in such a way that the strain energy per unit length, area or volume is proportional to the square of its value. For a planar beam element the characterizing stress can be shown as:

$$\sigma_{beam} = \sqrt{\left(M_i^2 + M_j^2 + M_i M_j\right)} \tag{3.72}$$

where M_i and M_j are the two end moments of the beam. In each case, the Normalized Stress Index (*nsi*) defines as in Equation 3.73;

$$nsi_i = \frac{\sigma_i}{\sigma_{i(\max)}} \tag{3.73}$$

where σ_i is the characterizing stress in a given element and $\sigma_{i(\max)}$ is the largest characterizing stress over all the elements of its kind.

Not all the vectors in matrix [*V*] are actually damage locating vectors (DLV). DLVs in general are vectors of [*V*] associated with negligible or zero singular values in matrix [*S*]. However, singular values in practice are seldom equal to zero and so a threshold is required to decide which vectors belong to raw space and which ones belong to null space and are in fact DLV.

To define such threshold, let's pre and post multiply Equation 3.71 by a vector of [*V*], for example V_i, which results:

$$V_i^T \Delta G V_i = V_i^T G_{\mathrm{D}} V_i - V_i^T G_{\mathrm{U}} V_i = S_i \tag{3.74}$$

This suggests that the singular values of ΔG (S_i) are the difference of the external work of the associated singular vector when it is applied to the damaged and undamaged states of the model as a load set. If it is assumed that the characterizing stress caused by applying V_i in undamaged and damaged states are adequately equal, then the difference in work is caused by changes in the strain energy in the damaged member, so:

$$s_i = \sum_{\Omega D} \alpha_j \sigma_j^2 \tag{3.75}$$

where j refers to the particular element and α is a constant that depend on the extent of the damage on each element except on j. If the vector V_i is multiplied by a constant, c_i so that the largest characterizing stress over the full domain is equal to unity, then:

$$c_i s_i = \sum_{\Omega D} \alpha_j nsi_j^2 \tag{3.76}$$

This Equation can also be written as:

$$c_i s_i = nsi_m^2\Big|_i \xi_i \sum_{\Omega D} \alpha_j \tag{3.77}$$

where nsi_m is the largest *nsi* in the damaged region and $0 < \xi_i < 1$. Let's assume that the vector that is associated with the largest value of Equation 3.77 is that where $i=q$. By normalizing this Equation with respect to its largest value and taking a square root on both sides one gets;

$$nsi_m^2\Big|_i = \rho_i svn_i \tag{3.78}$$

where,

$$svn_i = \sqrt{\frac{s_i c_i^2}{s_q c_q^2}} \tag{3.79}$$

$$\rho_i = nsi_m\Big|_q \sqrt{\frac{\xi_q}{\xi_i}} \tag{3.80}$$

Since the *svn* is computed without knowledge of the damage, then estimation of the largest *nsi* in Equation 3.78 over the damaged region is equivalent to selecting a value for ρ. In Equation 3.80, $nsi_m\Big|_q \leq 1$ and $\frac{\xi_q}{\xi_i}$ can be taken as equal to one. Choosing a value for nsi_m that does not exceed one obtains a cut on *svn*. If the flexibility matrices are very accurate and the errors in computing stresses are small, then the best results are expected at very low values of nsi_m. In practice however, such accuracy is not

attainable. So a safe cut-off value of 0.2 is recommended by (Bernal, 2002) to operate well for a wide range of conditions.

So as a result, only vectors with $svn \leq 0.2$ are taken as DLVs. When a group of vectors are selected as DLVs, the damage can be localized by calculating weighted stress index (*WSI*) using Equation 3.81.

$$WSI = \frac{\sum_{i=1}^{ndlv} \frac{\{nsi\}_i}{\overline{svn_i}}}{ndlv} \tag{3.81}$$

$$\overline{svn_i} = \max(svn_i, 0.015)$$

The members with *WSI* less than 1 are indicated as damaged members (Bernal, 2002).

CHAPTER 4: METHODOLOGY

4.1 Overview

This chapter describes all the methods that are used in this study. The contents of this chapter can be viewed in two categories i.e. modelling methods and analysis methods. Modelling methods are referring to the techniques and procedures that are used to model the frame structure in order to generate data. For examples, finite element simulations, laboratory set up and experimental modal analysis are within this category. The analysis methods are referring to those methods that are applied to analyze the generated data for different purposes in line with the objectives of this study e.g. model updating, mass normalization and damage detection. The general theories of these methods are presented in CHAPTER 3: and this chapter contains their implementation for this particular case study.

4.2 Frame Structure

A schematic of the frame structure used in this study is shown in Figure 4.1. It is a steel frame made of steel pipes as beam and column and also a steel plate as upper deck. The frame's height from the floor to top of the steel plate is 300±1 cm. The centre to centre dimensions of the frame are 115×130 cm at the base and 50×70 cm at the top. The steel plate, seating on top of the frame is 70×90 cm in dimensions and 4 cm in thickness. The columns are rising vertically in the rear YZ plane, but they are inclined in all other planes. All the columns are 7 cm in diameter and 5 mm in thickness and all the beams are 3.25 cm in diameter and 3 mm in thickness. The mass of the frame structure including columns, beams, 4cm tick steel plate, two shakers, two amplifiers and the frames of hanging blocks is approximately 320 kg.

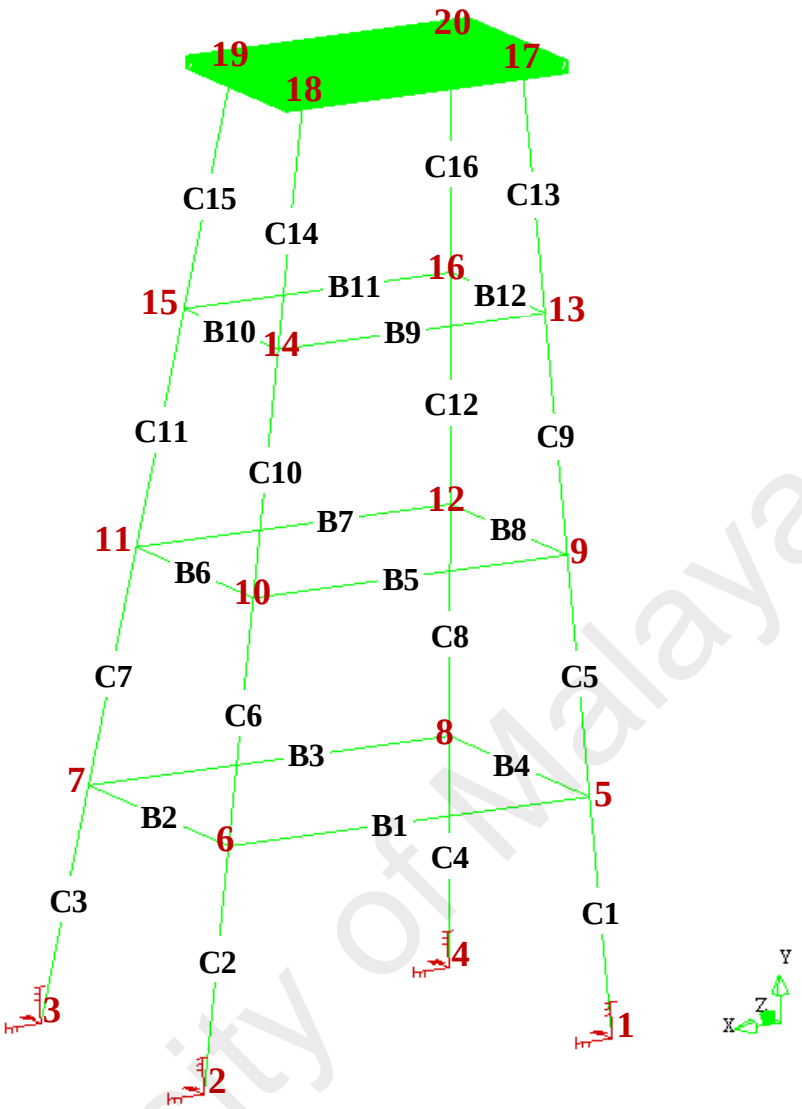

Figure 4.1: Frame structure with numbering of nodes, beams and columns

Selecting nodes and DOFs in any structural analysis method e.g. modal analysis, is very much depends on structure's type. In case of frame structures and trusts, joints are the preliminary choices for nodes. In finite element analysis, beams and columns of a frame structure might be divided further to increase accuracy. However, due to technical and financial limits, that is not usually applicable and even necessary for an experimental modal analysis. So, throughout this study, nodes are assigned in the intersection of beams and columns and no node is assigned in the middle of the members.

Figure 4.1 is illustrating the numbering of nodes, beams and columns and also the global coordinate axes. The node numbering sequence starts with node one which is a support located at the origin of global coordinate. The other 19 nodes are sequentially numbered clockwise from bottom to top. 16 columns and 12 beams are numbered accordingly.

In general, each node of a space frame has six degrees of freedom i.e. dX, dY, dZ, rX, rY and rZ. Although in case of this study, only translational DOFs are of interest (mainly because only translational sensors are available for the experiment). Considering that the frame has 20 nodes, this result on 60 DOFs in total. However, nodes 1 to 4 are supports and so the number of independent DOFs of the frame structure is 48. Table 4.1 is presenting the sequence of these 48 degrees of freedom. For example, DOF 36 is referring to translational DOF of node 16 along global Z axis. This sequencing is used throughout the study, for example in assembling flexibility and mass matrices etc.

Table 4.1: Sequence of DOFs of the model

Node number	DOF number			**Node number**	DOF number		
	X	Y	Z		X	Y	Z
1	Fixed	Fixed	Fixed	**11**	19	20	21
2	Fixed	Fixed	Fixed	**12**	22	23	23
3	Fixed	Fixed	Fixed	**13**	25	26	27
4	Fixed	Fixed	Fixed	**14**	28	29	30
5	1	2	3	**15**	31	32	33
6	4	5	6	**16**	34	35	36
7	7	8	9	**17**	37	38	39
8	10	11	12	**18**	40	41	42
9	13	14	15	**19**	43	44	45
10	16	17	18	**20**	46	47	48

4.3 FE Simulation

Finite element simulation is almost always a key part of any study in the field of structural engineering. Using FE, it is possible to simulate various structural systems and study their behaviour in almost no cost. In this study, FE modelling and analyses are employed in different ways and for different purposes. The first use of FE modelling was to give a general estimation of the structure's dynamic and modal behaviour prior to experimental set up. FE simulation also has a key task on examining the experimental results of various methods that are used in this study e.g. damage locating vectors, mass normalizations, etc. In all these cases, the analysis results of experimental data are compared to those obtained using FE modelling to acquire their reliability[1]. On top of these, FE simulation is in fact part of some methods that are used in this study. For example, in model updating method or DLV which will be describing later in this chapter, FE simulation has a different role other than just validating its equivalent experimental findings.

All the finite element simulations and analyses in this study are done using commercial finite element software, DIANA 9.3. DIANA has two different modules for FE modeling and FE analysis. The graphical user interface (GUI) of this package is iDIANA. Modeling the geometry, assigning elements, meshing, assigning input forces, constrains, material and physical properties etc. are all done in iDIANA environment. When the model is completed, DIANA's analysis module is used to run different FE analysis including linear static, linear dynamic, nonlinear static, eigen analysis etc.

[1] This statement is not suggesting that the finite element results are more reliable and must be used as benchmark. In case of modal properties, the most reliable and realistic results are those obtained by the experiment and any numerical simulation must be updated in reference to them. However, when it comes to examining the correctness of a particular method like mass change method or damage locating vectors, finite element simulation acts like a puzzle book with appended solutions and hints. So the correctness and reliability of the findings of those methods can be examined using finite element analysis, before they are employed experimentally where there is no hint to check whether their results are correct or not.

4.3.1 FE Modelling using iDIANA

Modeling the geometry of the frame structure in iDIANA is straight forward. Three types of structural elements are used to model the frame structure. L12BE two node beam elements are used to model columns and beams, HX24L eight node brick elements are used to model the steel plate and PT3T translational point mass is used to model the effect of extra weights and equipments placed on the model.

Diana offers three classes of beam elements. Class-I beam elements are the simplest form which are based on Bernoulli theory. They must only be specified with the general parameters i.e. area and moment of inertia, however, shear deformations can also be specified for this type of elements if required. Class-II beam elements are numerically integrated over their cross-section and along their axis. Therefore these elements may be used in geometrical and physical nonlinear analysis. Class-III beam elements comprise a number of curved (higher order) elements which are numerically integrated over their cross-section and along their axis.

None of the FE analyses in this study requires any of the advantages of class II or III beam elements. Nonlinear dynamic analysis in this study does not comprise any geometrical or physical nonlinearity to employ class-II beam elements. The local deformations of elements and members are also not important to this study. So as much as using class-III beam elements might offer some extra information on deformation of the members, it definitely does not worth the significant increase of computing time, especially in nonlinear dynamic analysis. Hence, L12BE which is the 3D version of class-I beam element in Diana is used for this study. For the same reason, HX24L was selected as the simplest form of brick elements to assign mass of the hanging blocks and the applied forces with minimum computing time.

The laboratory model of the frame structure includes two concrete blocks, hanging on the upper deck. Since the two blocks are not directly attached to the frame structure, their mass is not part of the mass matrix. The best approximation of their effect is their downward forces that are applied to the upper deck in 8 points. Some of the equipments are placed of the frame structure. Among them weight of two amplifiers are significant so their mass need to be added to the model. Moreover, there are extra weights that are used for mode shape scaling and need to be model (Refer to chapter 4.6). To simulate all these, 6 point mass elements (PT3T) were assigned to nodes 13 to 16, 18 and 20. PT3T is a three dimensional translation point mass/damping element. When applied to a node, this element directly adds the allocated amount of mass into three corresponding entries of that node in the mass matrix.

4.3.2 FE Analyses using DIANA

Based on the application, three different types of analyses are being performed on FE model i.e. eigen analysis, structural dynamic analysis and structural linear static analysis.

Eigen analysis of FE model is used to extract modal frequencies and mass normalized mode shapes directly from mass and stiffness matrices. The results of this analysis are used to study the overall modal properties of the model. They are also used as benchmark for mass normalization of the experimental mode shapes. The frame structure is assumed to have 48 degrees of freedom, so the full rank results of eigen analysis must include 48 modes. This is if only three translational DOFs are assumed for each node. However, L12BE element has 6 DOF at each node. So regardless of the assumption, rotational DOFs are included in stiffness and mass matrices in DIANA. Moreover, the steel plate on the deck is also meshed to smaller elements for some modelling reasons. Hence, the actual stiffness and mass matrices generated in iDIANA

is a lot larger than the assumed 48×48. Although this does not affect the results of extracted mode shapes. The final results are the translational modal vectors of the desired 16 nodes i.e. nodes 5 to 20 and for the lower modes.

Structural dynamic analysis is used to further investigate the modal behaviour of the model. Unlike eigen analysis, modal properties are not the direct results of this analysis procedure. The outputs of FE dynamic analysis are the response of each node to the input excitation. The quantity of excitation is force and the quantity of response is acceleration. The input force is the force signal that was recorded during the experiment. The original signal is recorded for 60 seconds with sampling rate of 3200 S/s. So the original signal contains 192,000 samples. This number is extremely large to be used in FE dynamic analysis. So the sampling rate was reduced to 320 S/s and the time was reduced to 5 seconds. So the final signal was containing 1,600 samples. This signal was used as input force to FE dynamic analysis. The analysis produces 1,600 accelerations for each DOF with the time intervals of 0.003125s. These data were used in ARTeMIS for modal identification.

The structural linear static analysis was used solely for DLV detection method. DLV, which is one of the detection methods used in this study, is based on calculating sets of loads with a special property. When these load vectors are applied to the structure, they induce zero or low stress on damaged member. To implement this, the load vectors were assigned to all 48 DOFs of the model in iDIANA. Then the stresses of all members were computed using linear static analysis of FE model.

4.4 Experimental Work

The frame structure shown in Figure 4.2 was fabricated and installed in the heavy structure laboratory of Department of Civil Engineering, University of Malaya. This

sub-chapter presents the methods that are used to test the laboratory model of the frame structure.

Figure 4.2: Laboratory model of the frame structure

4.4.1 Modal Testing Equipments

i. Accelerometer

Kistler 8702B50M1 K-Shear single axis accelerometer was used to measure the acceleration of the main DOFs of frame structure (Figure 4.3 - Left). This sensor has the acceleration range of ±50 g and the frequency range of 0.5 to 10 kHz. It can detect acceleration with the sensitivity of 100 mV/g. These accelerometers are connected to the model using a magnet mounted to their tip so they can be easily roved between

DOFs. 16 accelerometers of this type were available, but 14 of them had to be used simultaneously during the test. Four Kistler 8776A50 K-Shear single axis accelerometers were also used to record the acceleration of two concrete blocks and two shakers attached to them (Figure 4.3 - Right)

Figure 4.3: Kistler K-Shear accelerometers

ii. Force transducer

A PCB 208C02 force transducer was used to measure the applied input force to the frame structure (Figure 4.4). This sensor has the measurement range of 0.4448 kN in both tension and pressure. Using this sensor, the frequency of the applied force can be as low as 0.001 Hz and as high as 36 kHz, far beyond the range needed for this study. The sensitivity of the sensor is 11241 mV/kN.

Figure 4.4: PCB 208C02 force transducer

iii. Signal Analyzer

A 32 channel OROS OR-38 signal analyzer / data logger is using for this study (Figure 4.5). This device provides 40 kHz of real-time bandwidth on its 24 bit ICP inputs. The

input signals can go up to ±40 V. It is equipped with a 40 GB internal hard disk and any external device such as laptop or PC can be connected to it via its 100 Mb/s Ethernet. Its interface program is NVGate.

Figure 4.5: OROS OR38 signal analyzer

iv. Power Amplifier

Figure 4.6 shows the APS-125 power amplifier. The job of this device is to receive a weak low voltage signal from the analyzer or any other signal generator and amplifies it, so it become powerful enough to be used by the shaker to apply force to the structure.

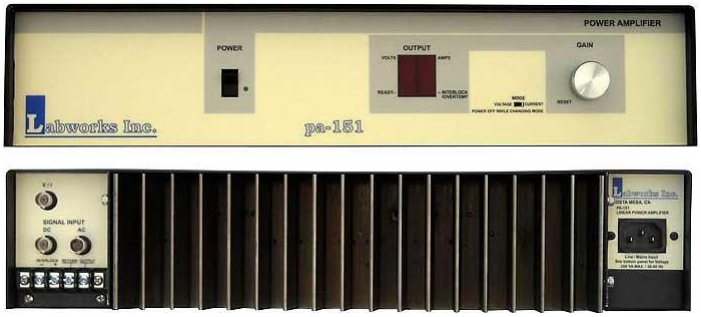

Figure 4.6: Labworks PA-151 power amplifier

v. Shaker

Figure 4.7 shows the ET-132-2 shaker used for this study. It provides the maximum load of 31 N for sinusoidal signals, 22 N for random signals and 67 N for shock forces. It has the maximum displacement of 1.3 cm peak to peak.

Figure 4.7: ET-132-2 shaker

4.4.2 Test Setup

4.4.2.1 Concrete Blocks

In laboratory, there are normally two ways of using the shakers to excite the model. First is by fastening the shaker to a fix support e.g. floor and using the rigidity of the support to provide the reaction force. Although sometimes it is difficult or not practical to support a shaker from a floor-mounted fixture. It particularly accrues in lateral excitation. In these cases, the solution is to hang the shaker from a support cable attached above the test article and attach masses to the base of the shaker to provide more inertia to push against the model (Figure 4.8). The whole concept of this set up is simple. In any modal testing, the job of shaker is to apply force to the model. For a shaker mounted to the floor or a stand etc, the reaction is provided by the stiffness of

that rigid body, while for a suspended shaker the reaction is provided by the inertia of shaker's mass, $F=ma$.

Figure 4.8: Shaker is hanged to excite the car via piano strings (www.businessmagnet.co.uk)

In this test set up, the same concept of suspended shaker is used with some modifications. The main difference is that the shakers-masses are not suspended to a side hanger. Instead, they are placed on top of the model, on the deck. For the relatively large model in this study, this is an advantage not to have a second hanger next to the model to just suspend the shaker. More importantly, this excitation method has potential of being extended and used in full-scale structures.

The main concern in this setup is that the mass should be placed on top of the deck in a way that it moves totally independent from it, at least in one direction. In other word

and assuming ideal conditions, if the deck moves, the mass stands still and does not follow the motion of the deck it is sitting on. This is possible by significantly diminishing the friction between the deck and the mass. A number of methods have been tested to reduce friction up to the point that is desired for the purpose of this study. The first proposal was to place rollers under the mass. It was tested by vibrating the block and measuring the input force and acceleration of it. Since the mass of the block was precisely measured, it was expected that the mass multiplied by its acceleration be equal to the input force. Although in this case, it was lower. This indicates that a fraction of the input force is overcoming the friction. Replacing rollers with bearings although improved the results significantly, but still was not up to the required level.

The third proposal was to suspend the concrete blocks. This is more similar to the suspended shaker method, although there are few concerns that need to be addressed. The main advantage of using rollers or bearings, if the friction can be cancel out, is that their motion is forth and back and unlike a hung body, it does not have a return or rest point. However, the motion of a suspended mass is like a pendulum (Figure 4.9). So even though the shaker is causing it to move forth and back, but it has its own oscillation characteristic i.e. swinging frequency that perhaps interferes with the input force. Moreover, this frequency might interfere with the vibration of the structure. So these effects need to be considered.

Two concrete blocks, weighted 67.8 and 68.2 kg, are hung to a steel frames using very thin steel cables, as shown in Figure 4.10. In this setup, the two blocks can freely swing in any vertical plan in a short span which means they act similar to simple pendulum. The word similar is used, because these blocks do not fulfill one important assumption of a simple pendulum. In a simple pendulum, one point mass is suspended to a relatively long and light inextensible string whereas in this case, each block is

suspended to four cables and the geometry of the blocks and the place where cables are connected to the blocks are making this system different from a simple pendulum. However some laws that are governing a simple pendulum can be approximately applied to this model.

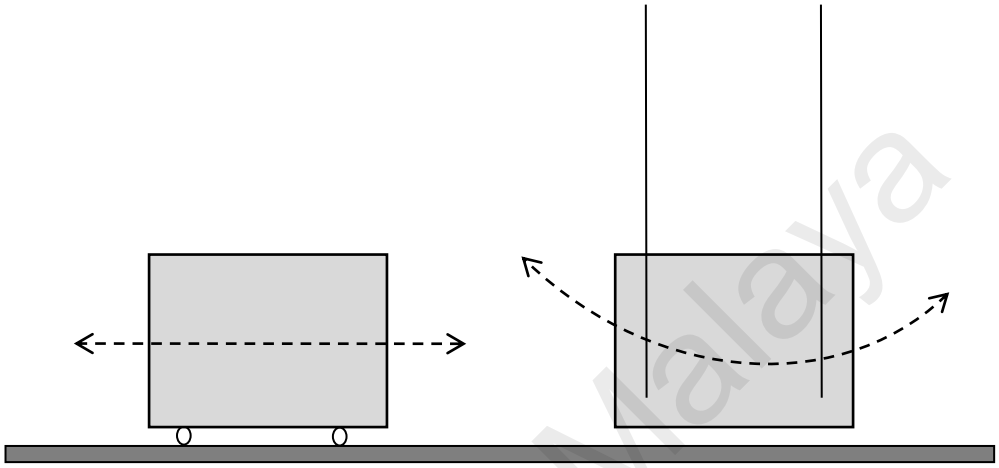

Figure 4.9: The difference between the motion of the block on rollers and suspended

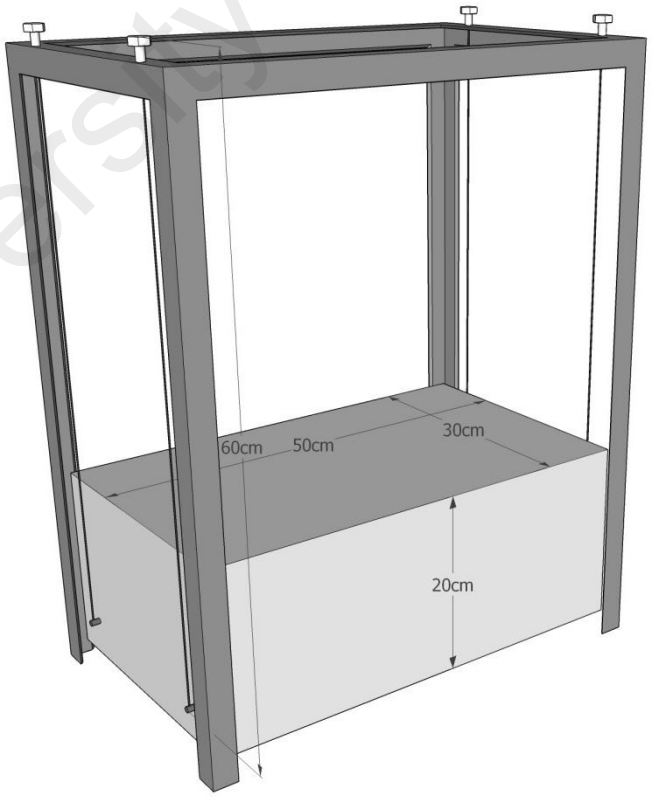

Figure 4.10: Schematic of concrete block suspended from a steel frame

Simple pendulums are nonlinear in general and their period is depending on initial angular displacement amplitude. However, with the assumption of small angles, $\sin(\theta) \approx \theta$, the frequency and period of the pendulum are independent from the initial angular displacement and are a function of length and acceleration of gravity (g). In this case, period of pendulum is:

$$T = 2\pi\sqrt{\frac{L}{g}} \tag{4.1}$$

where T is period of pendulum, L is pendulum's length and g is acceleration of gravity.

In case of these blocks and the way they swing (Figure 4.11), it is apparent that the block does not rotate around the pivot point. Because each block is suspended to two cables at each side, it maintains its horizontalness and moves up and down when it swings front and back. Figure 4.11 is showing the suspended block from the side. L is the length of each cable which is 60 ± 0.5 cm. d is the lateral displacement, h is the vertical displacement and θ is the swing angle. First, let's imagine the block is suspended to its frame and the frame is placed on the ground i.e. the frame itself is stationary. If the block swings within the small angle range, $\theta < 5°$, then the frequency of the block can be approximately calculated using Equation 4.2

$$f = \frac{1}{2\pi}\sqrt{\frac{g}{L}} \quad \text{====>} \; f = 0.65 \text{ Hz} \tag{4.2}$$

Vibrating characteristics of both blocks and their frames were tested on the ground. Table 4.2 is presenting the main resonance frequencies of the block which are 0.7 Hz laterally and 1.2 Hz angular. Other than these two, the test shows that the block has significant response in 2.3 and 17 Hz. The supporting frame also has 6 resonance frequencies within the range of this study as presented in Table 4.2. The two frames are

seating on rubbers that are acting as isolators. This is to minimize the vibration interference between the frame and the model itself. Although any trace of these 6 frequencies on the final results are going to be monitored.

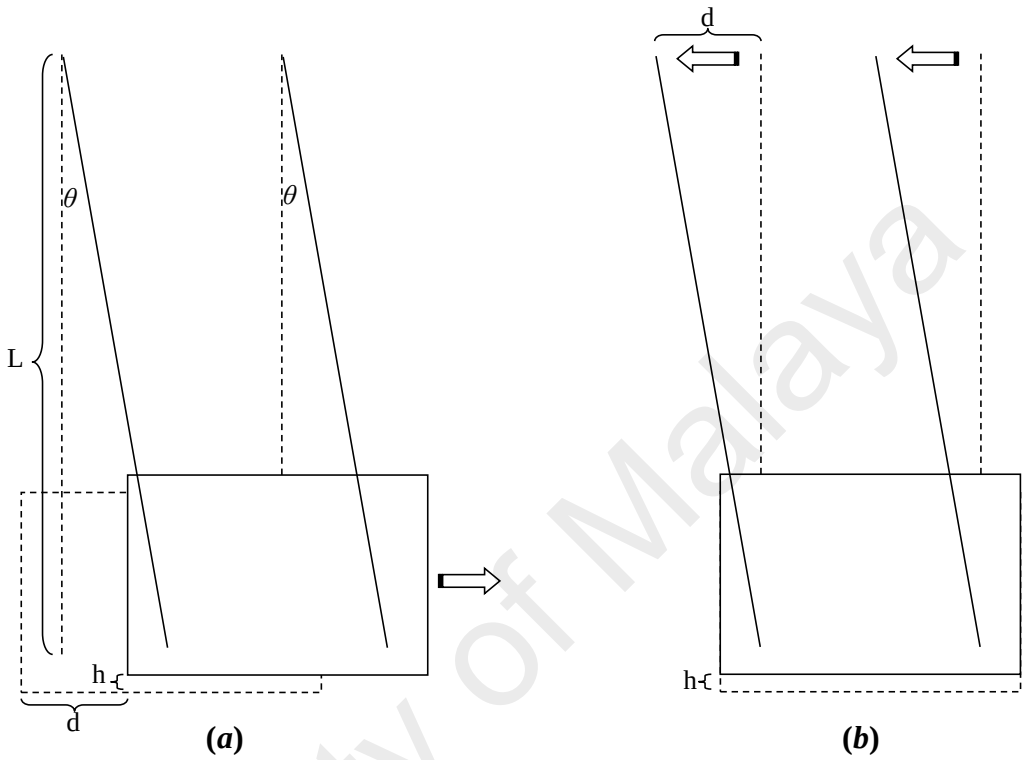

Figure 4.11: Motion of suspended concrete block relative to the deck

Table 4.2: Resonance frequencies of suspended concrete block and the supporting frame

	Vibrating Frequencies (Hz)					
Concrete Block		0.7	1.2	2.3	17	
Supporting Frame	21	24	113	162	186	222

The first three resonance frequencies of the block are not within the range of the input force, so the blocks are not excited in those frequencies. However there is another factor that significantly minimizes the effect of blocks oscillation on the model which needs to be discussed. What happened in an oscillating pendulum, or in this case the block, is

that it repeatedly converts kinetic energy to potential energy by gaining height and vise versa by gaining velocity. When the swing span is wide, $\theta > 5°$, this conversion relationship is nonlinear. For smaller span, conversion can be assumed linear. However if the span is too short it means the value of *h* (Figure 4.11) is very close to zero and so the pendulum's energy is much less than it needs to overcome frictions and it does not oscillate.

The other important concern is that the frames that are holding the blocks are seating on the deck and moving together with it. If the deck is stationary relative to the global coordinate (ground) and blocks are swinging or moving by an external force, the lateral displacement of the block, *d*, causes the block to gain height *h* as shown in Figure 4.11-a. Now let's imagine that the block is completely stationary relative to the global coordinate (ground) and the deck is moving (Figure 4.11-b). Any lateral displacement of the deck, *d*, causes the frame to move back and forth above the stationary block. In fact it does not matter whether the block is moving relative to the frame or frame is moving relative to the block. In both cases, the block gains height *h* for a relative displacement of *d* (Figure 4.11). So the best way of reducing the oscillating effect of the block is by minimizing its swing span as much as possible, specifying that the swing span is the motion of the block relative to the deck. In case of this study, *d* was monitored throughout the test using a laser proximity sensor and was not in any time more than 0.5 cm. So it is safe to assume that *h* is zero and the block is just moving laterally.

4.4.2.2 Excitation

The first important feature of any modal analysis is its type i.e. Experimental Modal Analysis versus Operational Modal Analysis. With a number of exceptions, EMA versus OMA in most cases can be rephrased to forced versus ambient excitation. Forced

excitation means that an external studied and known source of excitation applies to a known degree of freedom in order to measure the structure's response. This excitation can be a single sinusoidal signal, a random white signal, hammer impact force or a known deflection and release. This type of analysis requires a controlled condition which is only applicable in laboratory. There are many examples of experimental modal analysis of a full size structure e.g. wing or fuselage of an airliner or a car. However, in case of very large structures e.g. civil structures, EMA is not applicable as it is practically impossible to measure the excitation force(s) and therefore operational modal analysis is the only option. Operational modal analysis is based on the ambient and operational forces that excite the structure. Wave, wind, traffic, running machineries are some examples of ambient forces. The key fact is that these forces are not measurable and the modal analysis is entirely based on output signals.

Setting up a known excitation force is almost always possible in the laboratory, as it is possible for the 3 m height frame structure in this study. However, the main goal here is to exercise operational modal analysis to study its pros and cons. To do this, the experiment is set up in a way that fairly resembles the operational condition on the platform. Besides waves, wind and other environmental sources of excitation, an operational jacket platform is subjected to dynamic excitations produced by rotating machineries on the deck. A rotating machine like pump rotates at a particular frequency, so its vibration excites the structure at the same frequency and also at its harmonics. The machine's gearbox is also rotating at few different frequencies. Permutation of these excitations from different machines can be used to perform operational modal analysis.

In this study, the effect of running machines on the deck is tried to be mimicked by shaking hanging masses on the deck. The upper deck consists of two concrete blocks, hanged and precisely leveled inside steel frames and can freely swing in a short span. Each block is attached to the vibrating shaft of the shaker, while the shaker itself is

attached to the deck. Figure 4.12 is showing the position of the two concrete blocks on the deck. Blocks are placed at two sides of the deck and perpendicular to each other, so that they can excite the model along X and Z axes as well as rotationally around Y axis. Each block is attached to the shaker's shaft as shown in Figure 4.13. A force transducer is measuring the interaction force between the shaker and the block. Shaker itself is fixed to the deck from underneath using screws.

Figure 4.12: Two concrete blocks located on top of the frame structure

4.4.2.3 Measurement

Referring to Table 4.1, frame structure has 48 degrees of freedom that need to be measured. The number of available accelerometers was 16 and apparently it was not possible to measure all 48 DOFs simultaneously. So the model was divided to four segments, the acceleration of DOFs at each floor was measured using 12 accelerometers and the whole model was measured by roving these accelerometers in four steps. Although the amplitude of the amplifiers were not changed during the test, but these four sets of measurements are not directly compatible. In case of modal identification

using frequency response function, the response is divided by input force which consequently normalizes measurements of all DOFs. However in case of output only modal identification, the input force is not available and so the relationship between the amplitude of different measurement sets are unknown. For this reason, at least one DOF must be measured in all the measurement sets as reference. In this case, two reference DOFs i.e. 15X (31) and 16Z (36) were selected and two extra accelerometers were used permanently to measure these two DOFs.

Figure 4.13: Close view of block-shaker configuration.

Figure 4.14 is showing three accelerometers connected to a node. They are measuring the response of the node in its local coordinate which will later be converted to global coordinate of the model.

Other than measuring the acceleration of the main body, four accelerometers were used to measure the acceleration of the concrete blocks and the DOF which shaker is

connected to (Figure 4.13). Although the location of the shaker is not listed as one of the main DOFs of the model, but these two DOFs are required for FRF based modal identification using ICATS. Two force transducers were also measuring the interaction between the concrete blocks and the deck which can be translated to the input force at those DOFs (Figure 4.13).

Figure 4.14: The accelerometers connected to a node in its three local axes.

4.4.2.4 Modal Testing

Herein, the general procedure of modal testing is described. The specific exercises of introducing damage and adding extra mass are described in their respective subchapters. Assuming that concrete blocks and shakers are installed and adjusted, modal testing begins with installing all the sensors to the model and connecting each sensor to a channel of data analyses. The data analyzer used in this study has 24 channels, so all the 18 accelerometers (12 main, 2 references, 2 shaker, and 2 blocks) and the two force transducers can be attached to it simultaneously. A laser proximity sensor was also

connected to the 21st channel to monitor the relative motion of the concrete blocks. However data of proximity sensors and the acceleration of the concrete blocks were not directly reported and used in the present study. Two amplifiers were also connected to output channel of data analyzer to receive the force signals, amplifying them and send them to the shakers.

The final setups are done using NvGate, the graphic user interface of OROS. It is definitely not so relevant to explain all the setups in detail, but few are worth mentioning. The sampling rate was set to 3200 S/s for the entire test. This is about 7 to 8 times larger than the sampling rate needed for the objectives of this study; however the extra data was produced in no cost and could be used in further studies.

A variety of signals were also tested i.e. random white and pink signals, sweep sinusoidal and step sinusoidal. However only the data of random signals are used and this study. The bandwidths of input signals were between 3 Hz to 1.25 kHz. The 3 Hz lower band was selected to pass the first three frequencies of concrete blocks (Table 4.2), considering that the model vibrates at around 4 Hz in its first mode. NvGate automatically calculates the bandwidth by dividing the sampling rate to 2.56, which is equal to 1.25 kHz. So the upper band of input signal is selected accordingly.

At the beginning, the 12 main accelerometers were attached to nodes 5 to 8 in the first floor. The responses of these four nodes under different types of excitation were recorded before they are roved to the upper floor. For instance, there are three recordings for each random signal. Once the model was excited using shaker-1, then shaker 2 and then both shakers were working together. The recording length for each excitation scenario was 60s. There were also other forms of excitations which were not

used in this study. Only after all the excitation scenarios were tested, the main accelerometers roved to the next floor.

4.4.3 Modal Identification

All the objectives of this study are based on output-only modal testing. The modal identification method that is used for this purpose is EFDD which is described in chapter 3.1.2. ARTeMIS uses this approach to identify modal properties from output-only data. The academic licence of ARTeMIS Extraction Pro 3.2 is used in this study to extract modal frequencies and mode shapes of the model.

Besides OMA which is the primary identification method, FRF based modal identification methods are also used in some cases to reconfirm the results of OMA. For this purpose, ICATS 2008 (imperial college) was used in this study to perform FRF based modal identification and normalization. Both software's are licensed to Department of Civil Engineering, University of Malaya. The results of these identification methods are presented in the next chapter.

Figure 4.15 is illustrating the modal identification methods that are used in this study. This flowchart is showing that modal identification techniques are divided into two category of finite element and experimental identification methods. FE identification method is divided to eigen analysis and dynamic analysis. Both experimental modal analysis and FE dynamic analysis are employing EMA and OMA identification methods as shown in the Figure. Step 5 in the flowchart is showing that the excitation force that was recorded during the test is in fact being used as input force for the FE dynamic analysis.

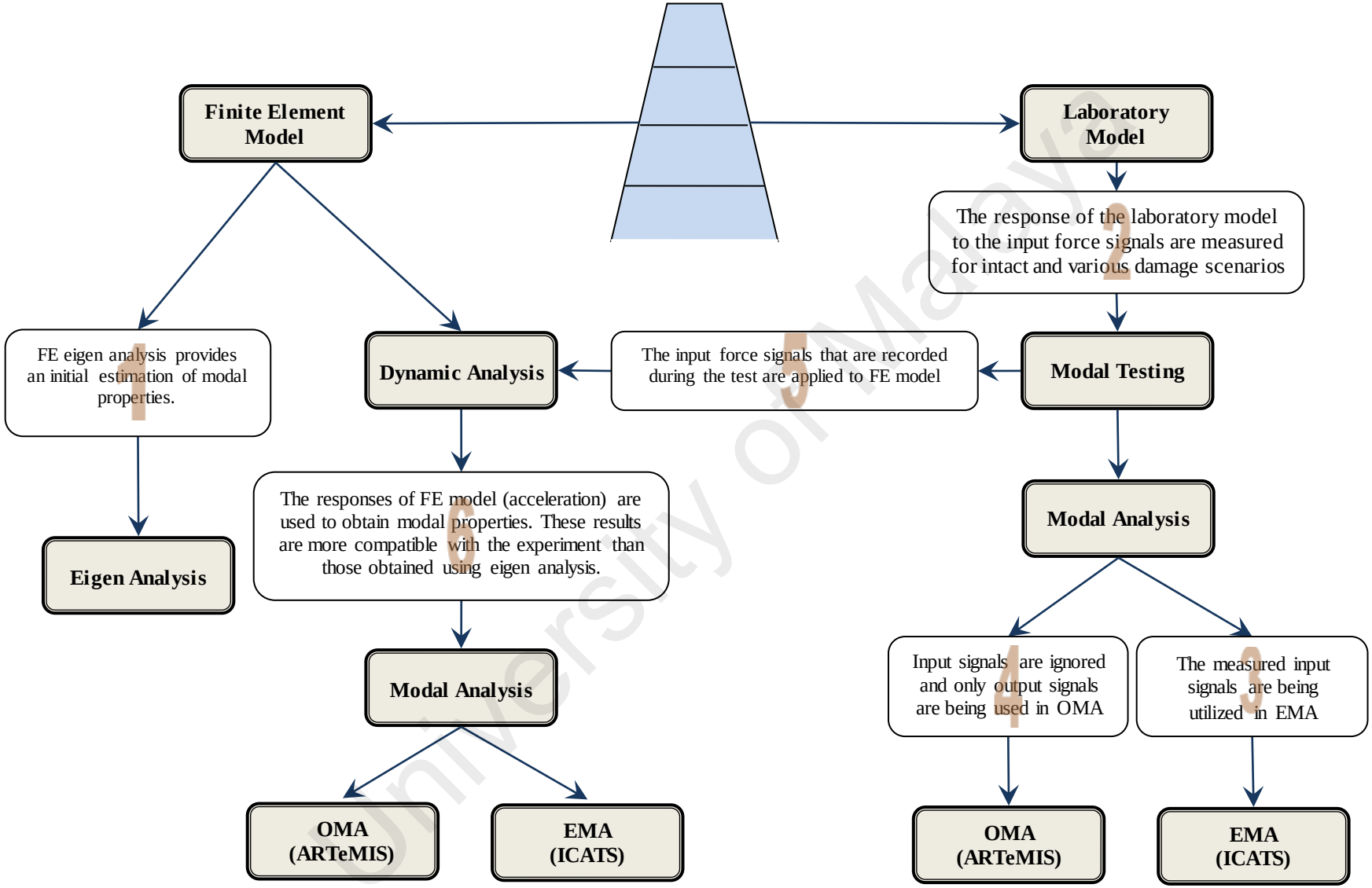

Figure 4.15: Flowchart of modal identification methods

4.5 Model Updating using CMCM

4.5.1 Complete Measurements

The background theory of CMCM model updating method is presented in chapter 3.2. This section describes how this method is implemented in particular case of this study. First, some positive and negative features of this method in respect to this case study need to be explained. CMCM method, like direct and iterative methods, is actually dealing with an optimisation problem. Although unlike iterative methods, it has the advantage of not requiring iteration and thus the computation time and possible of divergence are eliminated. Another important feature of this method is that the detected FE modes and experimental modes do not need to be paired. Moreover, those detected modes do not need to be scaled, neither relative to each other, nor to a property of the model e.g. mass (Hu, et al., 2007). However, this method has a significant limitation which is particularly a big concern in this case study and need to be addressed i.e. CMCM method cannot deal with incomplete mode shape. It should be noted that the main purpose of using this method in this study is to come up with a solution for damage detection when the lower DOFs of the frame structure are not experimentally measured.

Before dealing with the special case of model updating using incomplete mode shapes, let's begin with the case which mode shapes are complete. Equation 3.42 is the matrix form of Equation 3.41. Matrices C and E contain the stiffness and mass information and vectors α and β are containing stiffness and mass correction factors respectively. For simplicity, at first it is assumed that the mass matrix of the FE model and actual model are the same i.e. $M^*=M$. In this case Equation 3.42 is reduced to:

$$C\alpha = f \tag{4.3}$$

As mentioned above, in a simple form each element can be assumed to be updated by only one parameter. In case of stiffness, this parameter is the Young's Modulus of the member which is being corrected by α. This assumption can be close to reality in certain circumstances. For example if this method is being used for truss elements, this assumption can be used. Because truss is a single degree of freedom element (at each node) and has axial stiffness only. So either changing the size of the element or changing the Young's Modulus, both give the same result. On the other hand, beam elements have six degrees of freedom and in a simple form when only translational degrees of freedom are of interest, they are three DOFs elements. In this case, by changing only Young's Modulus the modification of axial and bending stiffness's are tight to each other and are changed all together. This could be acceptable, only if one is confident that the geometry of the element is correctly assumed and only material properties need to be modified.

4.5.2 Incomplete Measurements

The main purpose of employing model updating for this research is to come up with a solution for damage detection of frame structure when the entire mode shapes are not available. Although as mentioned before, one of the weaknesses of CMCM model updating method is that complete mode shapes are required. Considering this, it is important to come up with a practical solution to update the model using incomplete data.

By definition, every numerical modelling and prediction e.g. FE simulation is an idealized representation of reality. So they are not perfectly presenting the behaviour of the actual system which can be expressed as model uncertainty. Model uncertainty does not have one reason. In fact it has a number of types and sources which has been discussed in the work of many researchers such as (Der Kiureghian & Ditlevsen, 2009;

Kennedy & O'Hagan, 2001; Simoen, et al., 2015; Walker, et al., 2003). From these publications, model uncertainty can be summarized to three different types:

1- Model parameter uncertainty: This type of uncertainty is caused by inaccurate or uncertain parameters and inputs such as material properties, geometry, load characteristics, etc.

2- Model structure uncertainty: This type of uncertainty is the result of modelling simplifications and assumptions due to lack of knowledge or understanding of the true system. Simplifications of boundary conditions, governing physical equations and model order are few examples of this type of uncertainty.

3- Model code uncertainty: This type of uncertainty results from errors in the computer implementations and hardware and software errors. Nowadays this type of uncertainty is considered negligible compare to the other sources of error.

Other than these three uncertainty sources, there is another type of uncertainty which is related to the experimental data. This is not listed as one of the modelling errors above, because it does not act in any of the modelling stages, instead it acts during model updating process.

The proposed method here is addressing type-1 uncertainty which the modelling error is caused by material and physical properties of the members. It is based on the assumption that the modelling error in all the similar members i.e. beams and column, are more or less similar and by calculating the correction factor for a group of members, the rest can be updated accordingly and with an acceptable level of accuracy. This method also requires few iterations to give an acceptable estimation of updated model.

The main requirement of this method is to estimate paired modes in FE and experiment. This requires a precise simulation of the model to achieve as much compatibly as possible. It should be noted that only half of each detected mode shape is available from experiment which should be compared with the corresponding DOFs obtained from FE analysis. The other important point is that it is not really necessary to use higher modes, at least not for the first iteration, since it is more difficult to pair them.

As stated before, Equations 3.37 and 3.38 need complete mode shapes of FE and experiment i.e. ϕ and ϕ^*. All 48 DOFs are available in ϕ, but the first 12DOFs of ϕ^* are not estimated. In the first step, the missing DOFs of ϕ^* is filled with corresponding elements of ϕ as shown in Equations 4.4 and 4.5.

$$\phi = \begin{bmatrix} \varphi_1 \\ \vdots \\ \varphi_{48} \end{bmatrix} \tag{4.4}$$

$$\phi^* = \begin{bmatrix} \varphi_1 \\ \vdots \\ \varphi_{12} \\ \varphi^*_{13} \\ \vdots \\ \varphi^*_{48} \end{bmatrix} \tag{4.5}$$

The process of calculating the stiffness and mass correcting factors using ϕ and ϕ^* is the same as before, except that α is being calculated only for the upper half of the structure (B5 to B12 and C9 to C16). Since the size of similar members in this case study is the same, initially the same correcting factor can be used for similar members. In other cases, a combination of engineering judgment and try and error is needed to presume

correcting factors for the unmeasured members based on the correcting factors of measured members. This process needs to be repeated for few times until frequencies and available mode shapes converge.

4.5.3 Updating Stiffness and Mass Matrices

As explained before, there are a few ways to manipulate the stiffness of members in FE model. The easiest way is to change the Young's Modulus of each individual member. Although it is not very accurate since by changing Young's Modulus it is not possible to change axial and bending stiffness independently. So instead of material property, it is better to manipulate physical properties of each member. Figure 4.16 is showing the typical 6 degree of freedom beam element in the shape of a pipe that has been used in FE model together with its cross section. The physical properties of each member are the radius (r) and thickness (t) of the pipe. These are the two parameters that need to be changed in order to update the stiffness matrix of each member.

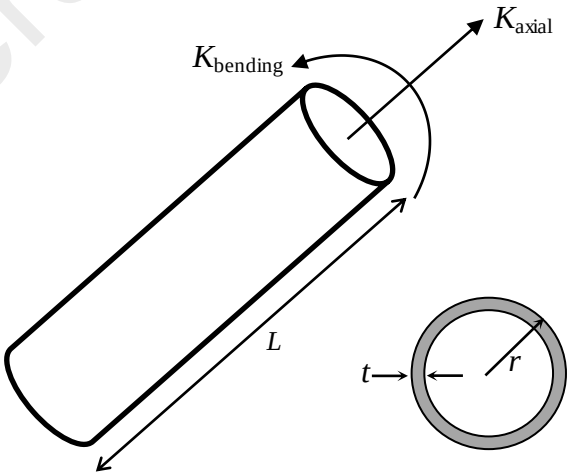

Figure 4.16: Schematic of a beam element with shape of a hollow pipe

The axial and bending stiffness in beam elements shown in Figure 4.16 are calculated using Equations 4.6 and 4.7

$$K_{axial} = \frac{EA}{L} \tag{4.6}$$

$$K_{bending} = \frac{12EI}{L^3} \tag{4.7}$$

where E is Young's Modulus, L is the length of the member, A is the cross section's area and I is the cross section's moment of inertia.

Figure 4.17 is presenting the stiffness matrix of a 6 DOF beam element based on its local coordinate i.e. the length of the beam is along X. In this matrix, DOFs 1, 2 and 3 are respectively corresponding to dX, dY and dZ of one end of the element and DOFs 4, 5 and 6 are for the other end with the same sequence. The reason why angular DOFs are not included in this matrix is that those DOFs are not measured in the experiment.

	1	2	3	4	5	6
1	$\frac{EA}{L}$	0	0	$-\frac{EA}{L}$	0	0
2	0	$\frac{12EI}{L^3}$	0	0	$-\frac{12EI}{L^3}$	0
3	0	0	$\frac{12EI}{L^3}$	0	0	$-\frac{12EI}{L^3}$
4	$-\frac{EA}{L}$	0	0	$\frac{EA}{L}$	0	0
5	0	$-\frac{12EI}{L^3}$	0	0	$\frac{12EI}{L^3}$	0
6	0	0	$-\frac{12EI}{L^3}$	0	0	$\frac{12EI}{L^3}$

Figure 4.17: Stiffness matrix of a 6 DOF beam element

It was stated that the stiffness matrix of each member is being corrected separately for each axis. So matrix K_n in Equation 3.37 only contains two rows and column of Figure 4.17 in each step i.e. 1 and 4 for axial stiffness, 2 and 5 for bending along Y and 3 and 6 for bending along Z. This results three separate correction factors for each member named α_a, α_{by} and α_{bz} respectively. Since the cross section of the members are circular which is symmetric along Y and Z axes, the bending stiffness along Y and Z are always the same and so α_{by} and α_{bz} cannot be used independently. So with the condition of α_{by} and α_{bz} not being significantly different, their average (α_b) may be used to correct bending stiffness of both directions, otherwise the cross section of that particular member must be changed to provide different stiffness along Y and Z axes. When correcting factors were determined, the corrected stiffness of n^{th} member can then be calculated using Equations 4.8 and 4.9

$$K'_{a,n} = K_{a,n}\alpha_{a,n} \tag{4.8}$$

$$K'_{b,n} = K_{b,n}\alpha_{b,n} \tag{4.9}$$

where K and K' are indicating the original and corrected values of stiffness respectively. Now with corrected axial and bending stiffness of the member being available, the physical properties of the member need to be updated. To do so, Equations 4.6 and 4.7 need to be written in terms of the section's physical properties i.e. r and t:

$$K'_a = \frac{EA}{L} = \frac{E\pi(r_o^2 - r_i^2)}{L} \tag{4.10}$$

$$K'_b = \frac{12EI}{L^3} = \frac{3E\pi(r_o^4 - r_i^4)}{L^3} \tag{4.11}$$

where r_o and r_i are outside and inside radius of the pipe respectively. The length and Young's Modulus of the member are known. So providing three additional conditions i.e. $r_o > 0$, $r_i > 0$ and $(r_o - r_i) > 0$, the corrected values of r_o and r_i can be calculated using the following system of nonlinear equations:

$$\begin{cases} (r_o^2 - r_i^2) = \dfrac{K_a' L}{\pi E} \\ (r_o^4 - r_i^4) = \dfrac{K_b' L^3}{3\pi E} \end{cases} \tag{4.12}$$

It should be noted that basically there is an easier way to introduce physical properties to DIANA. This is by introducing the cross section area, *A*, and area moment of inertia *I* directly, without having to set the size of the pipe. It is definitely much easier to calculate *A* and *I* using Equations 4.10 and 4.11 directly. Although the problem is that regardless of the assumption, beam elements in FE analysis are still 12 DOF elements so angular properties of the beam elements should also be introduced for each member. It must be reminded that angular properties of elements has always been and should have been part of the FE analysis. Because regardless of their DOFs being measured or not, they are naturally acting in the actual model too. However since their corresponding DOFs are not being measured, it is not possible to directly update angular properties of the elements. So it is more practical to estimate the size of the pipe using updated *A* and *I* and use it as physical properties and let the software calculate the rest of the information it needs based on them.

The FE model is then updated using the corrected physical properties of all members. Since the stiffness correction is performed by changing the dimensions of the members, this process alters the mass matrix as well. That is why it is better to update stiffness matrix before mass matrix and it needs to be reminded that the new version of mass

matrix should be corrected. Correction of mass matrix is much simpler than stiffness matrix since only one correcting factor is needed for each member which is applied to the member's mass density. The rest of the procedure is similar to what has been explained for correcting stiffness matrix.

The last thing that needs to be pointed out is the method of obtaining stiffness and mass matrices. It is possible to extract the global stiffness and mass matrices of the structure from FE model. However it does not provide the matrices of each individual member. So K_n and M_n have to be assembling using MATLAB. To make sure this manually assembled local matrix matches FE outputs, the global stiffness and mass matrices are also manually assembled and compared with FE results. For simplicity, the mass matrix in FE analysis is set to "lumped mass" to make it easier to reconstruct. After comparing the two results, the maximum difference between the two matrices were found to be very minimal. So it is safe to use manually obtained local matrices against FE generated global matrices. In case the difference is found to be significant, the proposed solution is to calculate the error individually for each DOF and scale the corresponding DOF of local matrix accordingly. The calculated local matrix can then be used against FE generated global matrix.

Figure 4.18 is illustrating the cross model cross mode model updating method in a simple flowchart form. It clarifies the role of each modal identification method in the process of model updating. As presented in the flowcharts, only the OMA identified modes are employing in this method while FE eigen analysis is only used to extract full rank stiffness and mass matrices.

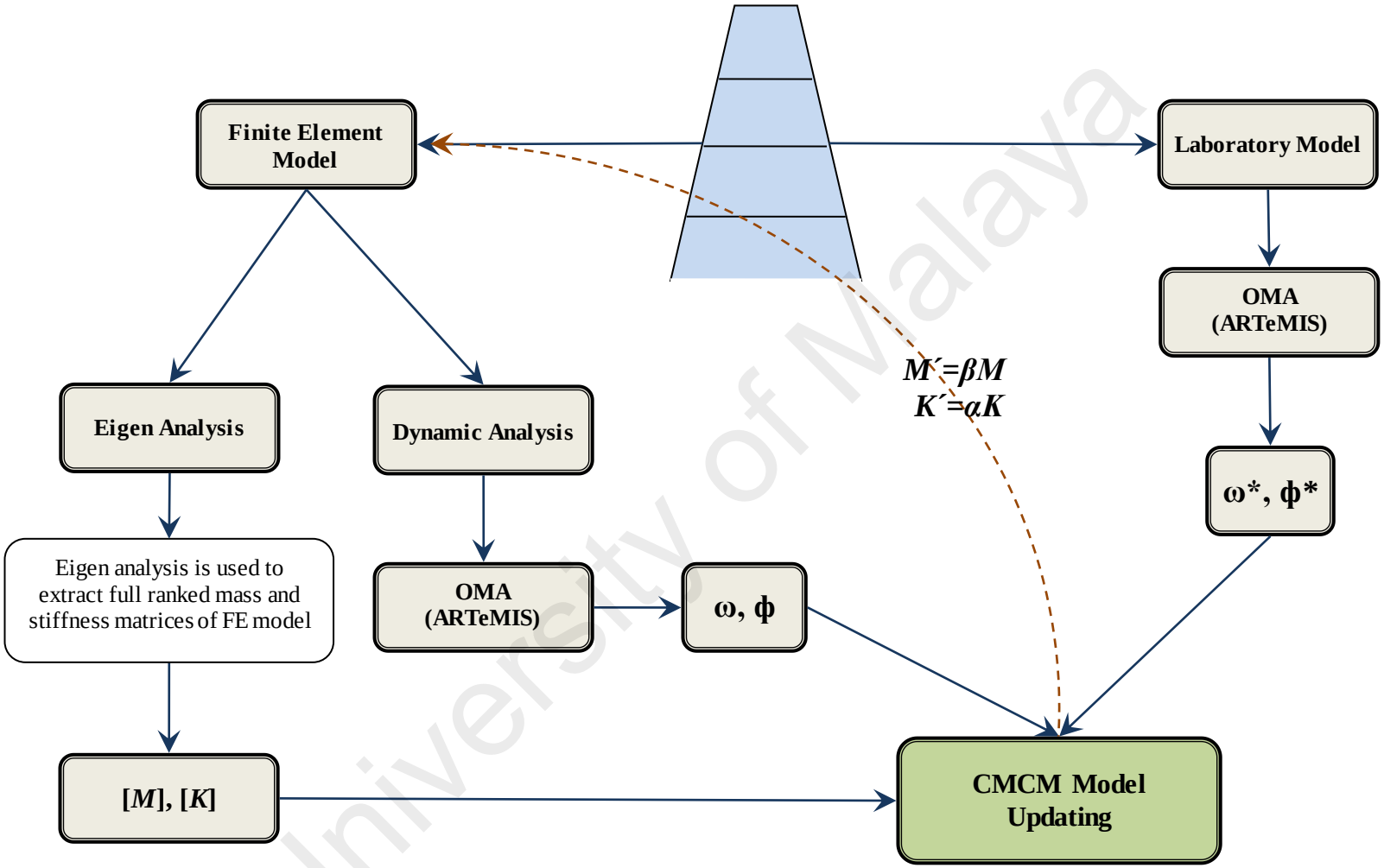

Figure 4.18: Flowchart of CMCM model updating method

4.6 Mass Normalization

The theory behind mass normalization using change in mass is described in chapter 3.3.2. In this chapter, the implementation of the method is presented.

One important factor is the mass change ratio i.e. the ratio of added mass to the mass of the structure. As mentioned in the theory of this method, the important assumption is the similarity of the mode shapes before and after mass modification. If the mass change ratio is so large, it changes the mode shapes significantly. On the other hand small mass change ratio might not affect the modal frequencies at all. So it is important to keep this ratio at its optimum level. (Hout & Avitabile, 2004) are suggesting the ratio of 5% for the best results.

The other important factors in mode shape scaling by change in mass is the position and distribution which the extra mass is added and/or shifted. While adding mass to a certain DOF can alter modal frequencies and mode shapes in certain modes, it might not affect some other modes significantly. There are few ways to assess the sensitivity of a mode shape to mass change in a particular DOF. For example (Parloo, et al., 2002) are presenting a method which not only the sensitivity of a mode in mass change is calculated, but the sensitivity of each DOFs of the mode is also elaborated. The important point is that in this method, mode shapes need to be properly scaled in order to calculate the sensitivity of mass change in modes.

To set up a mode scaling procedure using change in mass, it is quite important to have an initial estimation of the location of extra masses. The optimum position of mass in terms of their participation on the mode shape is entirely governed by the mode shapes themselves. Generally speaking, if a lumped mass is added to the "node" DOF of a mode shape, it causes minimum or no effect on that particular mode while if it is added

to an anti-node, the effect on the modal frequency and mode shape is utmost. Obviously adding mass to only one degree of freedom does not affect all the desired modes at the same level. Although if the location of the lumped mass is selected right, it can affect most or all desire mode shapes to a level which is required for mass normalization.

Based on some experimental limits e.g. a device occupies a joint, which can also be the case in a real platform, four joints has been selected as desire points to add mass. Nodes 14, 16, 18 and 20 (Figure 4.19) are labeled as points A, B, C and D consequently and any mass placed on any of these 4 nodes is denoted with the same letter. Initially, total of 10 mass change scenarios has been tested as follow:

a) Unmodified: The modal properties of the structure without any additional mass are elaborated which is denoted by letter "*U*"

b) Single point modification: 10 kg weight (approximately 3% of the structure's mass) is placed on points A to D separately which are denoted by the same letter and results in 4 separate cases.

c) Dual point modification: 2×10 kg weights (approximately 6% of the structure's mass) are simultaneously placed on points A to D which results in 6 different cases e.g. "AC" denotes that masses are simultaneously added to points A and C.

To study the optimum mass change modification for mass normalization, two finite element analyses has been carried out. First is FE eigen analysis which calculates modal frequencies and mass normalized mode shapes directly from mass and stiffness matrices. The existence of mass matrix and consequently mass normalized mode shapes provides an accurate reference to assess the accuracy of the scaling factor calculated by

each mass scenario. Basically, what eigen analysis provides are modal data which are ideal in any aspect. Calculated modal frequencies and mode shapes in eigen analysis are exact (regardless of whether or not they are in agreement with the experimental results) and so one can solely study the effectiveness of mass change scenario without having to consider the effects of measurement and identification errors which are existed in experimental results.

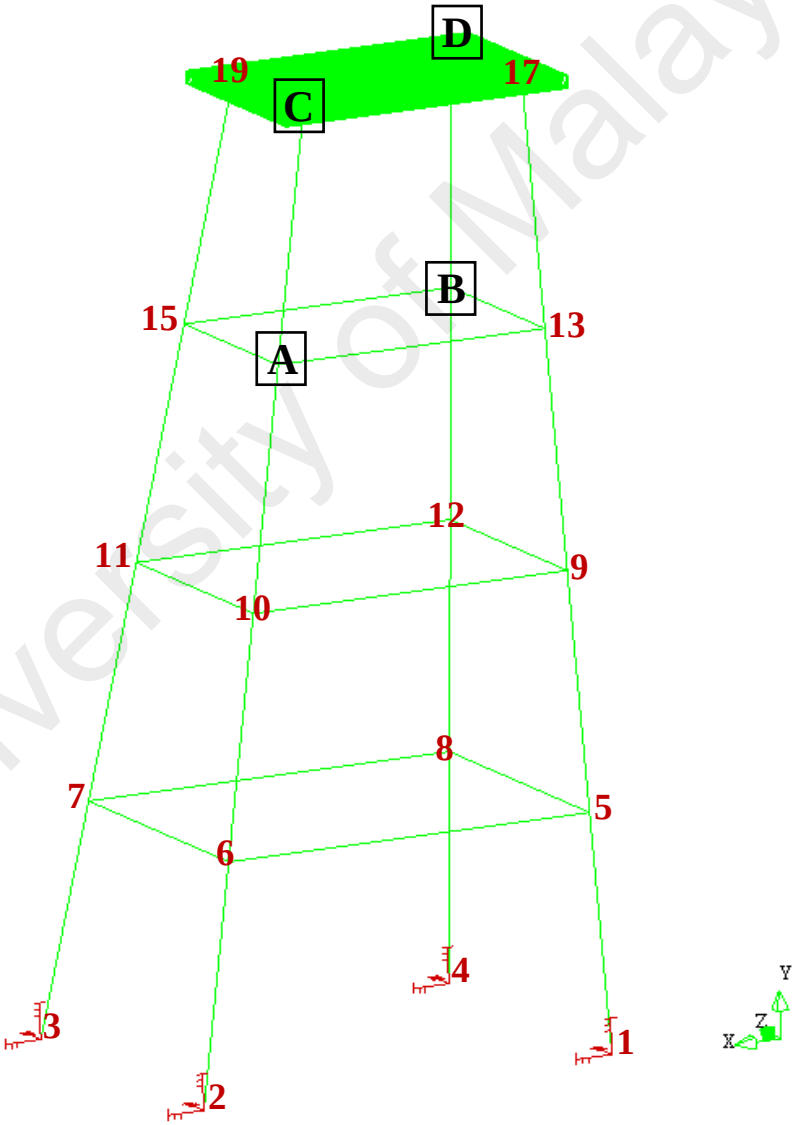

Figure 4.19: The location of external weights on the frame structure

FE dynamic analysis is used to mediate between the "perfection" of eigen analysis and "flaws" of experimental results. In FE eigen analysis, both measurement and modal identification are exact and free of systematic errors (although in FE eigen analysis, there is no actual measurement stage and it is all modal identification). On the other hand, Experimental modal testing suffers from error in both measurement and modal identification. In FE dynamic analysis however, the measurement stage is similar to eigen analysis and free of systematic errors while modal identification procedure is similar to the experiment.

FE dynamic analysis is the numerical replication of the experiments set up and test. Unlike FE eigen analysis, the modal frequencies and mode shapes in FE dynamic analysis are not numerically derived from mass and stiffness matrices. Instead, they are estimated using the response of the FE model to the applied dynamic loads, similar to what is done in modal testing. Dynamic input forces, the exact same force that has been measured during the experiment, are applied to the same DOFs of the finite element model. A nonlinear dynamic analysis calculates the response of the model in terms of acceleration in every time step which is equivalent of the sampling intervals. The measured response of the FE model is then used to determine the modal properties of the model, using similar method as the experimental data.

In the first step, FE eigen analysis is used to assess the effectiveness of the method. To do so, modal frequencies and mass normalized mode shapes of FE model are calculated for unmodified and all 10 mass scenarios using eigen analysis. The scaling factor of each mode and each scenario is then calculated using Equation 3.57.

Equation 4.13 is presenting the relationship between mass normalized mode shape (Φ) and the same mode shape, scaled to unity (Ψ), with scaling factor (α).

$$\Phi = \alpha\Psi \tag{4.13}$$

$$\Psi\Psi^T = 1$$

In general, the goal of mass normalization is to elaborate α in order to calculate Φ from Ψ, mentioning that any arbitrary mode shape can be scaled to Ψ. However in this case, since the goal is to check the results of mass normalization method, the procedure is reversed. Eigen analysis numerically calculates the precise mass normalized mode shapes. Therefore, the exact value of scaling factor can be calculated using Equation 4.14.

$$\alpha_{exact} = \sqrt{\Phi\Phi^T} \tag{4.14}$$

The same mass normalized mode shapes can be scaled to Ψ to calculate the scaling factor (α) using Equation 3.57, which is then compared with α_{exact} to evaluate its accuracy.

The next step is to evaluate the mass normalization results of FE dynamic analysis. The procedure of calculating scaling factor is exactly the same as for FE eigen analysis, except that the exact value is not available in this case. Instead, the estimated scaling factors of each mass scenario are compared with each other and also with the scaling factor that is calculated using FRF data, which in principle is more reliable and accurate. Using the results of FE eigen analysis and FE dynamic analysis, the best mass scenarios are selected and used in the experiment. Figure 4.20 is illustrating the mass normalized method using change in mass in the flowchart form.

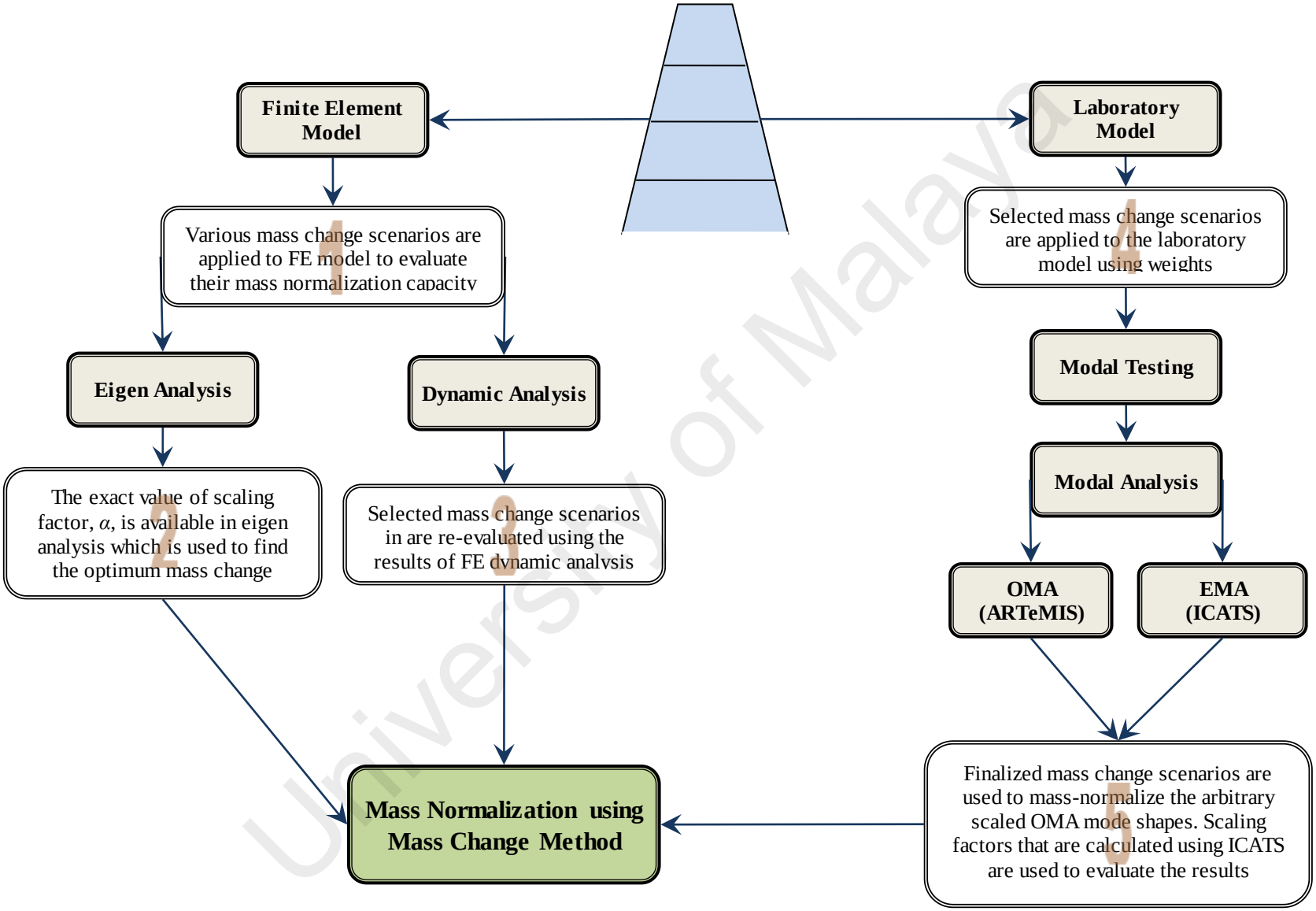

Figure 4.20: Flowchart of mass normalization method

4.7 Damage Detection and Localization

4.7.1 Damage Scenarios

Before getting to the details of damage scenarios, it is important to define terms "undamaged state" and "damaged state" clearly. An important assumption of this study is linearity. It assumes that the system remains linear throughout the test i.e. mass and stiffness matrices are constant. Although damage in this case is defined as change of stiffness (more correctly loose of stiffness) in one or more of the members which consequently alters the global stiffness matrix. So how is this definition consistent with linearity assumption? The answer is that the structure is not being seen as one nonlinear system, but instead as two different linear systems with similar mass matrices and different stiffness matrices and in fact it is required for each of the damaged states of the structure to be linear.

The other important assumption is that the stiffness matrices' difference is not due to geometrical changes; instead it is due to change in the stiffness of one or more members, either physically e.g. crack, or materially e.g. corrosion. It is not even necessarily loose of stiffness; it can be gain of stiffness by welding a crack. By this definition, damaged and undamaged states are totally relative. Undamaged is considered as "before the change" state and damaged is "after the change" state. So what is called undamaged structure here is not at all equivalent to intact structure. The intact model was incised and welded back a few times for other parts of the project. So if the original intact structure always be considered as "Undamaged state", the error of cutting and welding the members accumulates and eventually become significant. The solution is to repeatedly update the undamaged state to minimize this error.

Figure 4.1 is showing the numbering of columns and beams of the frame structure. Damages are introduced to the structure by incising one or few of these members using

a mini-cutter. In each case damages can be fixed by welding the damaged member, considering that the modal parameters of repaired structure might be slightly different from the original undamaged structure and need to be tested again. So to minimize the number of repairs and tests, damages are applied one after the other and then fixed one after the other. Table 4.3 is presenting damage scenarios in detail. As it shows, the test begins with case U1 which represents intact structure. Then a number of damages were introduced and fixed until all the members are welded back again. This stage of the structure is called U2. The same procedure of damaging and fixing produces few more damage cases until the structure is entirely fixed again, which is called U3. As presented in Table 4.3, total of 10 damage scenarios was produced and in each case, the reference case is show in the last column.

Table 4.3: Description of damage scenarios (refer to Appendix II for illustration)

Damage case	Damaged member(s)	Description	Reference
U1	-	Model is intact	-
D1	C5	C5 is incised in the middle	U1
D2	C2 - C5	**D1 +** C2 is incised below node 6	U1
D3	C2 - C5 - B5	**D2 +** B5 is incised at node 9	U1/U2
D4	C2 - B5	**D3 -** C5 is welded	U2
D5	B5	**D4 -** C2 is welded	U2
U2	-	**D5 -** B5 is welded	-
D6	B3	**U2 +** B3 is incised at node 8	U2
D7	B3 - B6	**D6 +** B6 is incised close to node 10	U2
D8	C5 - B3 - B6	**D7 +** C5 is incised in the middle	U2/U3
D9	C5 - B6	**D8 -** B3 is welded	U3
D10	B6	**D9 -** C5 is welded	U3
U3	-	All members are welded	-

4.7.2 Damage Locating Vectors

The theory of damage locating vector is presented in chapter 3.4 . In this section, the process of applying the method for this study is described. As the first step, the modal flexibility matrices of undamaged and damaged scenarios need to be calculated using Equation 3.68. In this Equation, modal frequencies and mass normalized mode shapes are the requirements. The mass normalization method is described in chapter 4.6 and its results are going to be discussed later in Chapter 5. So let's just assume that a few numbers of modes are identified and their mode shapes are scaled with an acceptable accuracy. With this assumption, using DLV involves a number of steps as follow:

i. Obtaining modal flexibility matrices

It was mentioned before that flexibility matrix is global, so Equation 3.68 converges using global mode shapes i.e. lower frequencies. In other word, only the first few modes are required to estimate the modal flexibility matrix and existence of higher modes only increase the accuracy of the matrix. In this case, modal flexibility matrices were calculated using different number of modes i.e. 6, 9 and 12 modes. However, the core of the study is based on the modal flexibility matrices that are calculated using the first 9 modes. Assuming that 9 modes are available, matrix $[\Phi]_{48\times 9}$ in Equation 3.68 has 48 rows corresponding to DOFs and 9 columns corresponding to mode shapes. The dimension of eigenvalue matrix is equal to the number of available modes and so $[\Lambda]^{-1}$ is a 9×9 matrix. This shows that regardless of the number of available modes, the calculated flexibility matrix in Equation 3.68 is always 48×48.

ii. Calculating SVD of flexibility change matrix

The flexibility change matrix is $[\Delta G]_{48\times48} = [G_D] - [G_U]$. The singular value decomposition of $[\Delta G]$ was calculated using MATLAB and the result of this operation were matrices $[U]$, $[S]$ and $[V]^T$. Matrix $U_{48\times48}$ is not of interest. Matrix $S_{48\times48}$ is a diagonal matrix that contains singular values. Matrix $V_{48\times48}$ is an orthogonal matrix which its columns are either vectors of raw space or null space. Ideally, the locating vectors are those columns of V that are associated with singular values of zero. However the singular values are not exactly zero in practice and so a criterion is needed to decide on which columns of V are DLVs.

iii. Selecting DLVs

To select which vectors of $[V]$ are DLVs, first all 48 vectors must be applied to the undamaged model. To do this, the entries of each vector were applied as a force to its associated DOF in FE model. This resulted on 48 different FE models which every one of them were subjected to 48 point forces. By performing a linear static analysis for each model, the characterizing stresses of all 28 members were computed. With these results and using a series of operations that was described in chapter 3.4, the *svn* index was calculated for each vector. Load vectors with $svn \leq 0.2$ were selected as DLV.

Although this is the standard procedure of finding DLVs, but it should be emphasised that this procedure is very difficult and time consuming in practice, particularly in case of this study. The number of DOFs (sensor locations) and consequently the number of load vectors in this study is relatively large and having to run 48 FE analyses just to select DLVs among them does not seem to be practical. Fortunately, it is not at all

necessary to apply all load vectors in practice, at least not in this case. As mentioned before, DLVs are those vectors that are associated with very small or zero singular values. So the best was of evaluating the load vectors is to calculate *svn* of those vectors associated with the lowest singular values until it hits the cut-off values. Although not impossible, but it is very unlikely that one of the load vectors with higher singular value results on *svn* lower that the cut off value. So it is not necessary to evaluate those load vectors. In case of this study, always the 10^{th} to 15^{th} last load vectors out of 48 were considered as DLVs.

iv. Calculating WSI as damage indicator

Ideally, the damaged member can be located using only one DLV. All it takes is to analyze the model under its loading and to find the member with zero or negligible characterizing stress. Although in reality the calculated DLVs are not so perfect. Weighted stress index (*WSI*) combines the information from multiple DLVs in a way that introduces additional robustness into the technique.

Weighted stress index (*WSI*) of each member were calculated using Equation 3.81. For example, imagine that 10 load vectors were selected as DLVs and the *WSI* index of column C5 was being calculated. The first step is to calculate the *nsi* indices of column C5 for all 10 DLVs. In each case, the calculated *nsi* were normalized by *svn* value of its associated DLV. *WSI* is simply the average of all 10 normalized *nsi* values of column C5. The *WSI* of all beams and columns were similarly calculated. Any member with *WSI* index below 1 is considered as damaged member. Figure 4.21 is illustrating the method of employing damage locating vector in the flowchart form.

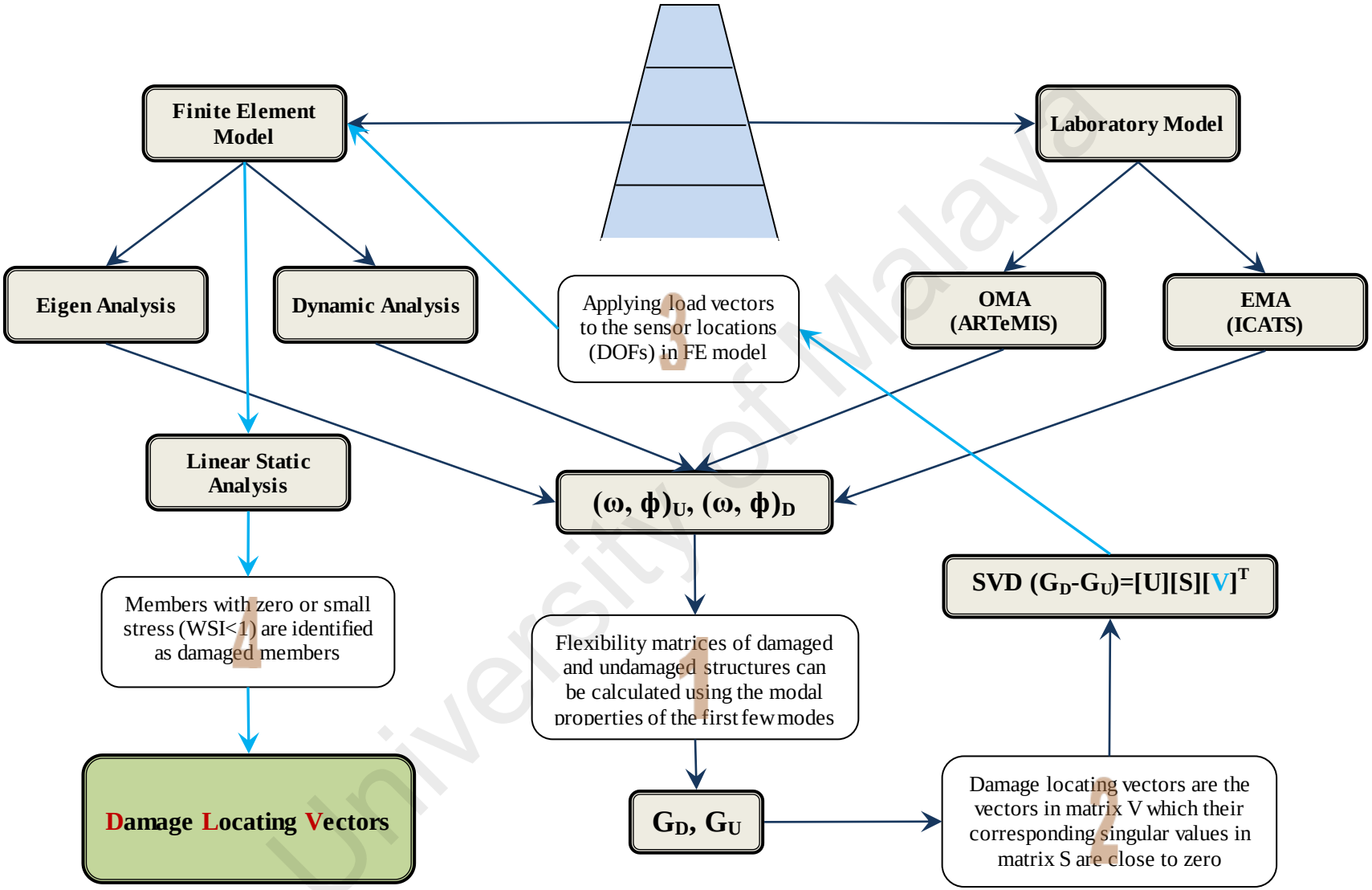

Figure 4.21: Flowchart of damage detection using damage locating vector

4.7.3 Damage Detection using Incomplete Measurements

4.7.3.1 Overview

One of the first steps in structural analysis is dividing the model into smaller components i.e. elements to do numerical modelling and analysis. Choosing the number, size and type of these elements in different parts of the structure is a decision that one must take based on type of the structure, type and purpose of the structural analysis, the capability of the available hardware and software etc. This process which can be referred to as "meshing" is determining the number of nodes and DOFs and consequently the dimension of mass, stiffness and damping matrices. When it comes to experimental modal analysis, modelling the structure with fine meshing and large number of DOFs is not really applicable. That is because the number of sensors are limited which governs the number of nodes and DOFs. The bottom line is that in general, it is unnecessary and pointless to introduce DOFs and to expand the size of structural matrices without measuring them all. If one is decided to divide a beam into 60 nodes, but can only measure 20 of them, this fine meshing is pointless and the size of the model must be reduced to 20 DOFs.

Sometimes the structure itself imposes a minimum number of elements and DOFs that should be assigned. For example in frame and truss structures, the number of joints is usually the minimum number of nodes that are assigned in modelling. That is the case where certain nodes and DOFs must be assigned regardless of whether they can be measured or not. There might also be some other valid reasons to introduce DOFs that cannot be measured. This is how the term "incomplete measurement" is defined; the nodes and DOFs those are assigned for a legitimate reason, but cannot be experimentally measured. In a jacket structure for example where parts of the structure is under water, it is obviously very difficult to measure underwater DOFs.

The review of former studies on this subject was presented in CHAPTER 2:. Despite of their interesting approaches and promising results, it is rather apparent that not every method is necessary suitable for every problem. Particularly in this case, due to the complex geometry of the frame structure, these methods are not entirely applicable to address incomplete measurement problem. Nonetheless, this study proposed a simple and handy technique to estimate the location of damaged member of a frame structure using incomplete measurements.

4.7.3.2 Frequency Shift Vectors

It is known that incomplete measurements do not affect the estimation of modal frequencies. A solo sensor in the right location can fairly measure all the modal frequencies of the structure. Incomplete measurements result on incomplete mode shapes which consequently affects the assessment of modal flexibility matrix. The core damage localization of this study i.e. DLV is entirely based on the modal flexibility matrix. So if some DOFs are missing from flexibility matrix, it makes DLV insensitive to damaged members associated to those DOFs. The detail of how the missing DOFs are affecting DLV is discussed in chapter 5.6.2 based on the results. Briefly, when the missing DOFs are in a specific part of the frame structure e.g. all the nodes in first floor, DLV is unable to evaluate members that are attached to those DOFs. However, if the damaged member is a column, it is at least able to identify the foot (not the exact member) which is involved in damage, only if the two end of the foot are measured or known (supports). Damaged members that are not associated to unmeasured DOFs can still be detected by DLV in an incomplete measurement. So in such case, DLV can partially evaluate the damage scenario of the frame structure. Although the absent or uncertain part of its results need to be cover with another detection method.

To do this, a frequency based method is proposed to provide additional information to identify possible damaged members located in unmeasured part of the structure. This method, in general, is based on studying the frequency shifts of updated FE model caused by known damage cases and comparing them with the experimental frequency shift caused by unknown damage scenario. With a methodical comparison, it is possible to approximation the damaged member with a reasonable level of confident.

To explain the method, let's use a hypothetical frame structure with a number of unmeasured DOFs. Let's assume that the unmeasured DOFs are associated with 5 members, m1 to m5. Unmeasured member is defined as a member which either one end or both ends of it are linked to an unmeasured node. Furthermore, unmeasured node here is defined as a node which none of its DOFs are measured. This hypothetical structure is subjected to an unknown damage scenario, *D*. The first 10 modal frequencies and mode shapes of the model are estimated experimentally for undamaged and damage cases. Apparently, only measured DOFs are presented in mode shape vectors and consequently in modal flexibility matrices. As mentioned, these incomplete modal flexibility matrices can still be used to calculate DLVs, but since no DLV is calculated for missing DOFs, the calculated *WSI* indexes of m1 to m5 are not reliable. However, the estimated *WSI* of other members are reliable and can be used to evaluate their condition.

In case which the damaged member in damage case *D* is one of the measured members, it can be identified using DLV. Although if one of the unmeasured members are involved, DLV is unable to detect it. Even if DLV identifies one of the measured members as damaged, there is a chance that *D* is a multiple damage case and unmeasured members are contributing to it as well. So regardless of the results of DLV,

damage case *D* cannot be certainly determined without the knowledge of unmeasured members.

The first step to check the possible contribution of unmeasured members in *D* is to simulate five damage scenarios d1 to d5 by reducing the stiffness of m1 to m5 respectively in updated FE model. The level of stiffness reduction should be set in a way that the overall frequency shifts in FE results do not be significantly different from those obtained in the experiment. In other word, the damage severity in FE should not be extensively different from the actual case; however the tolerance is fairly high. This can be achieved by a number of tries and errors.

The modal frequencies of intact FE model and d1 to d5 are then estimated using FE dynamic analysis. It should be reminded that the FE model is updated, so the modal frequencies of undamaged FE and experimental models are adequately similar. The proportion of the frequency shifts relative to undamaged cases are then calculated for d1 to d5 as well as for *D* and are named fs1 to fs5 and FS, respectively.

Let's imagine that m2 is the sole unknown damaged member which means m2 is responsible for FS. Since FE model is updated, the frequency shifts caused by d2 are supposed to be similar to the frequency shifts caused by *D*, i.e. FS = fs2. However this statement is extremely ideal. The detected modal frequencies in both FE and experiment are not totally accurate. Although FE model is updated, but there is always a level of error in any simulation. The position and magnitude of stiffness reduction in FE is just an approximation of the unknown damage case. All these factors and many more are the reason why the frequency shifts in FE and experiment are never the same.

Although the similarity of the two frequency shift vectors is not possible, but there is a valid question; is there any meaningful relationship between the two vectors? Because if

such relationship can be evaluated, it can be used as an indicator to locate the damaged member.

4.7.3.3 Assessing the Relationship between FS and fs2

The definition of relationship and association and their difference is presented in appendix I. Based on that definition, the aim is to find a causal relationship between FS and fs2. The simplest way of assessing the relationship between two variables is by calculating their Pearson's correlation. So in case there is a relationship between FS and fs2, their correlation coefficient must be significant. This is absolutely true, but correlation coefficient is unable to find an exclusive relationship between the two variables. The reason, as was explained before, is that it is very possible for fs1 to fs5 to be moderately or even highly correlated with each other. This makes fs2 a "cofounding variable" between them and FS. So all these variables would have some level of correlation with FS and fs2 cannot be identified. The method of identifying cofounding variables using multiple linear regression is described in chapter 0. This approach is used here to distinguish between the causal relationship of fs2 and FS and the association of other possible correlated variables.

Smart-PLS statistical software is used to calculate the linear regression coefficients. This software does structural equation modelling (SEM) using partial least square regression analysis (PLS). Structural equation modelling is a method of fitting a network of variables to data. This software is a powerful statistical tool which is very famous in the area of social science (Hair Jr, Hult, Ringle, & Sarstedt, 2016). Smart-PLS is capable of fitting a large number of variables with very complex relationships. However in case of this study, it was just used as a calculator to do very simple multiple linear regression analysis. The Flowchart in Figure 4.22 is showing the method of using frequency shift to detect damage in unmeasured part of the structure.

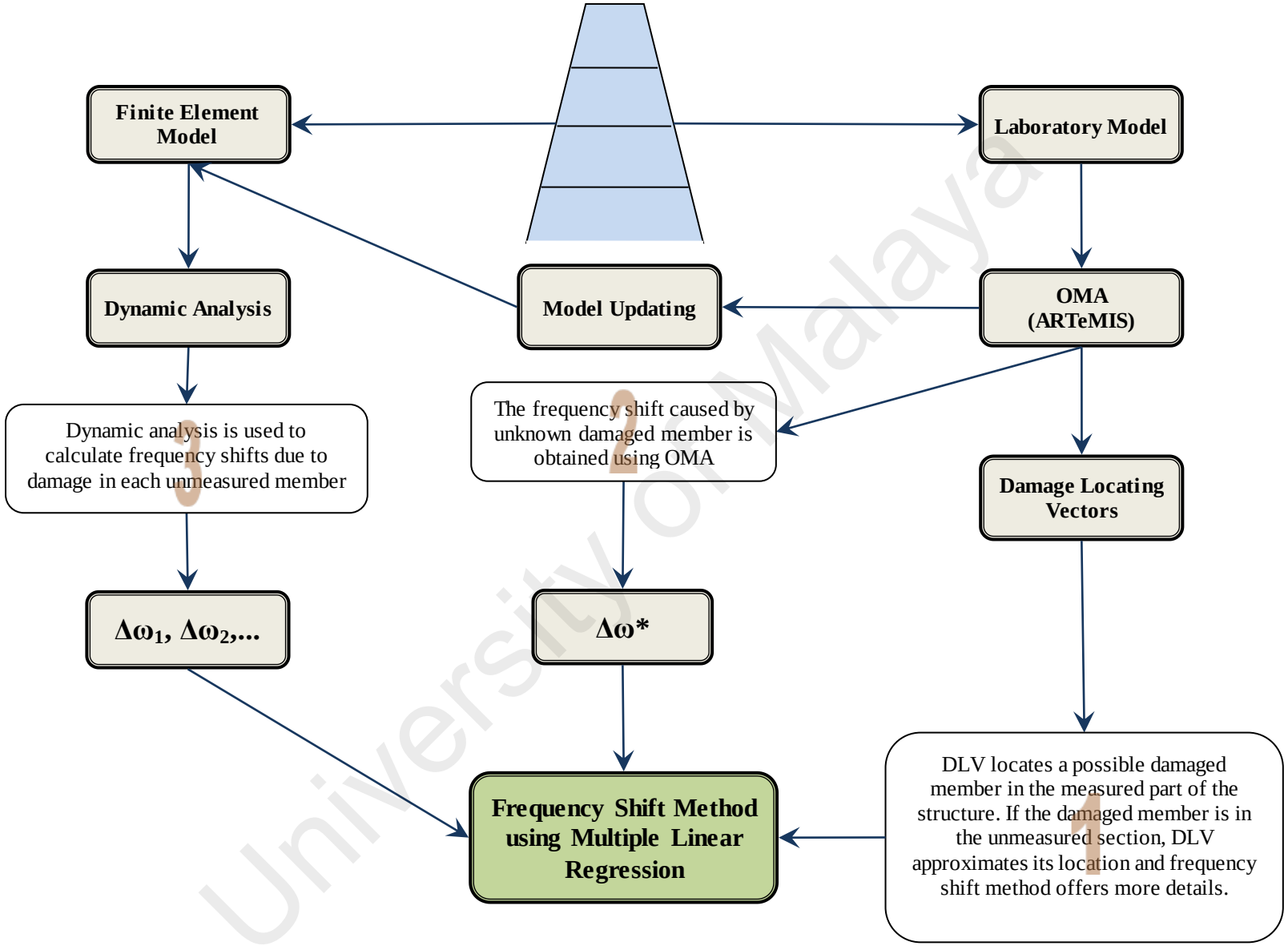

Figure 4.22: Flowchart of damage detection using frequency shift method

CHAPTER 5: RESULTS AND DISCUSSION

5.1 Overview

This chapter includes presentation and discussion of the results of this study. For most cases, the methods of obtaining the results e.g. measurements, analyses, calculations etc. and also the theories that have been used are presented

The chapter contains four main topics:

i. The first topic discusses about the results of mass normalization using mass change method. This subchapter has two objectives. First is to verify the results of this mass normalization method and to propose a technique to assess the accuracy and reliability of its findings. For this purpose, numerically generated data are used to study the relationship between mode shapes correlation, frequency shifts and estimated scaling factors. The second is to apply this method for mass normalization of experimental mode shapes. The results are then being used in other parts of the study.

ii. The second topic of this chapter includes the results of model updating. Model updating is about utilizing experimental data to update the numerical FE model to acquire maximum similarity between reality and simulation. The primary purpose of using model updating in this study was its necessity for the proposed damage detection method that uses incomplete measurements. However, it was also used as a standalone detection method which enhances the reliability of damage locating vectors.

iii. The third topic discusses about the results of "Damage Locating Vectors". The method is applied to 10 damage scenarios to evaluate its ability to detect damaged member in different circumstances. Three different sets of data are used for this purpose. First are the results of FE eigen analysis. The mode shapes in eigen analysis are numerically scaled, so its results are used as benchmark. The second sets of data are obtained using FE dynamic analysis. This method benefits from the ideal measurements similar to eigen analysis, but its modal identification and scaling processes are similar to the experimental modal analysis. So it mediates between FE eigen analysis and the experiment. Finally, damage locating vector is used to predict different damage scenarios using experimental data.

iv. The last topic of this chapter presents and discusses the proposed method of damage detection using incomplete measurements. The proposed method is based on the frequency shifts of the updated FE model under certain damage scenarios and studying their relationship with the experimental data using multiple linear regression analysis. Being paired with DLV, this approach can predict the damage scenario with an acceptable accuracy.

5.2 Modal Identification

The academic license of ARTeMIS Extractor Pro. 3.2 is used in this study to extract modal properties of FE and experimental model. In both cases, the measured acceleration of each DOF in cm/s^2 is imported to the software. In case of experimental data, the local coordinate of each measurement is not perpendicular to the global coordinate of the frame structure. So in each case, the measured accelerations of each

node in its local XYZ axes need to be converted to global coordinate. ARTeMIS is capable of importing the data in its local coordinate and does the conversion.

After data sets are processed, ARTeMIS draws the average of the normalized singular value of spectral density matrices of all data sets (Figure 5.1). Modes are identified at this step by manual peak picking as shown in Figure 5.1. Peak picking requires a general understanding of the system as some peaks might be not useful or some desire modes might not be shows as an individual peak. For example the results are showing a sharp peak at 50 Hz; however former FE eigen analysis of the frame structure did not identify any mode close to this frequency. In fact this peak is always presented in the results and is caused by the noise that the alternating current is inducing to the system which is exactly 50 Hz. The other example is the two peaks that are identified at 30.4 and 31.9 Hz. At the first glance, the first peak might look not so significant and the second peak be selected. However FE results are showing that the model has two modes at this range with very close frequencies, but different mode shapes; one is the second bending along Z and the other is second bending along X. Since the two modes are very close, to clearly identify the first mode and its mode shape, another data processing is required with the data sets along Z directions to solely identify this mode.

After all the desired modes are selected, ARTeMIS exports all the required information of the modes including modal frequencies, mode shapes and modal damping of each mode. Figure 5.2 is showing the first 6 experimental mode shapes identified using ARTeMIS.

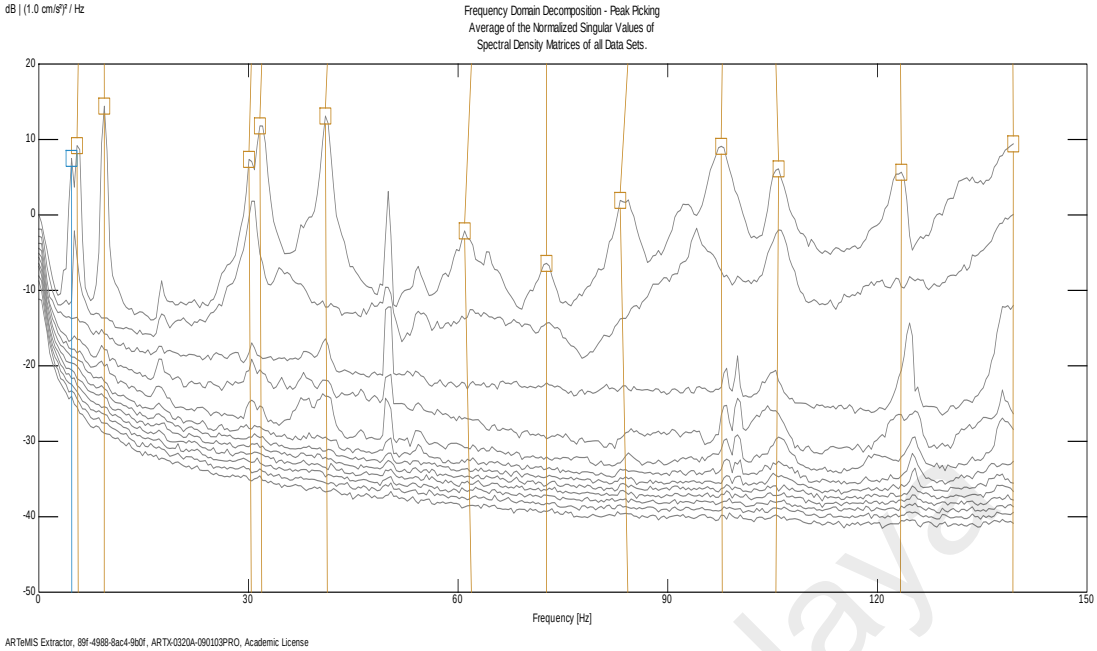

Figure 5.1: Enhanced FDD peak picking in ARTeMIS

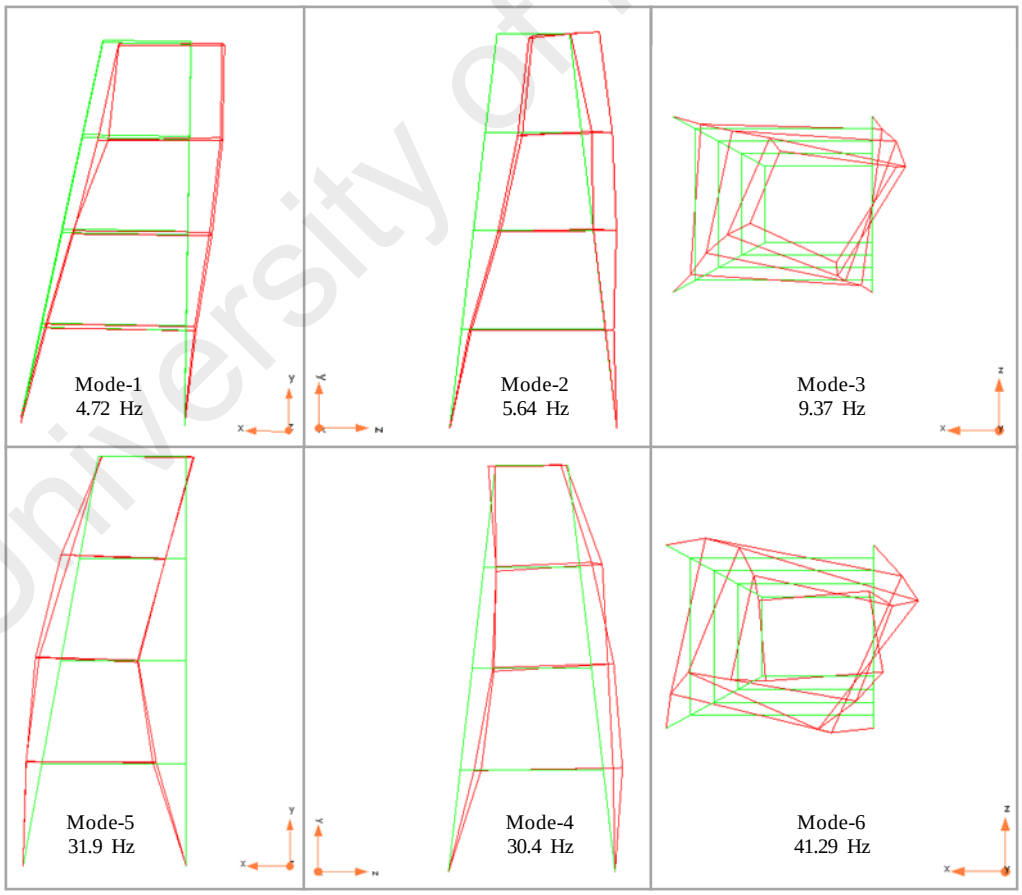

Figure 5.2: The first 6 experimental mode shapes identified using ARTeMIS.

5.3 Mass Normalization

The background theory of mass normalization using mass change is presented in chapter 3.3.2. The methods of utilizing this approach in this study are also described in chapter 4.6. So this part only focuses on presentation of the results of this approach and also discussions about them. This section has two main objectives. One is to verify this approach numerically and experimentally and based on that propose few suggestions on how to effectively apply this method and enhance its reliability. The second goal is to produce required data to be used for other parts of the study.

This part is presented in three sections:

i. All 10 mass modification scenarios that are presented in chapter 4.6 are tested using finite element eigen analysis. Precise mass normalized mode shapes are available in eigen analysis; therefore they can be used as reference to validate the findings. The aim is to realize which parameters are playing a role on validity and reliability of the results.

ii. All 10 mass modification scenarios are tested using finite element dynamic analysis. Unlike eigen analysis, the mode identification method in FE dynamic analysis is similar to the experiment. So its results and findings are more compatible with the experiment. In general, the main goal of these two FE analyses is to find which mass modification scenarios are more suitable for the task.

iii. The modification scenarios that are selected by FE analysis are then used to normalize the experimental mode shapes.

5.3.1 Mass Normalization using Eigen Analysis

10 mass modification scenarios were simulated in iDIANA by adding point mass elements to respective joints. The updated modal frequencies and mass normalized mode shapes of each case are then obtained using eigen analysis. Using modal frequencies and mode shapes of original and modified cases, the scaling factor for each mass scenario and each mode was calculated using the method described in chapter 3.3.2.

i. Single 10 kg mass scenarios

Figure 5.3 is presenting the scaling factors calculated using 4 single mass scenarios. The reference line which is the numerically calculated scaling factor of original case is also shown by dotted line.

The results are showing that the estimated scaling factor of all mass scenarios perfectly fits the exact value for the first 3 modes. Case B is showing a tolerable fit for modes 4 and 5 too. Other than this, the estimated scaling factors are far from being acceptable. To explain this, two important factors must be discussed i.e. correlation and frequency shift.

As mentioned before, one of the main assumptions in Equations 3.57 and 3.63 are that the mode shapes after mass modification should not be significantly changed. They assume that the two mode shapes remain identical and so they only use Ψ_1 to calculate α. So to describe why the results are so erroneous after mode four, the frequency and mode shapes changes might offer some explanation.

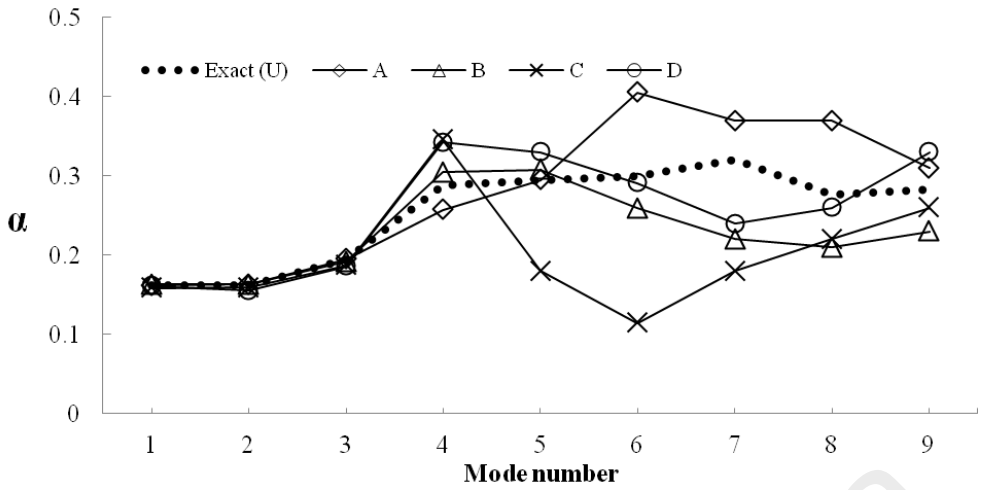

Figure 5.3: Scaling factor estimated by a single 10 kg mass placed on points A to D (FE eigen analysis)

Figure 5.4 is presenting the correlation between the mode shapes of original model and single mass scenarios. It shows that the mode shape correlation of all cases are close to 1 for the first three modes which partly explains the perfect estimation of scaling factor for these three modes. Modes 4 to 9 (except for mode 6) are showing a very low correlation for case A which means they do not satisfy the assumption of Equations 3.57 and 3.63 and should be eliminated. For case B, the correlations of modes 4 to 6 are acceptable, although a bit low for mode 5, but it still explains the exactable results that were mentioned above.

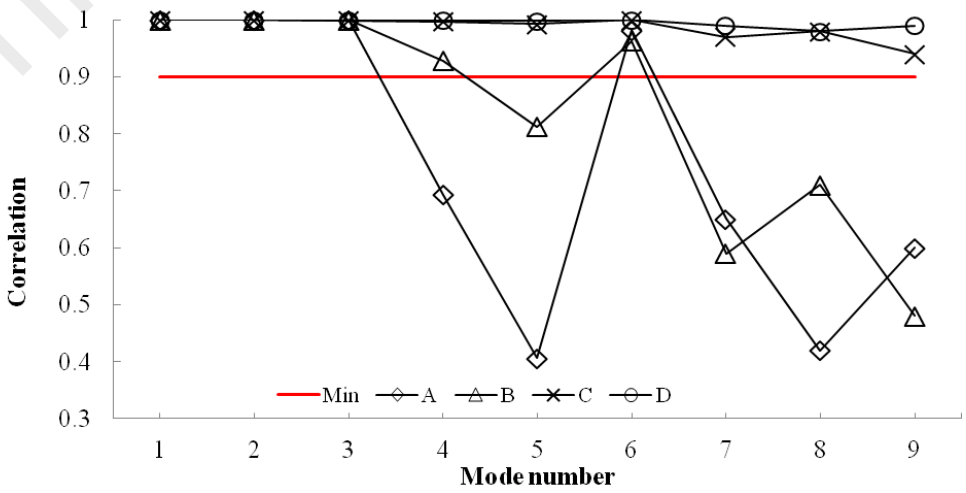

Figure 5.4: Correlation of original and modified mode shapes in single mass scenarios (FE eigen analysis)

It should be noticed that a high correlation value does not necessarily results in a good estimation of α. It is because correlation between two modes can be high simply because the extra mass had no effect on that mode shape and did not changed it at all. The value of frequency shift is another factor that can help assessing the reliability of estimated scaling factors (Figure 5.5). For example in cases C and D, although the correlation is close to 1, but the frequency shift of modes 4 to 6 are significantly low, less than 0.05% which is far less than the minimum of 1% suggested by (Brincker & Andersen, 2003). It means the extra masses in these two points did not participate in these 3 modes. The reason is that the upper deck is node of mode 4 to 6 i.e. the standing point of vibration which makes the extra mass ineffective. Although since Upper deck is the anti-node of mode shapes 1 to 3, the extra mass placed on points C and D effectively change the modal frequency and provides a perfect estimation of scaling factor. In case of points A and B however, lower deck is not on the node of any of the 6 mode shapes and so they alter all the modes and give a reasonable estimation of α.

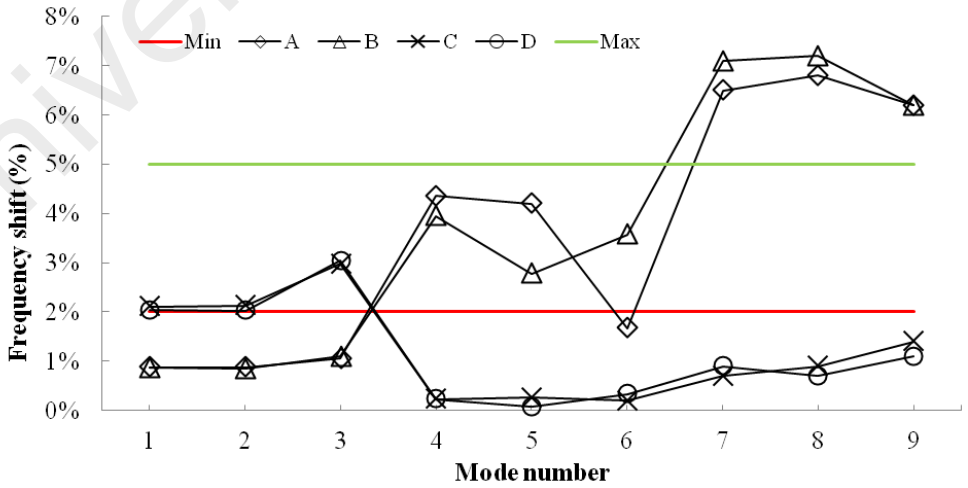

Figure 5.5: Frequency shifts of modified mode shapes in single mass scenarios (FE eigen analysis)

ii. Dual 10 kg mass scenarios

Figure 5.6 is presenting the scaling factors calculated using 6 dual mass scenarios. The results are showing a significant improvement in the accuracy of calculated scaling factors in compare to single mass scenarios. BC-BD and CD are presenting acceptable fit with the exact value for all modes. However, the results of AB, AC and AD are starting to deviate from the exact value after mode 4. Further investigation of correlations and frequency shifts of these cases (Figure 5.7 and Figure 5.8) indicates that these inaccurate scaling factors are suffering from either low correlation factor or an improper frequency shift, or even both.

Results of eigen analysis are showing that among 10 mass modification scenarios, only BC, BD and CD are providing reliable results.

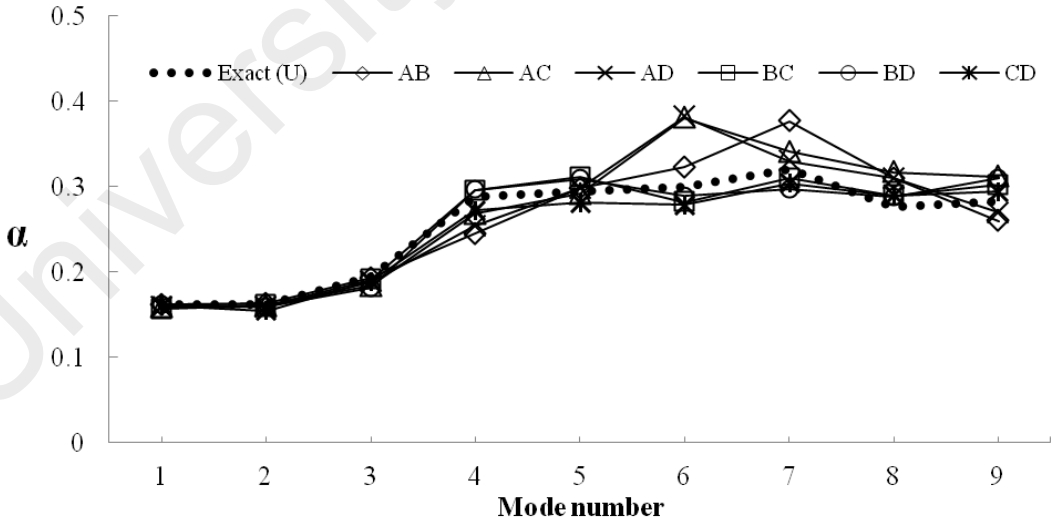

Figure 5.6: Scaling factor estimated by dual mass scenarios (FE eigen analysis)

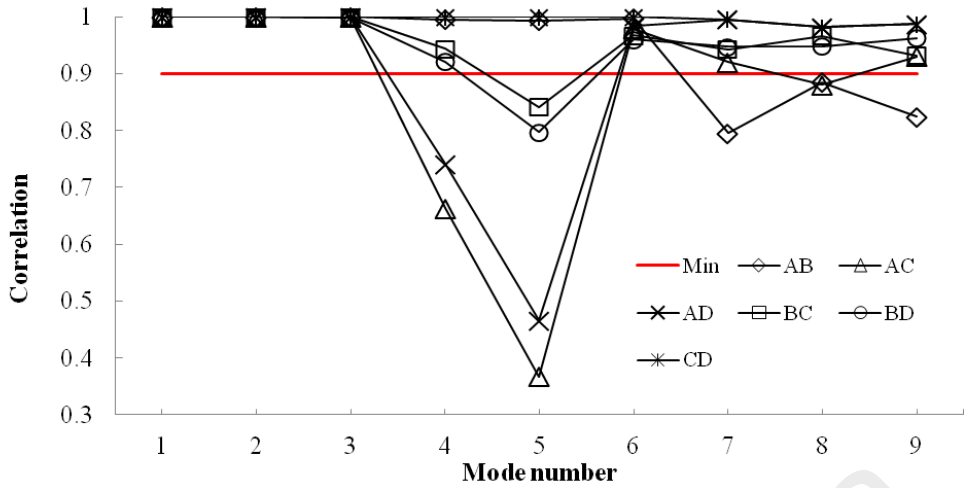

Figure 5.7: Correlation of original and modified mode shapes in dual mass scenarios (FE eigen analysis)

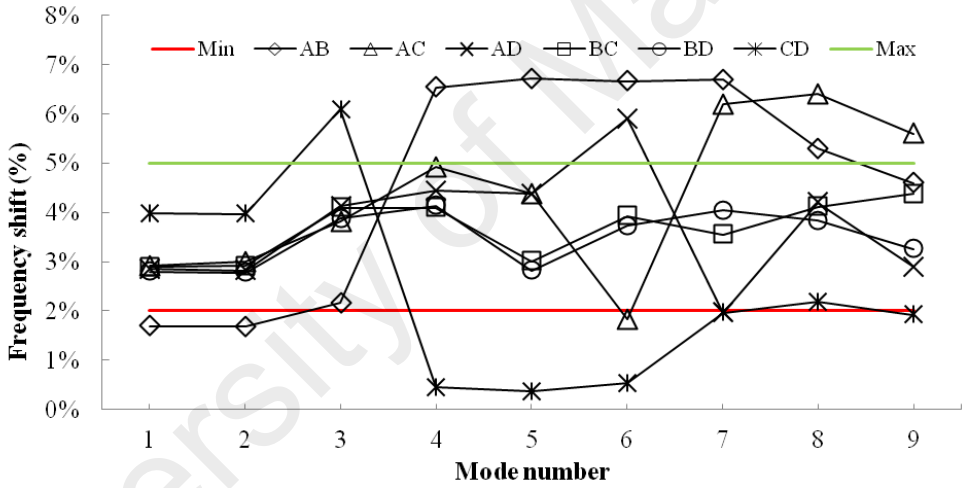

Figure 5.8: Frequency shifts of modified mode shapes in dual mass scenarios (FE eigen analysis)

5.3.2 Mass Normalization using FE Dynamic Analysis

FE eigen analysis can be considered as the most accurate way of calculating the modal frequencies and mode shapes. What makes it so accurate is that the modal parameters are calculated directly from mass and stiffness matrices. Although this could be not so favorable when the results are being use to validate the experiment. FE dynamic analysis is used to provide modal parameters that are more similar and more compatible with the experiment. To do so, the very same input forces that have been recorded

during experimental tests are applied to the FE model with the same sampling frequency, 320 Hz, and to the same points. The acceleration of each DOF is also recorded at the same sampling frequency. Table 5.1 presents the frequency of the estimated FE modes of Eigen analysis, dynamic analysis using ARTeMIS and dynamic analysis using FRF. Unlike eigen analysis, in dynamic analysis the first 12 modes are extracted and being used for damage detection.

Table 5.1: Frequency of detected modes in eigen and dynamic FE analysis

Finite Element	Description	Frequency (Hz)		
		FE Eigen	FE Dynamic (ARTeMIS)	FE Dynamic (FRF)
Mode 1	1st bending along X	4.08	4.099	4.2
Mode 2	1st bending along Z	4.64	5.661	5.62
Mode 3	1st torsion around Y	8.51	8.644	8.73
Mode 4	2nd bending along Z	26.59	26.25	26.28
Mode 5	2nd bending along X	26.93	26.25	26.82
Mode 6	2nd torsion around Y	30.01	35.21	35.59
Mode 7	3rd bending along X	62.32	53.27	52.9
Mode 8	3rd bending along Z	72.27	66.13	66.76
Mode 9	3rd torsion around Y	77.88	76.54	76.31
Mode 10	4th bending along X	NA	89.05	89.33
Mode 11	1st vertical along Y	NA	93.68	94.13
Mode 12	4th bending along Z	NA	96.36	96.92

Figure 5.9 and Figure 5.10 are showing the estimated scaling factor of the first 12 modes of FE dynamic analysis using 4 and 6 mass scenarios respectively. The scaling factor calculated using FRF is also presented in these Figures as reference line. It should be noted that although the results calculated using FRF are expected to be more accurate than the results of mass change method, but it cannot be used as a reference the same way it was used in eigen analysis. One reason is that although accurate, the scaling

factors calculated using FRF are not as accurate as those calculated in eigen analysis[2]. The other reason is that the scaling factors that are estimated using FRF belonging to their own detected modes which are not entirely similar to those that are estimated using ARTeMIS

Similar to the results of FE eigen analysis, the single mass scenarios are not promising at all. If the line of FRF is considered as an approximate reference line, most of the estimated scaling factors are significantly far from this line. Moreover, the results of different mass scenarios in Figure 5.9 are not at all close to each other, except for the first 3 modes. This shows that single mass scenarios were unable to accurately or even approximately estimate the scaling factors.

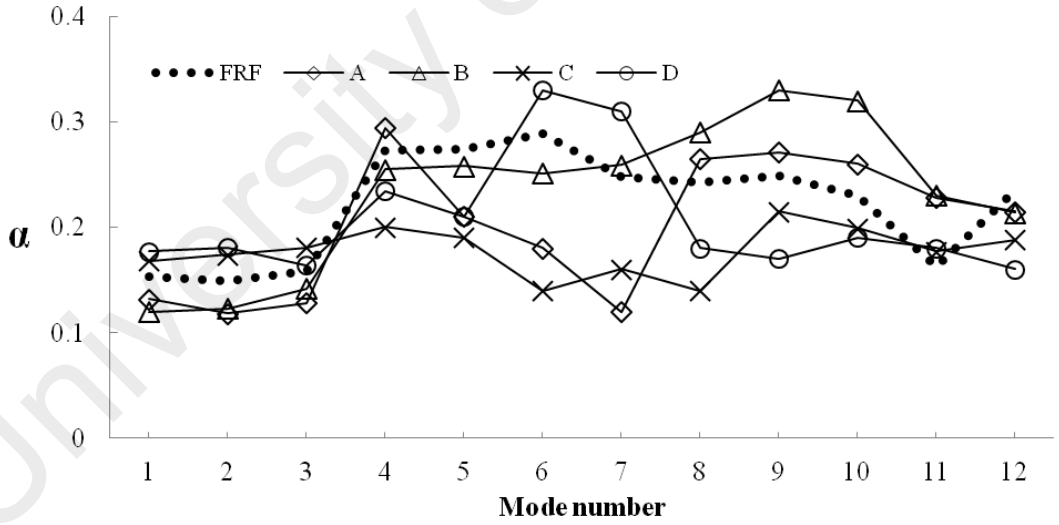

Figure 5.9: Estimated scaling factor in FE dynamic analysis for single mass scenarios

[2] This statement should not be misreading as if the findings of eigen analysis are more accurate and reliable than other modal estimation methods. In case of modal estimation, it is clear that the experimental results are the benchmark and any other findings should be compared and updated in respect to them. But when it comes to investigation of a method that employs modal parameters, the findings of each modal estimation technique is evaluated internally. For example, the scaling factors of the eigen analysis mode shapes that are estimated using mass change method, are being compared with the numerically obtained scaling factors using eigen analysis. Apparently, this internal comparison is significantly more reliable.

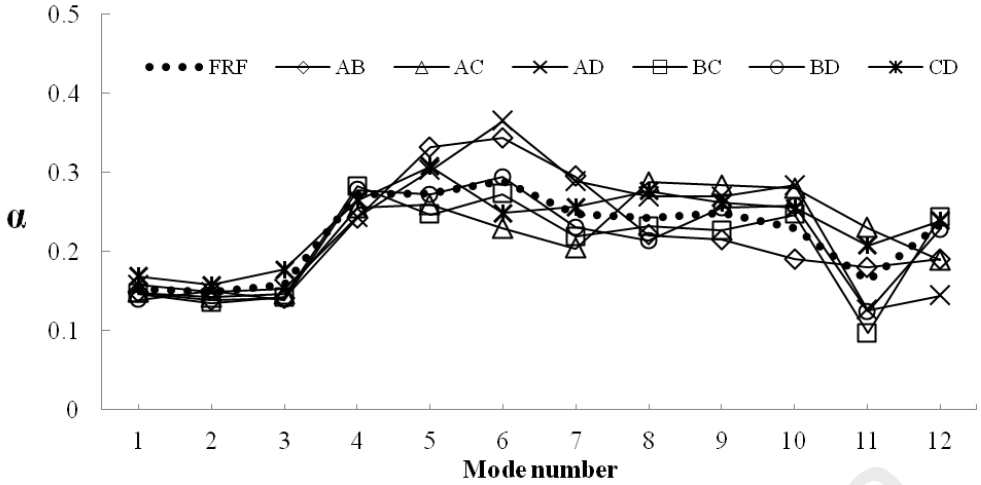

Figure 5.10: Estimated scaling factor in FE dynamic analysis for double mass scenarios

The estimated scaling factors of double mass scenarios in Figure 5.10 are noticeably more concrete compare to single mass scenarios. In most cases, they are following the same trend as each other and also compare to FRF results. Among the 6 dual mass scenarios, three of them are showing the best estimation in all 12 modes i.e. BC, BD and CD. Similar to FE eigen analysis, the correlations and frequency shifts are being used to evaluate the estimated scaling factors (Figure 5.11and Figure 5.14). Both correlation value and frequency shift of a mode must be within the range in order to accept the scaling factor. The results are showing that with few exceptions, for each of the cases with correlation and frequency shift within the range, the estimated scaling factors are closer to each other and also to FRF line.

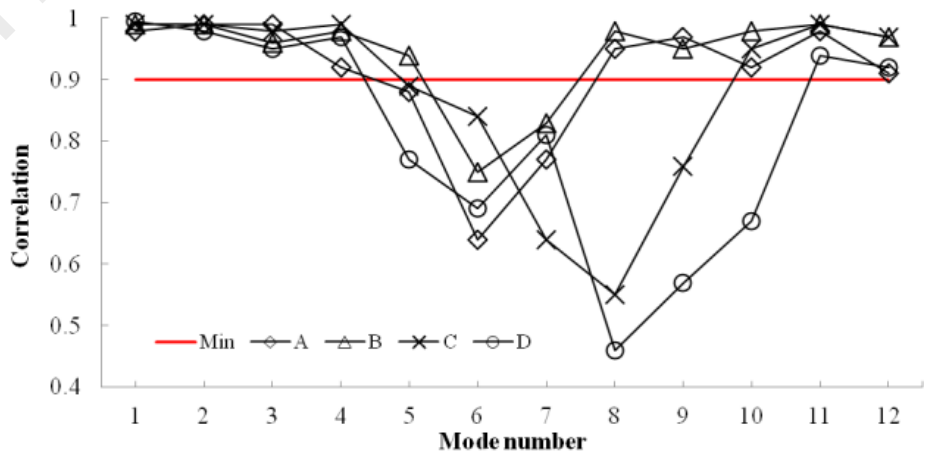

Figure 5.11: Correlations of unmodified and modified mode shapes in single mass scenarios (FE dynamic analysis)

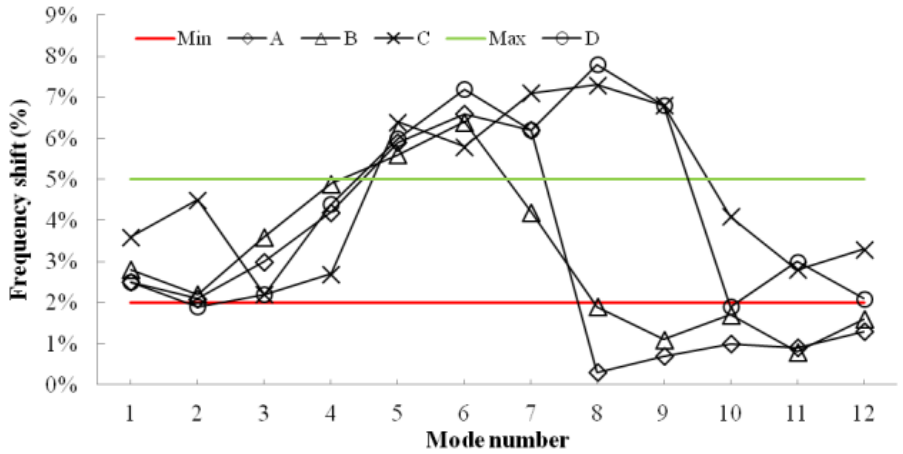

Figure 5.12: Frequency shifts in single mass scenarios (FE dynamic analysis)

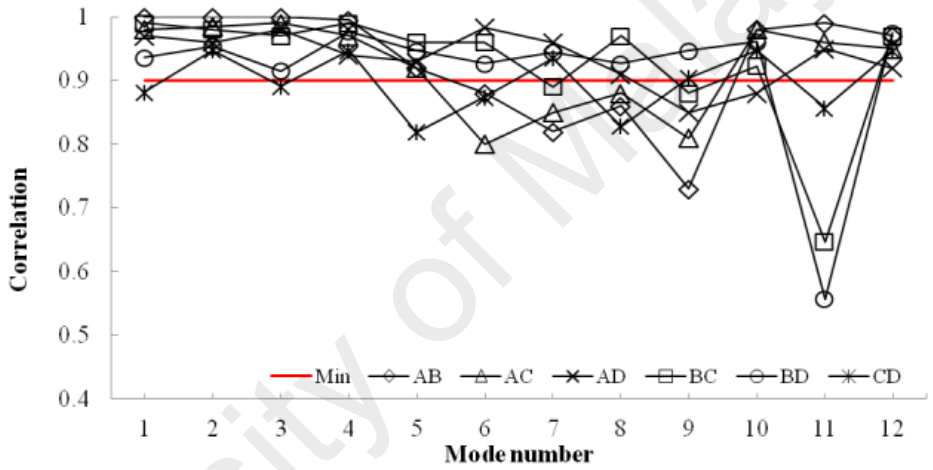

Figure 5.13: Correlations of unmodified and modified in dual mass scenarios (FE dynamic analysis)

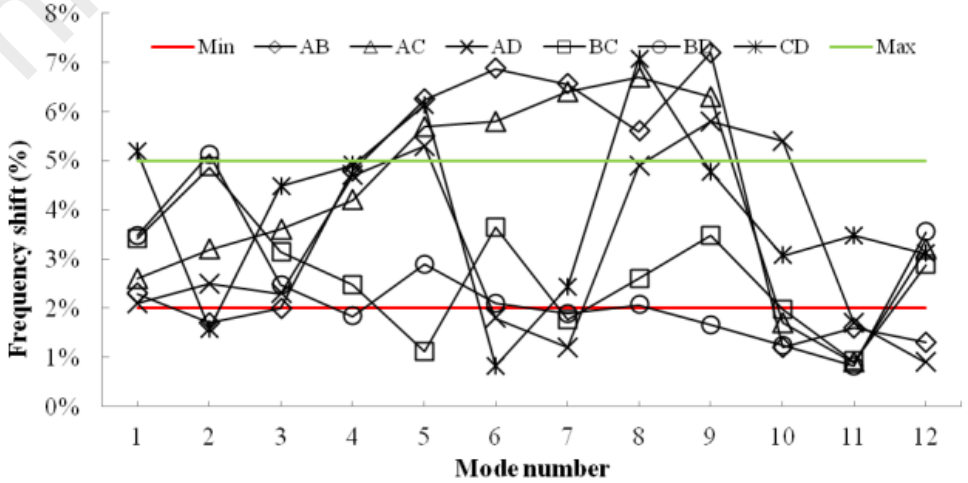

Figure 5.14: Frequency shifts in dual mass scenarios (FE dynamic analysis)

5.3.3 Rules of Assessing Reliable Scaling Factor

The results of FE eigen analysis and FE dynamic analysis are suggesting a relationship between the correlation of Ψ_1 and Ψ_2 and also the frequency shift and the reliability of the calculated scaling factor. From the results of all previously examined mass scenarios it was concluded that when the correlation of the two mode shapes is high (Correl > 0.9), the estimated scaling factor is smaller than its actual value. It is because the mass change were unable to adequately change the mode shape which happened when the mass is very small or it is placed on the node of that particular mode shape.

If the correlation of the two mode shapes is low (Correl < 0.8), but the frequency shift is high ($\Delta\omega$ > 3%), it shows that the added mass is large, causing the mode shape to change which is in contrary with the assumption of this method and so the calculated scaling factor is not reliable. Although rare, it is possible for both correlation and frequency shift to be low. This happens when the amount of added mass is sufficient, but its position or distribution (in case multiple masses are added) is critical in a way that it significantly affects some DOFs of the structure and not the others. Regardless of what the reason is, this case should also be rejected.

The most favorable situation is when the correlation of the two mode shapes is high (Correl > 0.9) and the frequency shift is sufficient ($\Delta\omega$ > 1%). Although the optimum values for correlation and frequency shifts are (Correl > 95%) and (2%< $\Delta\omega$ <5%). This criterion is very useful to evaluate the truthfulness of the calculated scaling factors in actual cases where the exact value is not available.

Using these rules, the reliability of experimentally estimated scaling factors is being examined. Based on the results of FE eigen analysis and Fe dynamic analysis, only three mass scenarios was tested experimentally i.e. BC, BD and CD.

5.3.4 Mass Normalization of Experimental Modes

Table 5.2 is presenting the frequency of the first 12 experimental modes. Comparing Table 5.1 and Table 5.2 shows that the first 8 mode shapes of experiment and FE dynamic analysis are generally paired. Although when it goes to higher frequencies, the detected modes are different. Furthermore, the modal frequencies of the first modes are similar and when it goes to higher modes, they become more different.

Table 5.2: Frequency of detected experimental mode shapes using FRF and ARTeMIS

Experiment	Description	Frequency (Hz)	
		ARTeMIS	FRF
Mode 1	1st bending along X	4.72	4.76
Mode 2	1st bending along Z	5.64	5.70
Mode 3	1st torsion around Y	9.37	9.37
Mode 4	2nd bending along Z	30.40	30.31
Mode 5	2nd bending along X	31.90	32.03
Mode 6	2nd torsion around Y	41.29	41.25
Mode 7	3rd bending along X	61.90	61.64
Mode 8	3rd bending along Z	72.66	72.89
Mode 9	Atypical shape	84.29	84.45
Mode 10	3rd torsion around Y	97.81	97.53
Mode 11	Atypical shape	105.5	104.94
Mode 12	Atypical shape	123.3	123.83

The scaling factors of all 12 modes are estimated using three mass scenarios i.e. BC, BD and CD which are presented in Figure 5.15. The comparison of the estimated scaling factors with themselves and also with FRF line shows that in almost all cases, the results are more or less following the same trend with an acceptable proximity. Only in mode 4, the distance of the data is significant.

Examination of correlation values and frequency changes (Figure 5.16 and Figure 5.17) are also showing that the results of mode 4 are not reliable. Another interesting observation is the inconsistency between correlation value and frequency shift in mode 4. Low correlation value in mode 4 is indicating that the mode shape is significantly

changed which is suggesting that the effect of mass changes were significant in this mode. This should be normally coupled with a high frequency shift. However the frequency shifts of this mode are below 1% in all three cases. As explained before, this could be because the extra mass only affects the neighboring DOFs without actually altering the mode itself. It could also be due to an error on mode shape estimation in this particular mode. This possibility is more probable since all three mass scenarios are having the same problem. However, no matter what causes this problem, the results of mode 4 are not reliable and this mode should be ignored.

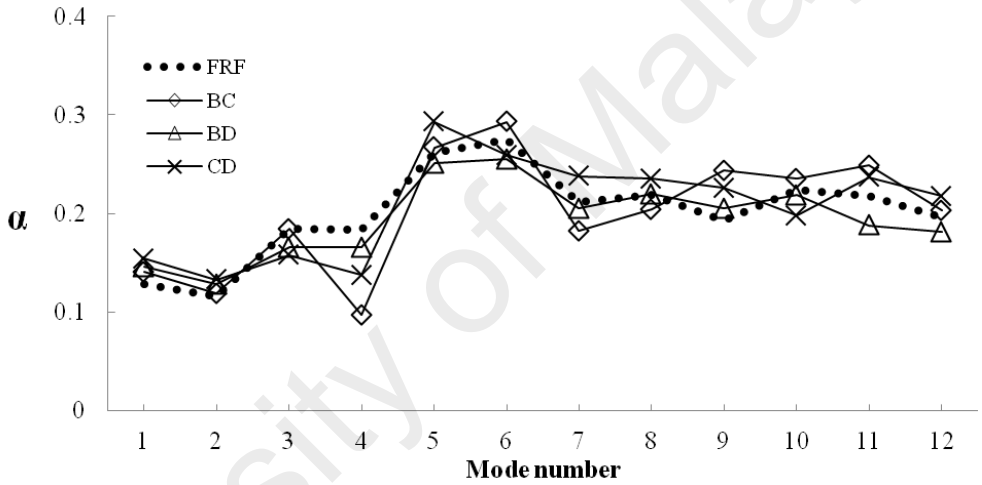

Figure 5.15: Estimated scaling factor using selected mass change scenarios obtained experimentally

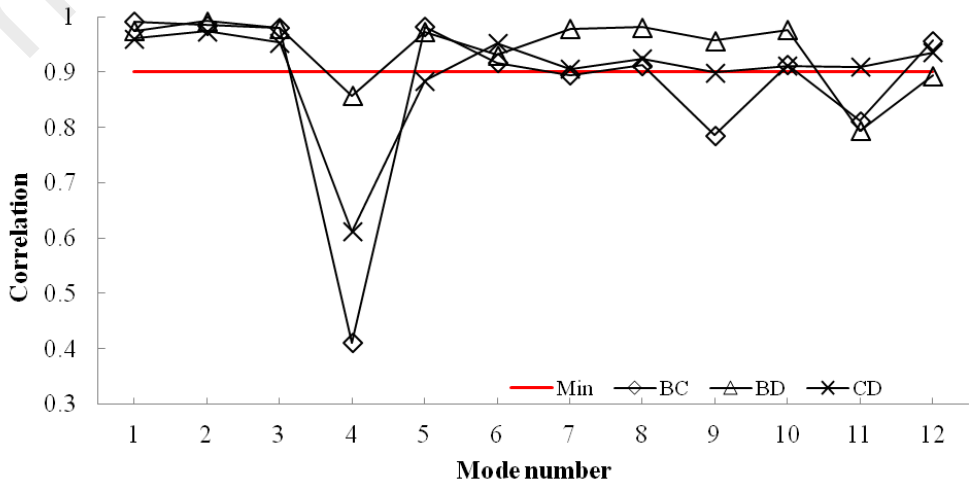

Figure 5.16: Correlation of unmodified and modified mode shapes obtained experimentally

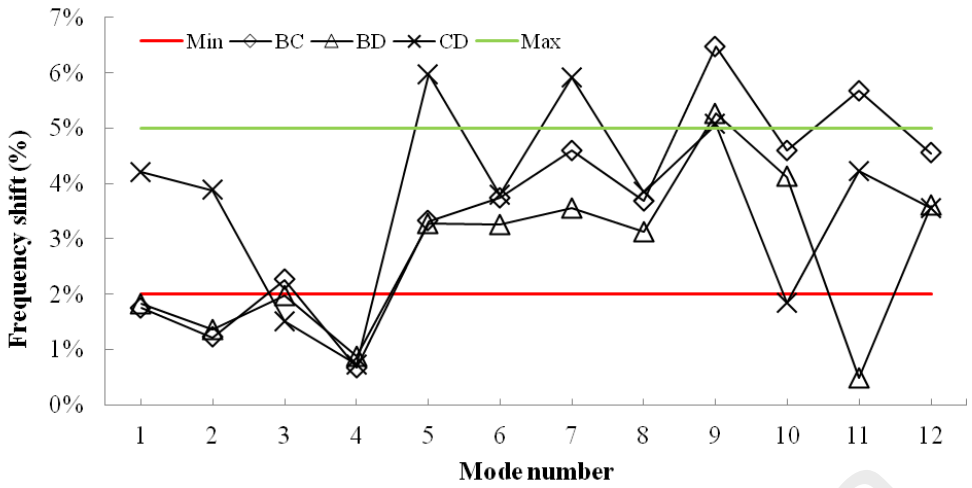

Figure 5.17: Frequency shift of modes obtained experimentally

5.4 Model Updating

5.4.1 CMCM using Complete Measurements

The theory of CMCM model updating is explained in chapter 3.2 and its implementation method is described in chapter 4.5. This section is presenting step by step updating of FE model using this method. For this purpose, the first 9 modes of both FE dynamic analysis and experiment are being used. Figure 5.18 is presenting the modal frequencies of the first 9 modes. The Figure shows that over all, the estimated frequency in FE is lower than what has been obtained from the experiment. This shows that the stiffness of FE model in general is lower than what is estimated in the experiment.

The first step to update the FE model is finding the correcting factor of the stiffness of each member. As mentioned before, three stiffness correcting factors are calculated for each member, one for its axial stiffness and two for bending stiffness's. Figure 5.19 and Figure 5.20 are presenting the stiffness correcting factors of columns and beams respectively, calculated in first step. The estimated correction factor is above one in all cases which indicates that the axial and bending stiffness of the members need to be

increased. To apply corrected stiffness to FE model, the physical property of each member is calculated using Equation 4.12. In case the estimated size of a group of members are very close to each other, their physical properties can be assigned in bulk for simplicity. However it is always better to model all the members individually if possible.

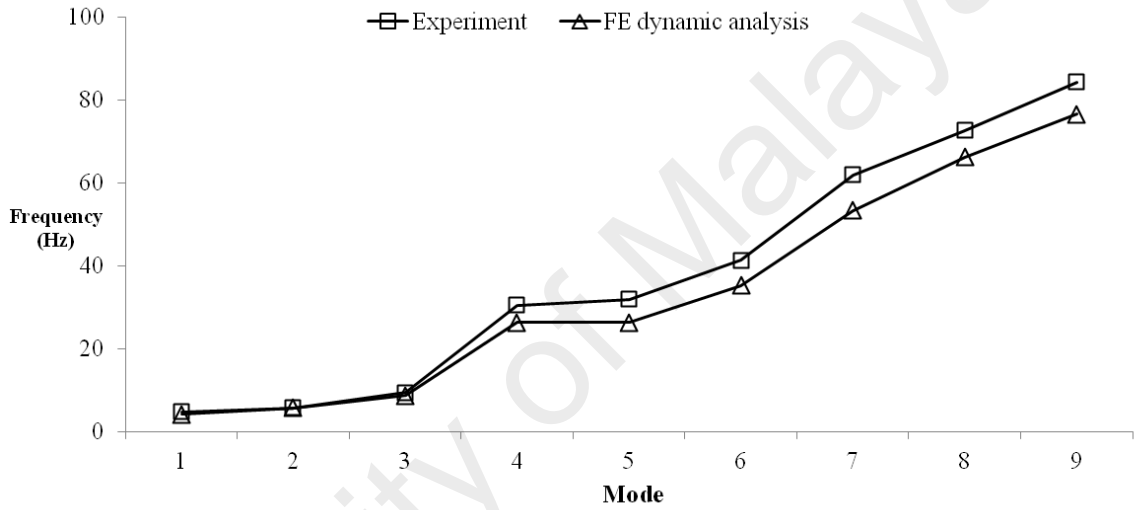

Figure 5.18: FE and EX comparison of the frequencies of the first 9 modes

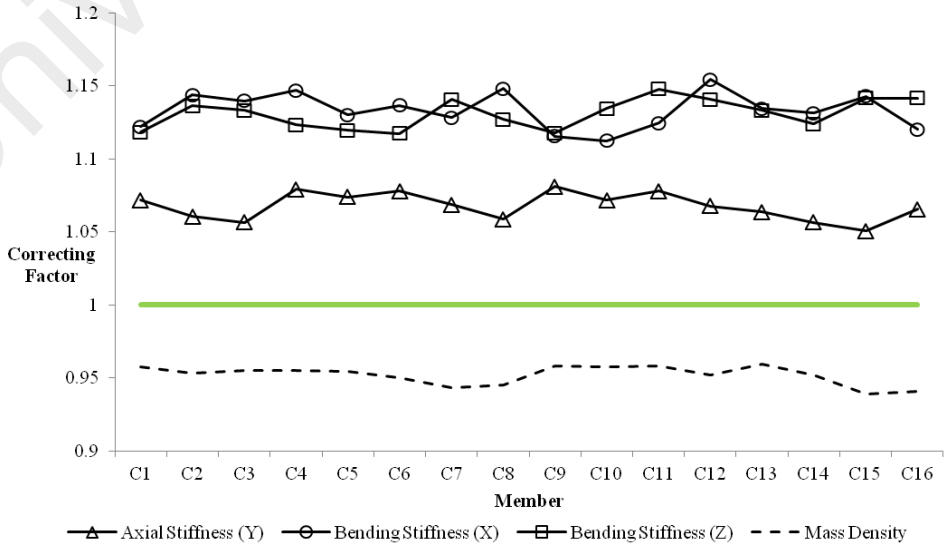

Figure 5.19: Stiffness and mass correcting factors of columns using complete measurements (Step 1)

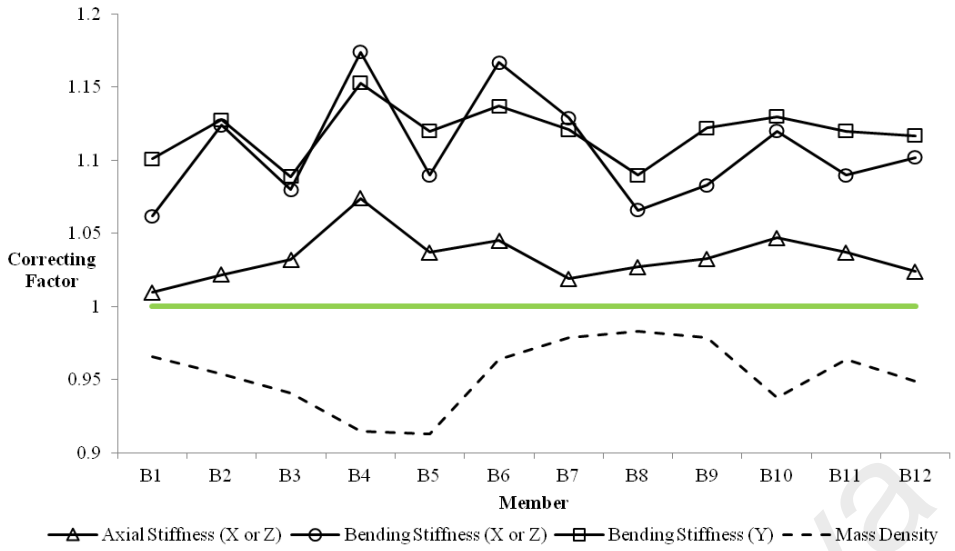

Figure 5.20: Stiffness and mass correcting factors of beams using complete measurement (Step 1)

After stiffness matrix is updated, it is time to calculate the mass correction value of each member. It is possible to use the mass matrix and modal properties of the original FE model to update the mass matrix and then apply the correcting factors to the stiffness updated version of the model. This is approximate, but saves an additional modal estimation step. However to get more accurate results, especially in case which the stiffness correcting factors are relatively large, it is better to recalculate modal properties and mass and stiffness matrices after each updating stage. The calculated mass updating factor for columns and beams in step 1 are presented in Figure 5.19 and Figure 5.20 respectively. As it was expected, the calculated mass correcting factors for all members are below 1, indicating that the overall mass of the model need to be reduced. It is reasonable since mass reduction would increase the overall frequencies of the model. Although it should also be noticed that only part of the estimated mass correcting value is corresponding to the original model. A segment of it is acting on the extra mass that was increased by increasing the size of the members. This explains once more why it is better to recalculate modal properties after each step.

After both stiffness and mass matrices are updated, the whole process is repeated again to check the results. Figure 5.21 and Figure 5.22 are presenting the calculated correcting factors of the second step. The results are showing that the estimated correcting factors of mass and axial stiffness of all members are close to one. Bending stiffness of columns are just slightly higher than they should be and bending stiffness of beams need to be reduced. The dimensions of all members need to be updated again to apply the new sets of correcting factors.

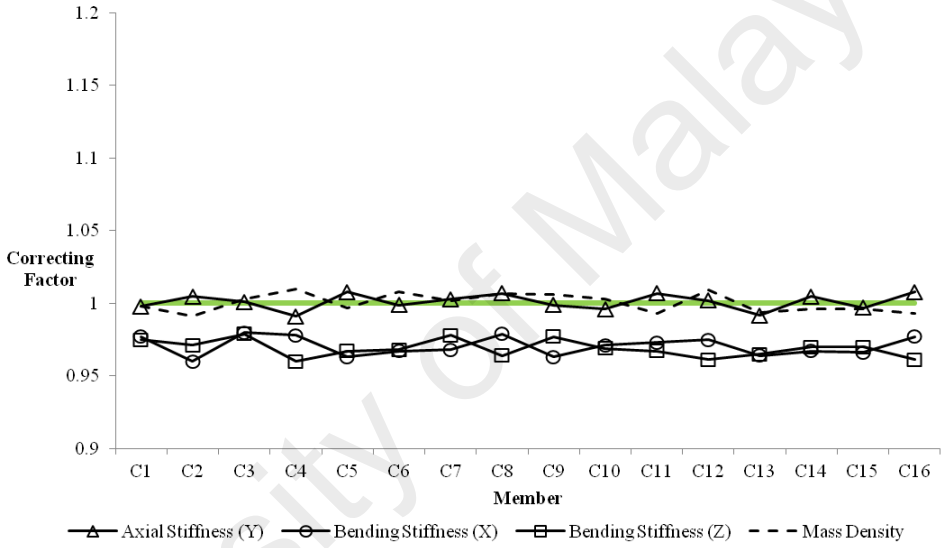

Figure 5.21: Stiffness and mass correcting factors of columns using complete measurements (Step 2)

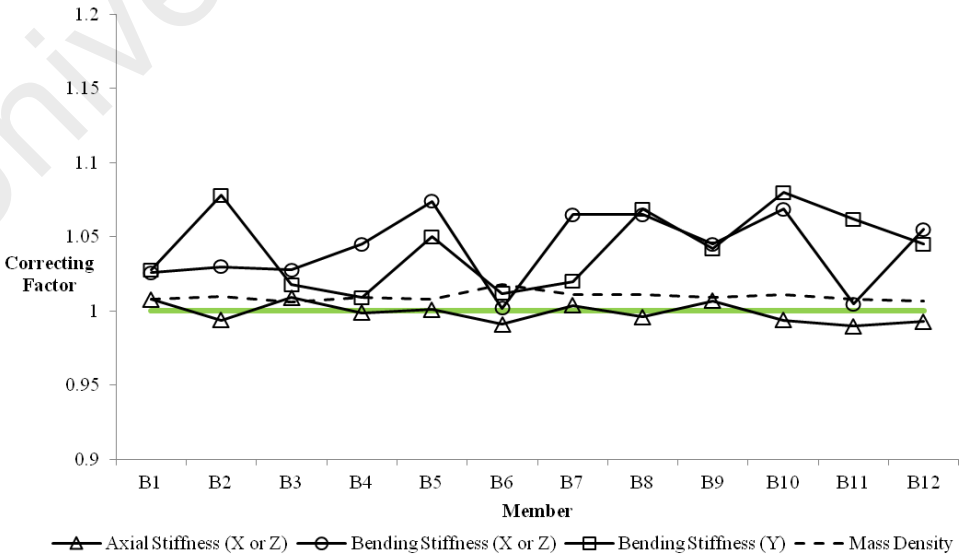

Figure 5.22: Stiffness and mass correcting factors of beams using complete measurements (Step 2)

After updating the model in second stage, the correcting values are calculated again to see if they are converged. Figure 5.23 and Figure 5.24 are showing the third sets of stiffness and mass correcting factors of columns and beams respectively. All the correcting values are close to one which indicates that the model is converged.

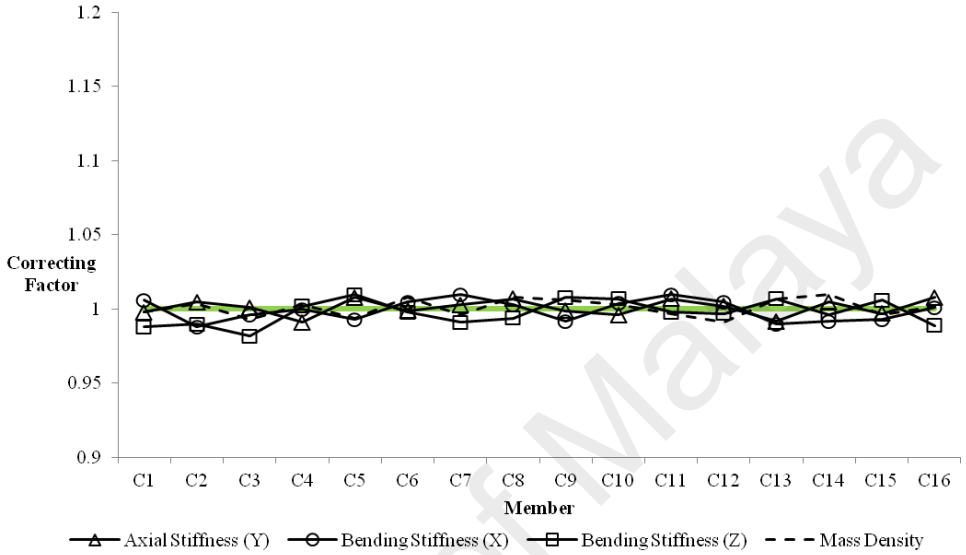

Figure 5.23: Stiffness and mass correcting factors of columns using complete measurements (Step 3)

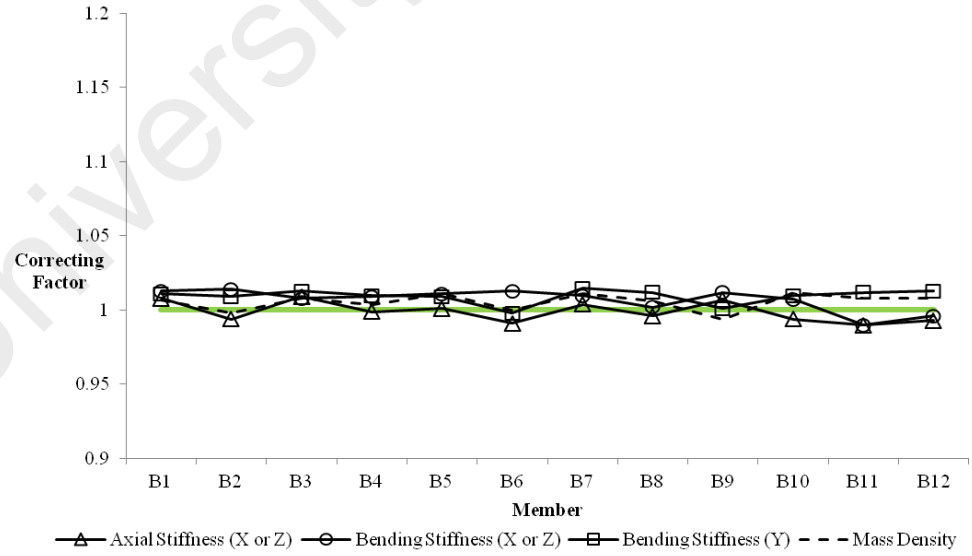

Figure 5.24: Stiffness and mass correcting factors of beams using complete measurements (Step 3)

The updated model can be examined by comparing the frequencies and mode shapes of FE model and experiment. Figure 5.25 compares the frequencies deviation of original model and 1st and 2nd corrected models. It shows that the frequencies of the model after second update are not more than 2% different from the experiment. The correlations of updated mode shapes are also above 98%.

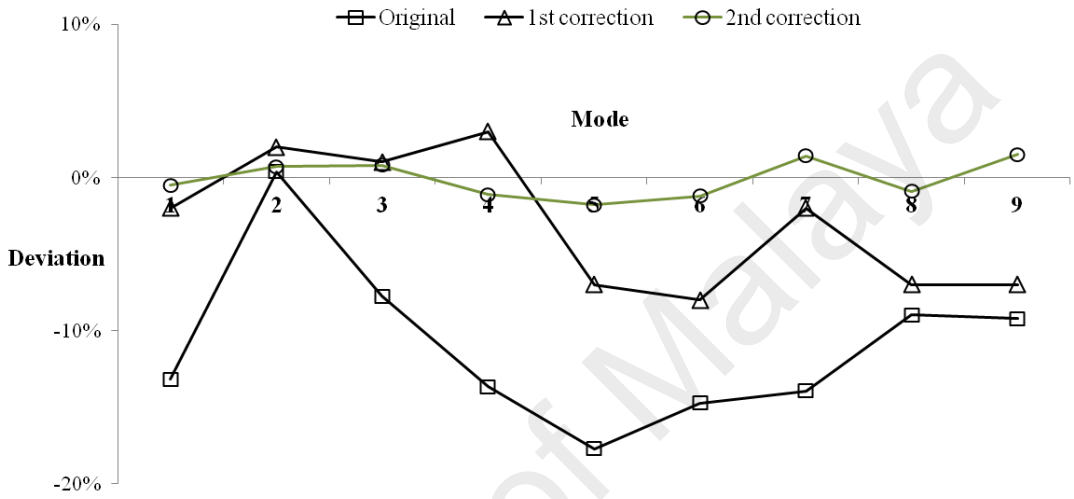

Figure 5.25: Comparison of the frequencies of original model and 1st and 2nd corrections

5.4.2 CMCM using Incomplete Measurements

The main reason for model updating in this study is to find a solution for detecting and locating damage in parts of the structure that are not measured. That is why it is important to find a way to update the model using incomplete data. The proposed method of model updating using incomplete data is presented in chapter 4.5.2. In general, the method approximates the missing items of the experimental data i.e. mode shape components, based on the available corresponding items obtained from FE. Equations 5.1 and 5.2 are presenting the modal vectors obtained from FE model and experiment in matrix form:

$$\phi = \begin{bmatrix} \phi_u \\ \phi_m \end{bmatrix} \tag{5.1}$$

$$\phi = \begin{bmatrix} \phi_u^* \\ \phi_m^* \end{bmatrix} \tag{5.2}$$

where ϕ_u and ϕ_m are FE mode shapes corresponding to the unmeasured and measured DOFs and ϕ_u^* and ϕ_m^* are experimental mode shapes corresponding to the unmeasured and measured DOFs respectively. It should be noted that vectors of ϕ and ϕ^* are arbitrary scaled. All the items of the two matrices above are known except for ϕ_u^* which can be approximately estimated using Equation 5.3:

$$\phi_u^* = \phi_u \sqrt{\frac{\phi_m^{*T} \phi_m^*}{\phi_m^T \phi_m}} \tag{5.3}$$

With ϕ and ϕ^* both available, the first step is to estimate the stiffness correcting factor of each element. It should be reminded that although the missing part of the ϕ^* is filled, but it is approximate and so it is not able to estimate the correcting factors of its corresponding members. The point is that updating the stiffness of measured DOFs gradually converges that piece of information which in return improves the accuracy of the correcting factor in each step.

Figure 5.26 and Figure 5.27 are presenting the results of the stiffness correcting factors estimation for columns C9 to C16 and beams B5 to B12 respectively. The estimated correcting factors are used to update their corresponding columns and beams' stiffness. As mentioned before, the size of columns and beams are similar throughout the model and so it is a good approximation to use the average of correcting factor of each case for similar unmeasured members, which is show in Figure 5.26 and Figure 5.27 by dotted lines in each case.

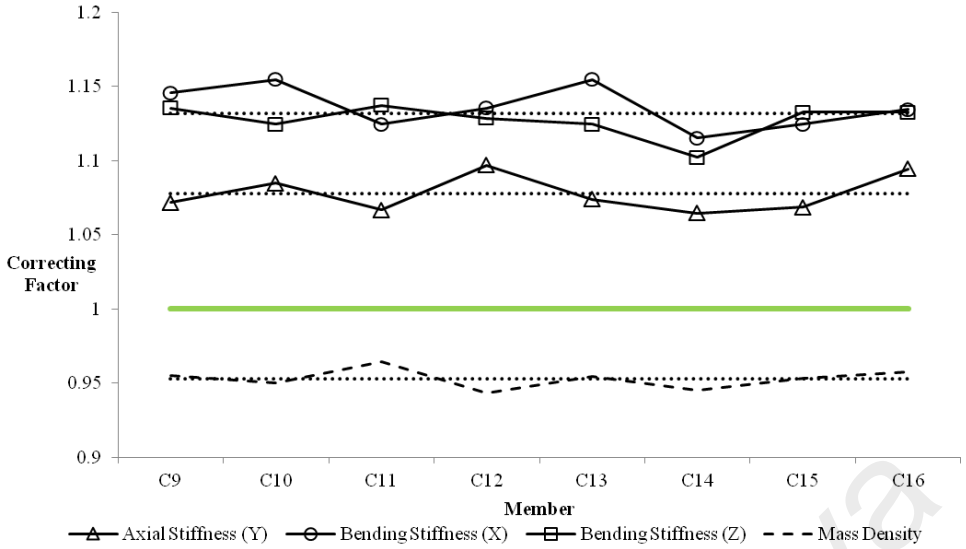

Figure 5.26: Stiffness and mass correcting factors of columns using incomplete measurements (Step 1)

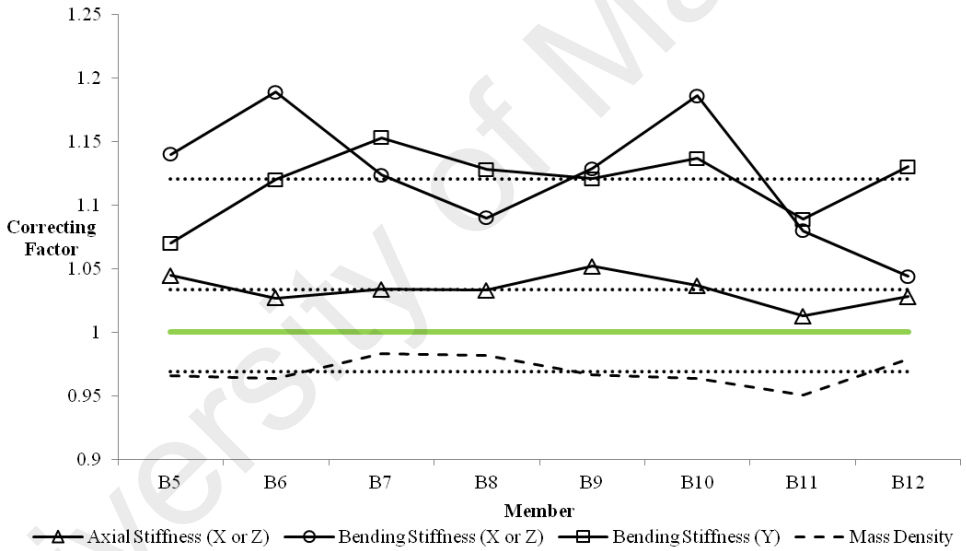

Figure 5.27: Stiffness and mass correcting factors of beams using incomplete measurements (Step 1)

Similar to what as explained previously, the global and local stiffness and mass matrices need to be recalculated after stiffness is updated. Furthermore, it is very important to recalculate ϕ_u^* after each step. The updated information are then used to estimate the mass correcting factor of each measured member and its average value is used to update mass of the unmeasured members.

The second round of updating stiffness and mass matrices are similar to the first one and its results are presented in Figure 5.28 and Figure 5.29. The results are showing that the axial stiffness of beams is already converged in one step, but the rest still need to be updated. The mass matrix of all members is also converged. However, since mass of the member is a function of its physical properties, stiffness updating alters mass matrix and so it should be estimated after each step.

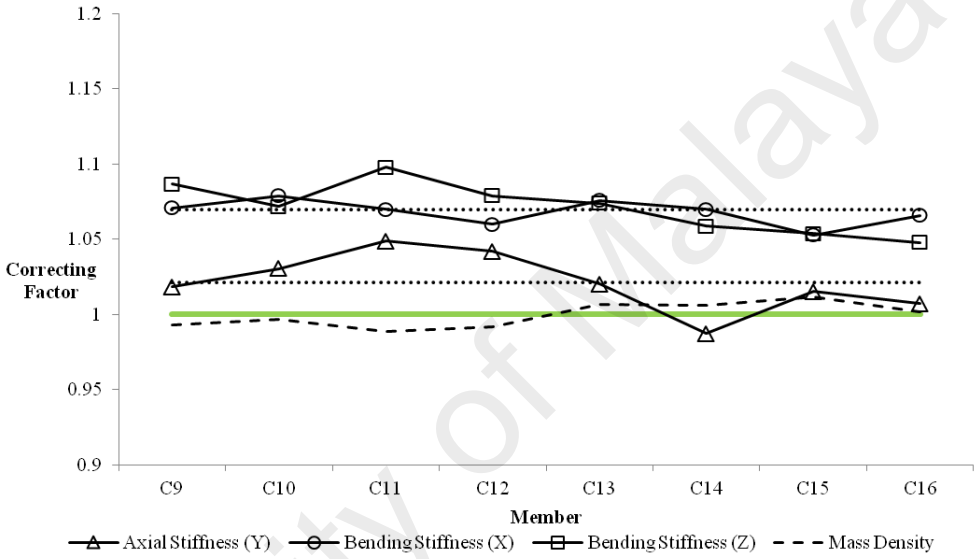

Figure 5.28: Stiffness and mass correcting factors of columns using incomplete measurements (Step 2)

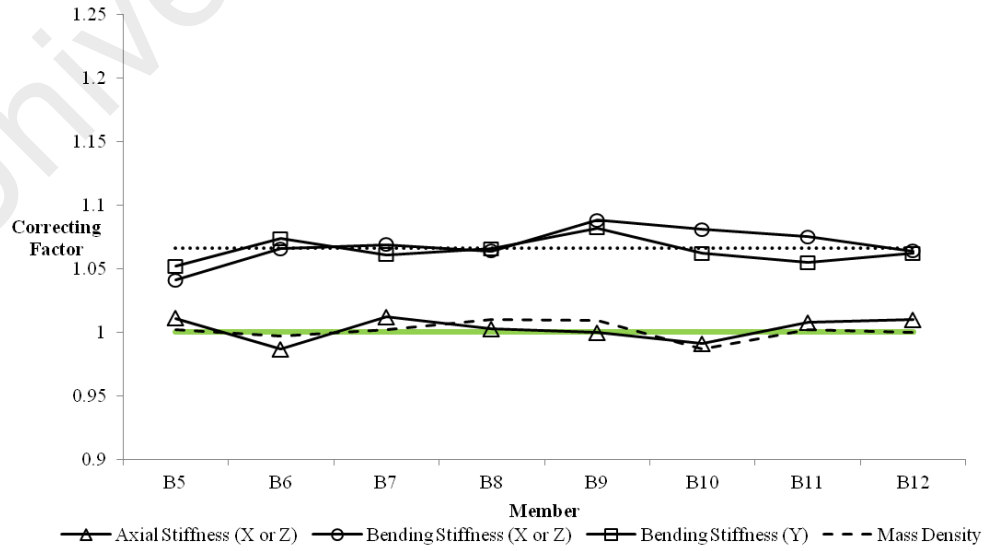

Figure 5.29: Stiffness and mass correcting factors of beams using incomplete measurements (Step 2)

Figure 5.30 and Figure 5.31 are showing the results of the third updating step. As it shows, the stiffness of the beams and axial stiffness of the columns are converged, but bending stiffness of columns are not. Figure 5.32 shows the results of the columns 4th updating step which the entire model is eventually updated.

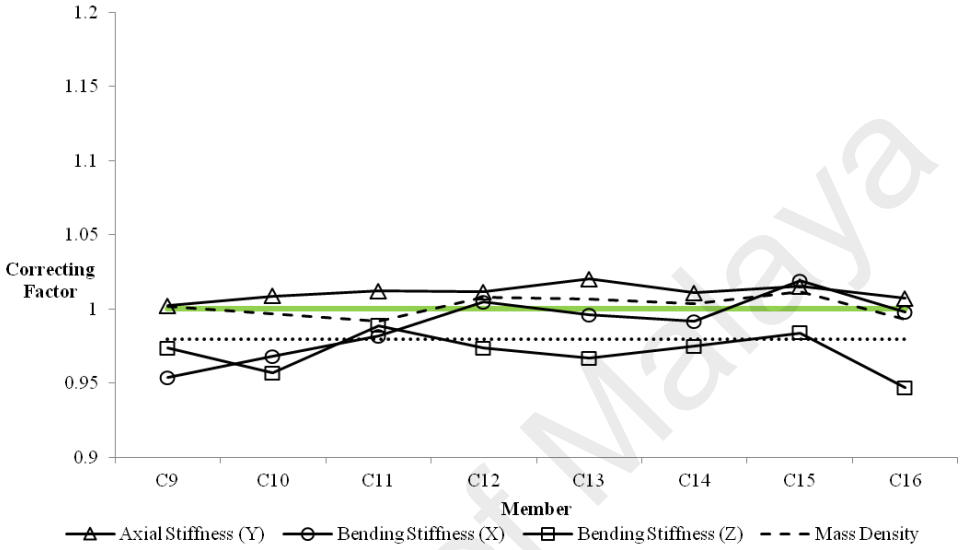

Figure 5.30: Stiffness and mass correcting factors of columns using incomplete measurements (Step 3)

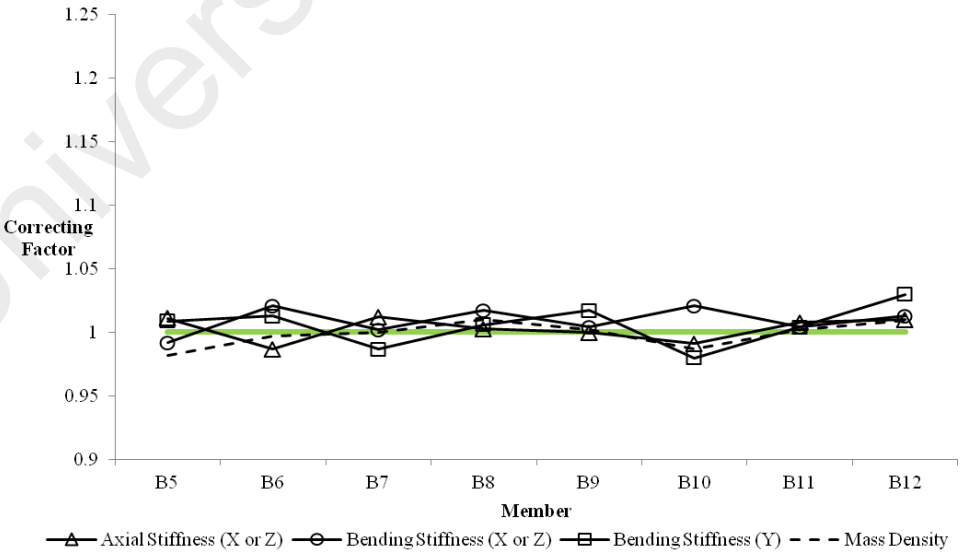

Figure 5.31: Stiffness and mass correcting factors of beams using incomplete measurements (Step 3)

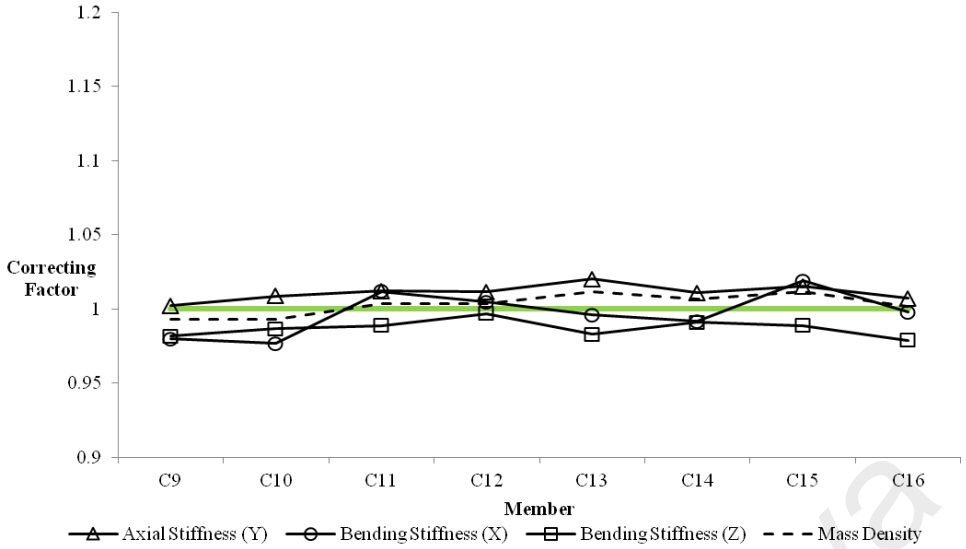

Figure 5.32: Stiffness and mass correcting factors of columns using incomplete measurements (Step 4)

5.5 Damage Detection and Localization

5.5.1 Damage Locating Vectors

5.5.1.1 Finite Element Results

The theory and implementation of damage locating vector is presented in chapters 3.4 and 4.7.2. In this chapter, the results of damage locating vectors are presented and discussed. The first step is to verify the ability of damage locating vector in locating damaged members in different damage scenarios. For this purpose, FE eigen analysis is used considering its ultimate accuracy in mode identification and mode shape normalization. All 10 damage scenarios that have been presented in Table 4.3 are simulated in FE model and modal frequencies and mass normalized mode shapes of undamaged and each damaged scenarios are used to construct flexibility matrix. Using DLV method, 48 sets of load vectors are calculated for all DOFs and those with lower singular values are used to calculate *WSI* index which is damage indicator.

Figure 5.33 is presenting *WSI* index of the first four damage scenarios using FE eigen analysis. The horizontal axis shows the member's number and the vertical axis shows *WSI* value. Members with index values less than one are identified as damaged member. In horizontal axis, members 1 to 16 are referring to columns and members 17 to 28 are referring to beams. So the column's numbers are the same as their respective member's number e.g. member 9 is column 9, but beam 5 in this sequence for example is numbered as member 21.

The results are indicating that in all cases, *WSI* index of the damaged members are less than one and they are located with ultimate accuracy. The case is similar for the rest of damage scenarios which are presented in Appendix III. Such perfect and accurate results confirm that when all the governing factors such as the number of detected modes, the number of measured DOFs, the accuracy of identified modes and mass normalization are in their best shape, damage locating vector is able to accurately and with no doubt locate the damaged members. From this ground, the effects of each of these factors are going to be analyzed and discussed.

Figure 5.34 and Figure 5.35are presenting the *WSI* index of the first four damage scenarios using FE dynamic analysis. Figure 5.34 shows the case which modes are identified and normalized using FRF while Figure 5.35 is presenting the case which modes are identified using ARTeMIS and normalized using mass change method. In both cases, *WSI* of most of damaged columns are less than one which indicates existence of damage. However in case of beams, *WSI* are more than one, especially in case of multiple damage scenarios. However they are all relatively small enough to be identified as damaged member.

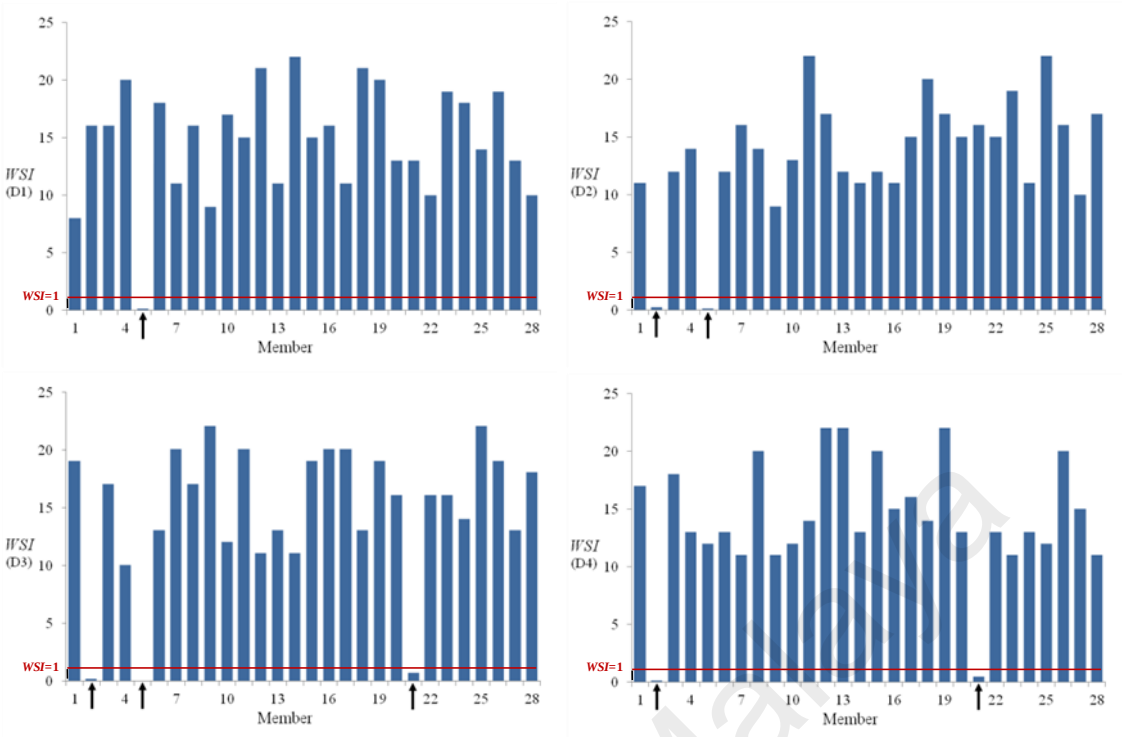

Figure 5.33: *WSI* index of the first 4 damage scenarios using FE eigen analysis
(members with *WSI* less than one are considered as damaged)

It should be reminded that Figure 5.34 and Figure 5.35 are presenting the results of FE analysis. Similar to any other numerical simulation, these results are not suffering fro m some of the errors that are usually expected in an experiment. For example, the results are not influenced by environmental noises or calibration errors etc. However in this case, FE dynamic analysis shares some uncertainties with experimental results, when it comes to mode identification and normalization. For example, the effect of sampling rate and the frequency resolution on mode identification are in fact putting FE dynamic analysis and experimental analysis at the same side, compare to a numerical method like eigen analysis which provides absolutely accurate results in modal identification and normalization.

Figure 5.35 and the rest of these diagrams that are presented in Appendix III are verifying that for FE dynamic analysis results, the mass normalization using change in

mass and also the proposed method of accepting/rejecting the calculated scaling factor is up to the accuracy required for flexibility based damage detection.

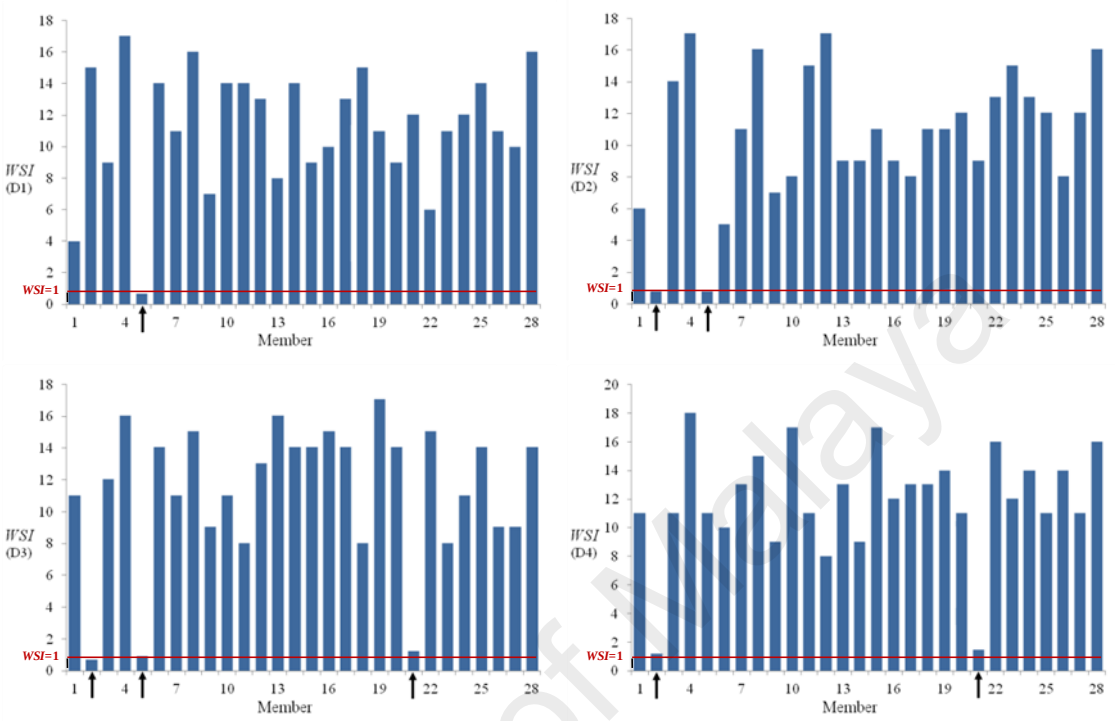

Figure 5.34: *WSI* index of the first 4 damage scenarios using FE dynamic analysis and FRF identification method in ICATS

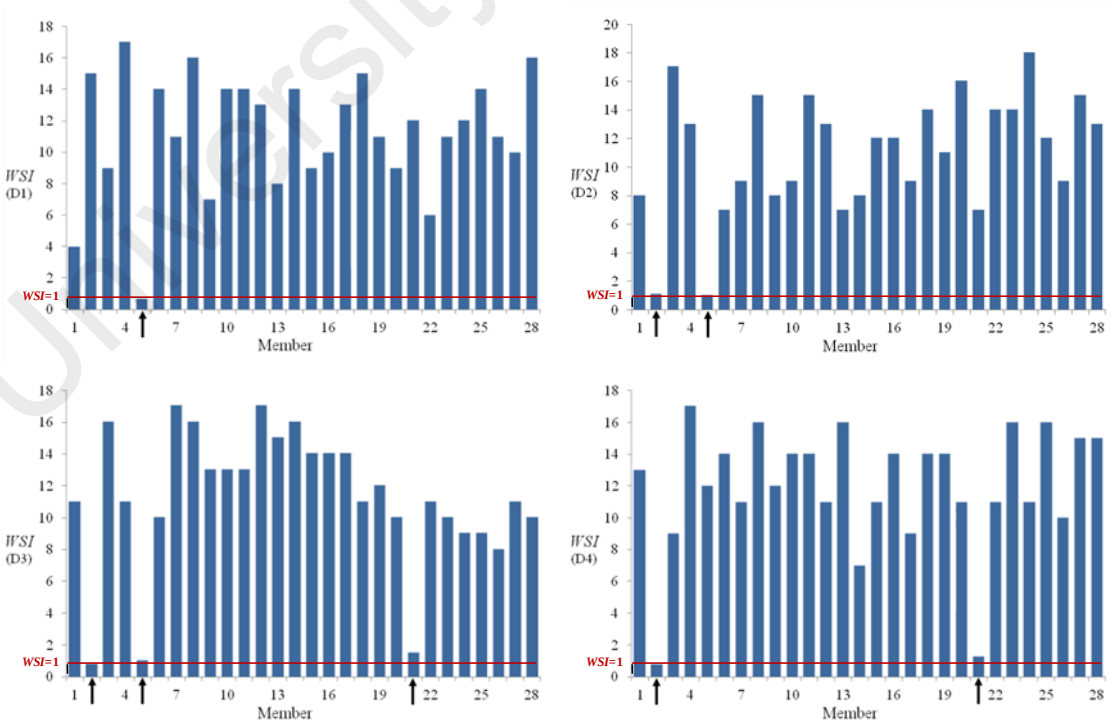

Figure 5.35: *WSI* index of the first 4 damage scenarios using FE dynamic analysis and EFDD identification method in ARTeMIS

5.5.1.2 Experimental Results

Figure 5.36 and Figure 5.37 are presenting the *WSI* index of the first four damage scenarios of experimental modal analysis. Figure 5.36 shows the case which modes are identified and normalized using FRF and Figure 5.37 is showing the case which modes are identified using ARTeMIS and normalized using mass change method. Unlike FE dynamic analysis, almost none of the damaged member's indices are less than one. However, in all cases, the index values are low enough for damaged members to be distinguishable. The worse results are for *WSI* value of beam 5 (member 21) in D3 and D4.

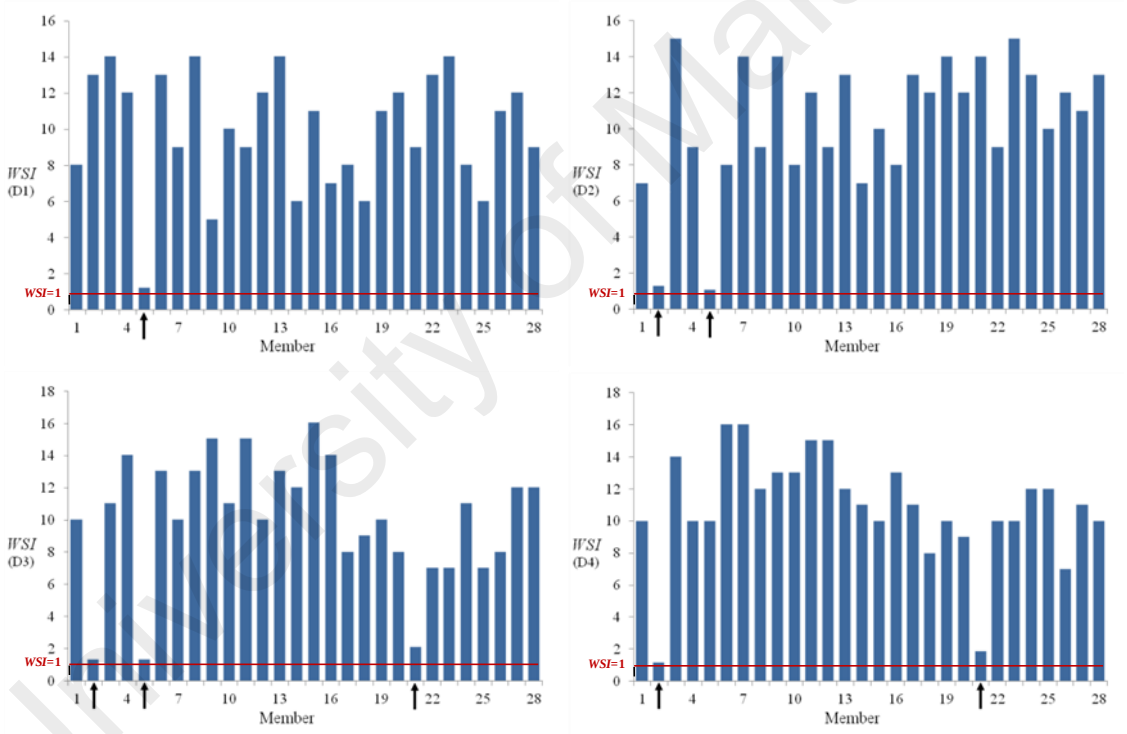

Figure 5.36: *WSI* index of the first 4 damage scenarios of the experiment using FRF identification method in ICATS

In general, in this type of structures, damage in columns is much easier to be detected than in beams. There are two reasons for this. The first reason is the geometry. In a frame structure, columns are in line with each other. So any change in the stiffness of a column alters more entries of the stiffness matrix than those of a beam. In other word, damage in columns has more "global influence" than damage in beams. This makes it

easier to identify change of stiffness in a column. The second reason is that the beams of these types of frame structures are smaller than the columns. So their stiffness change is less effective in the stiffness or flexibility matrix.

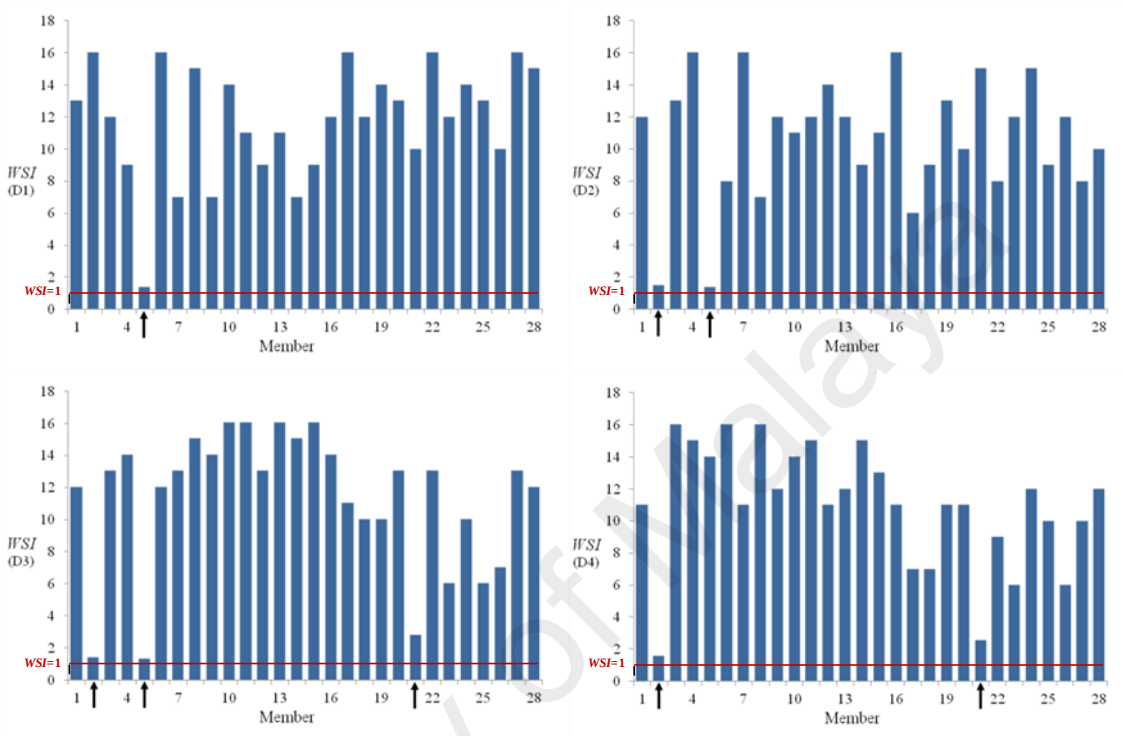

Figure 5.37: *WSI* index of the first 4 damage scenarios of the experiment using EFDD identification method in ARTeMIS

5.5.1.3 Effect of Absence of Higher Modes

To study the effect of the number of detected modes, particularly higher modes on the accuracy of this method, the experimental results have been repeated using only th**e** first 6 modes. The results of this test are presented in Figure 5.38 and Figure 5.39. The results are showing that for the first two damage scenarios where only columns are involved, the damaged members are easily identified, although the index is higher than one. However in damage cases 3 and 4 beam 5 is not undoubtedly distinguishable as the damaged member. This interesting observation agrees with the previous statement about sensitivity of columns and beams in this method. Since damage in a column has more global effect on the stiffness matrix, it is detectable using only the first 6 modes which

are also more global. Although when it comes to a beam with more of a local influence on stiffness matrix, the presence of higher more local modes is vital for detecting damage on them.

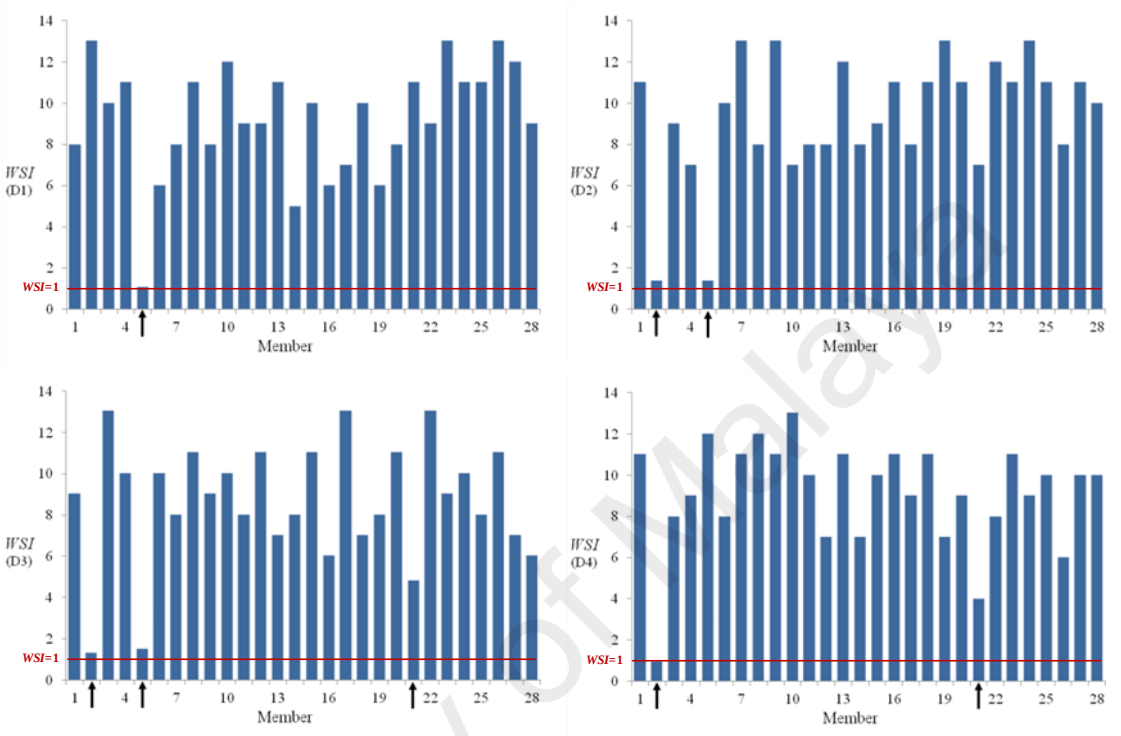

Figure 5.38: *WSI* index of the first 4 damage scenarios using the first 6 modes (Experiment- FRF)

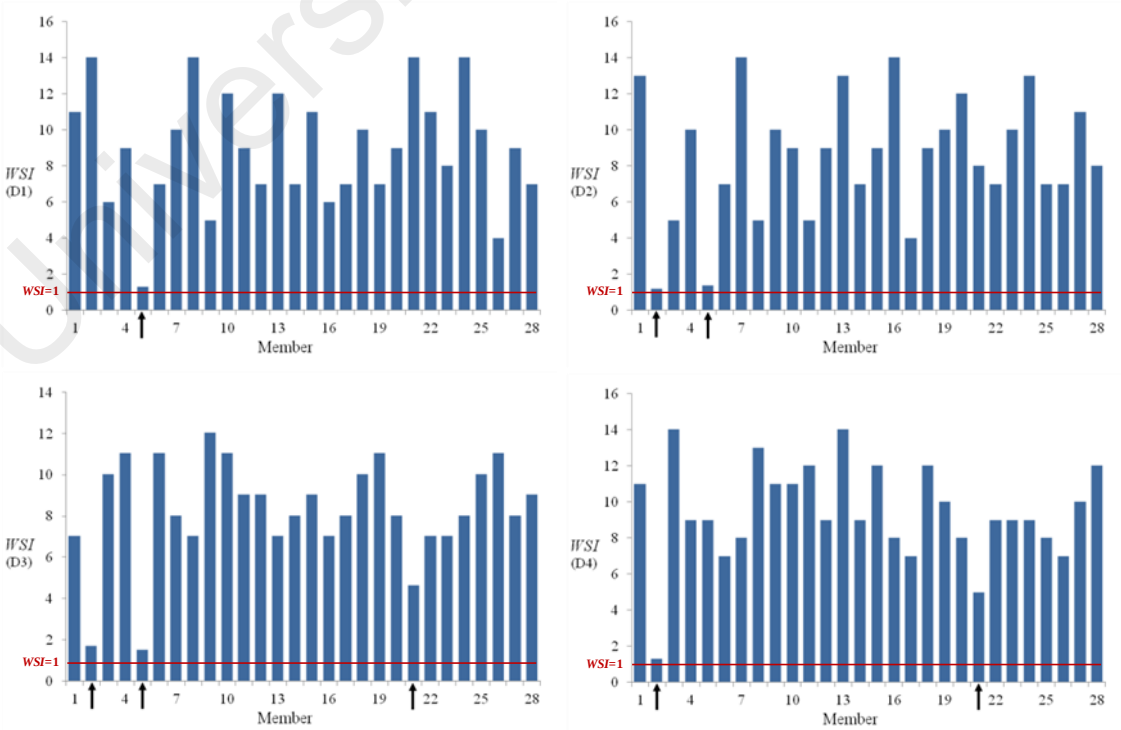

Figure 5.39: *WSI* index of the first 4 damage scenarios using the first 6 modes (Experiment - ARTeMIS)

5.5.2 Utilizing CMCM as Damage Indicator

5.5.2.1 Damage Detection based on CMCM

Originally, CMCM is a model updating method. However its ability to track changes on the stiffness of the members makes it a possible damage indicator. CMCM as damage detection method has some advantages over DLV. The most important advantage is that it does not need mass normalized mode shapes and works with any arbitrary scale. This alone is important enough, because scaling mode shapes in OMA analysis is not so easy and straightforward. However, there are some other aspects in favour of DLV. Unlike DLV that works with the more global "Flexibility Matrix", CMCM needs local "Stiffness Matrix". Flexibility matrix is global and so it converges by using lower frequency modes. However stiffness matrix cannot be extracted from these modes. So the stiffness matrix of the experimental model is not available. The only way it can be estimated or better to say approximated is by updating the FE model.

Implementing CMCM so that it can be used as damage detector has two main steps:

1- First step is to update the FE model using the experimental results of damaged structure. To achieve the best results, the updating process must be performing as accurate as possible.

2- The updated FE model should then be updated against experimental results of undamaged structure.

Lets K and M be the stiffness and mass matrices of FE model. Equations 5.4 and 5.5 are used to update matrix K and M:

$$C_{n,ij} = \frac{(\phi_i)^T K_n \phi'_j}{(\phi_i)^T K \phi'_j} \tag{5.4}$$

$$D_{n,ij} = \frac{(\phi_i)^T M_n \phi'_j}{(\phi_i)^T M \phi'_j} \tag{5.5}$$

where ϕ_i is the i^{th} mode shape of FE model and ϕ'_j is the j^{th} mode shape of damaged model obtained experimentally. The process of updating is similar to what has been presented before and is not repeated here. Now let's K^* be the stiffness matrix of FE model after being updated by damaged results. The second step is updating K^* using experimental results of undamaged structure, as shown in Equation 5.6:

$$C_{n,kl} = \frac{(\phi'_k)^T K_n^* \phi''_l}{(\phi'_k)^T K^* \phi''_l} \tag{5.6}$$

where ϕ'_k is the k^{th} mode shape of updated FE model and ϕ''_l is the l^{th} mode shape of undamaged experimental model. $C_{n,kl}$ is then used to estimate stiffness correcting factor. Any member with stiffness correcting value more than one is marked as damaged member. Besides, the correcting value itself is a good measure of damage severity.

Since this method is based on comparing the two sets of modal frequencies and mode shapes, a question might rise that why modal properties of undamaged and damaged state of the model cannot be compared right away to calculate *C*. The answer is simple; because in that case *K* is not available. This is the key point of this method. Since stiffness and mass matrices are not available in the actual model, it uses FE model to intervene between the two sets of data. Since mass and more importantly stiffness matrices are available in FE, they can then be used to relate frequency and mode shape

changes to the DOFs and geometry of the structure. So to achieve the best results using CMCM, it is important to do an accurate FE modeling and updating.

Figure 5.40 is presenting the results of damage detection using CMCM for the first 4 damage scenarios. As it shows, the method clearly identifies all damaged members. Moreover, the correcting factors associated with each damaged member are corresponding with their damage severity which is around 30 to 35% in this case.

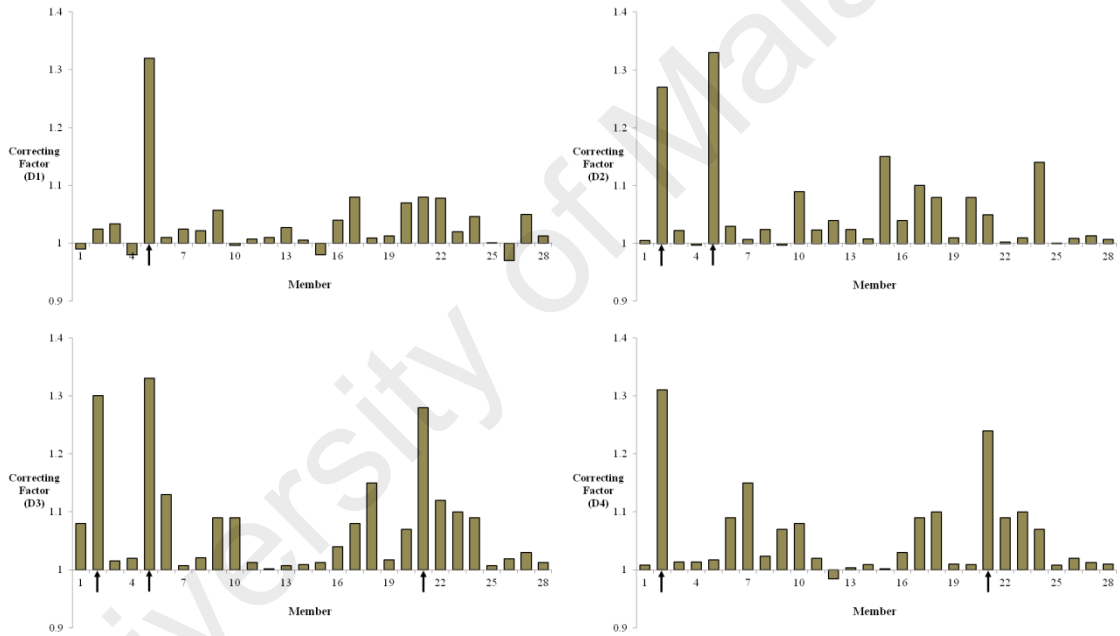

Figure 5.40: Damage detection using CMCM

However the correcting factor value of 1.3 in Figure 5.40 are clearly identifying them as damaged members, but the results are also showing relatively high values for intact members too. However there is a significant difference between the calculated value of damaged members and mistakenly identified intact members, but this error causes uncertainty on damage localization and is a flaw of this method. Close examination of the geometry of the structure reviles that in most cases, the incorrectly detected

members are at one end connected to the damaged member. Since damage in a member alters DOFs of its two ends, it indirectly influences the other members that are in one end connected to those DOFs. This can help to do a better judgment on pointing to the damaged member.

5.5.2.2 Enhancing DLV using CMCM Indicator

While CMCM based detection method that is presented here and DLV method are both showing some major errors in detecting damaged members, particularly in multi damage scenarios, but there is an interesting difference between their types of error. An overall investigation of all the damage detection results that are obtained using DLV suggests that the errors of this method are generally similar to what is known as "Type II" error. On the other hand, results of CMCM are suggesting that this method in general suffers from what is known as "Type I" error.

Let's define these two types of error and their differences, but to do so, let's briefly define a statistical term called "null hypothesis". In statistics, the term "null hypothesis" refers to a general statement or default position that there is no relationship between two phenomena (Everitt, 1998). This definition is generally used in social science and this study has nothing to do with statistic. However this term can somehow be redefine to suit the purpose of this study. Let's say that in this case, the default state of each member in each set of damage detection analysis is being undamaged. In other word, the "null hypothesis" of each member is for it to be undamaged. So the job of the detection method is to simply "reject" this hypothesis or default state whenever it comes to a damaged member. Now let's see in how many ways a detection method might fail doing its job.

Type I error, also known as false positive, is defined as "incorrect rejection of a true null hypothesis". It means the null hypothesis is actually true, but the method incorrectly rejects it. Reminding that a true null hypothesis in this case means the member is actually undamaged, then "incorrect rejection" of it means that the detection method incorrectly marked an intact member as damaged. On the other hand, type II error, also known as false negative, is defined as "the failure to reject a false null hypothesis". It means the null hypothesis is actually false, but the method fails to rejects it. Again, reminding that when the null hypothesis is false, it means that the member is damaged. So the detection method should be able to reject the null hypothesis, but it fails and marks a damaged member as intact. It is clear that although these two examples are both called error, but they are so different and has different impact on the final results and conclusions.

A closer look at all the results obtained from CMCM and DLV shows that CMCM is generally suffering from "type I" error. As it rarely fails to detect a damaged member, but it occasionally marks some undamaged members as damaged. In contrary, results of DLV are suggesting that it generally suffers from "type II" error. As it rarely marks an undamaged member as damaged, but it sometimes fails to detect an actual damaged member. It should be noted that this statement is not ruling out the effect of other sources of error. "CMCM rarely fails to detect damaged member" does not imply that this method is always successful on locating damaged member. The ability and accuracy of any damage detection methods depends on many external factors e.g. modal testing set up, equipments, quality of raw data, method of modal analysis, accuracy of extracted modal parameters, accurate numerical simulation of the model etc. Assuming that most of these factors are considered and are in their best shape possible, there are always imperfections that cause errors and uncertainty. The statement above is

describing how these errors are influencing the final results and which conclusion made by those results are more uncertain.

It should be emphasized that the DLV's error type that is explained here as being false negative should not be misunderstood and being compared by the term "false positive" that is discussed in earlier studies by (An, et al., 2014; Gao, 2005; Gao, et al., 2007). The false positive detection that is reported by them is referring to a problem caused by insufficient number of measurement points. This causes the absence of a damage locating vector between two or more members and if one of those members is damaged, it is possible that other members be falsely marked as damaged. This issue is further described in 5.6.1.

The important point of describing types of errors is that when there are two methodologies to address a problem, each with one of the two types of error, they are able to cancel each other's uncertainty in some extend. Figure 5.41 is presenting the results of DLV method for damage scenarios D7 to D10. These damaged cases are chosen since they involved two damaged beams and the results of DLV are very uncertain to detect these damaged members. The reason is that the *WSI* index calculated for damaged members, particularly beams are way above one which is the suggested limit for damaged member to be detected. Furthermore, the *WSI* indices of undamaged members are as low as 6 for some cases. For example *WSI* index of the damaged beam B6 (member-22) in D8 scenario is 5.1 while the *WSI* of undamaged beams B2, B5 and B11 (members 18, 21 and 27) are 6. This makes it very difficult to assertively detecting the damaged member.

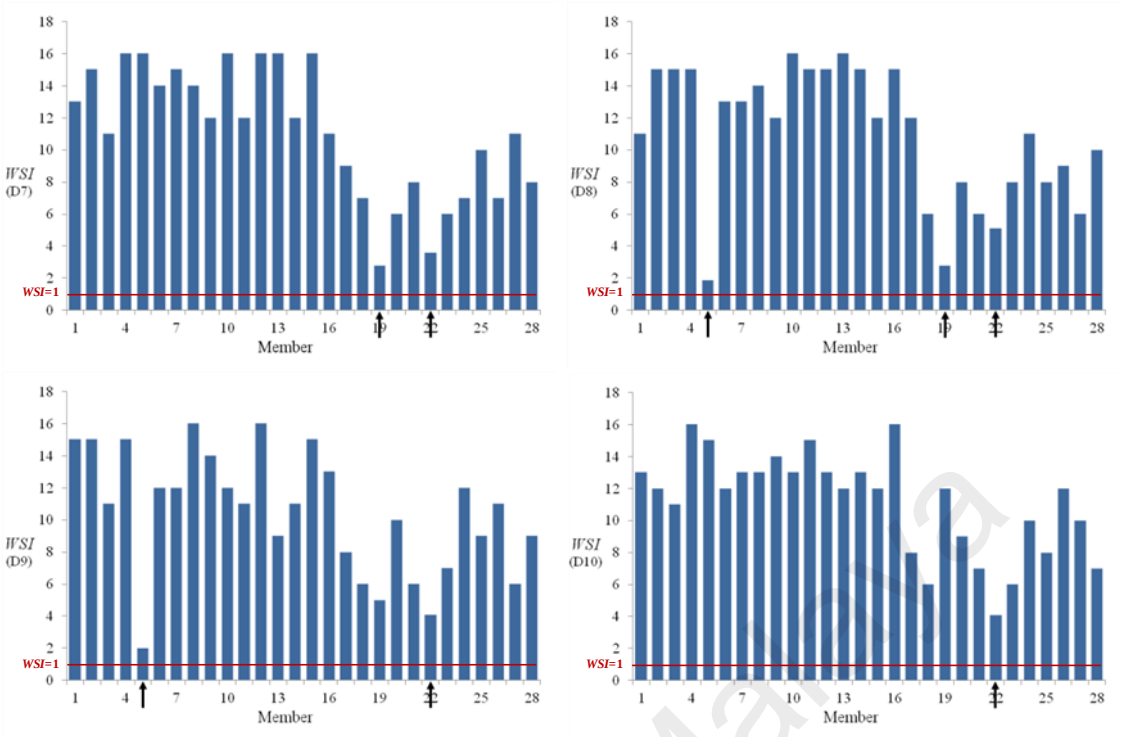

Figure 5.41: Results of DLV for damage scenarios D7 to D10. (Output only)

In Figure 5.42 and Figure 5.45, the left diagrams are presenting the results of CMCM damage detection for damage scenarios D7 to D10 respectively. As mentioned before, since the nature of error in this method is type I, all damaged members are detected, but meanwhile many undamaged beams are also having significant value of correcting factor which is a false positive. In Figure 5.42 and Figure 5.45, the right diagrams are showing the results of CMCM that are normalized by *WSI* index respectively. The normalizing process is very straight forward, simply dividing the correcting factor by *WSI*. Although since the scale of correcting factor starts from 1, it is first subtracted by 1 as shown in Equation 5.7;

$$i = \frac{(\alpha - 1)}{WSI} \tag{5.7}$$

where α is correcting factor and i is the normalized damage indicator. The value of i itself has no particular meaning and it is just a ratio between the lower and higher points

of the diagram. So it is again normalized to one to make it more sensible. The results of normalized damage indicators are showing that combining the two damage detection methods is significantly improving the reliability of the final results.

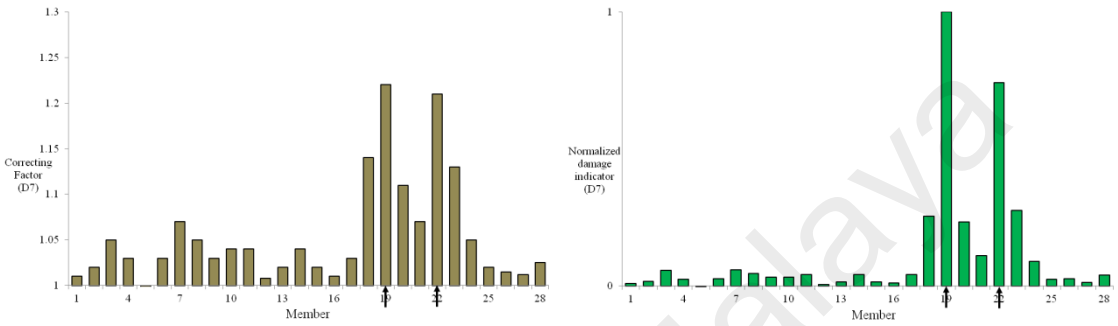

Figure 5.42: CMCM damage detection (left) and CMCM normalized by *WSI* (right) for D7

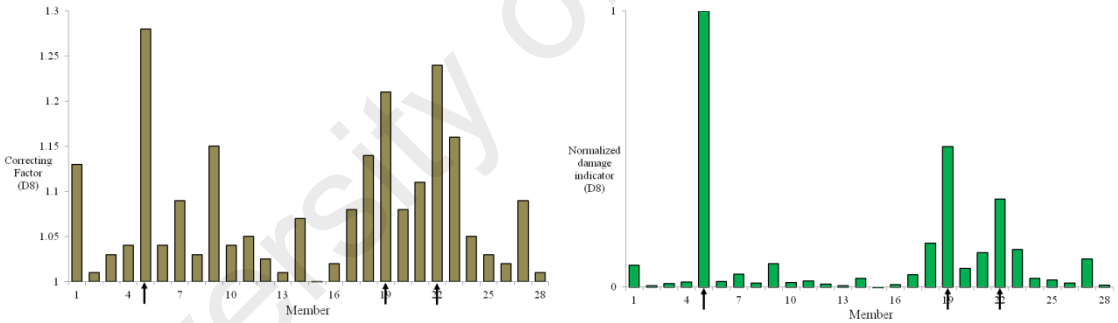

Figure 5.43: CMCM damage detection (left) and CMCM normalized by *WSI* (right) for D8

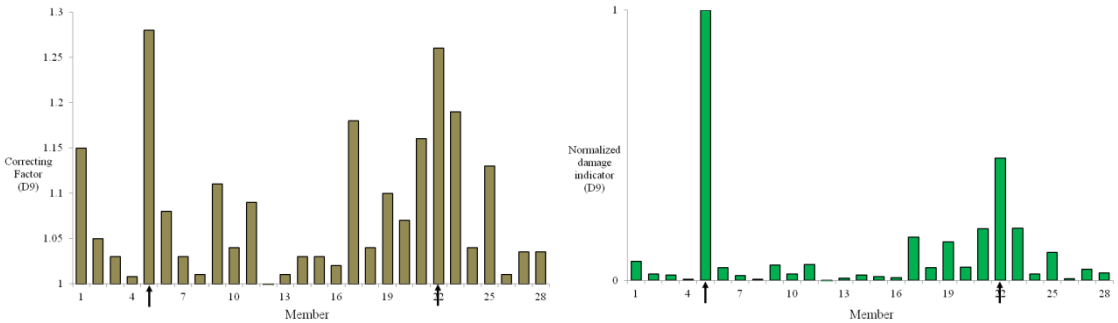

Figure 5.44: CMCM damage detection (left) and CMCM normalized by *WSI* (right) for D9

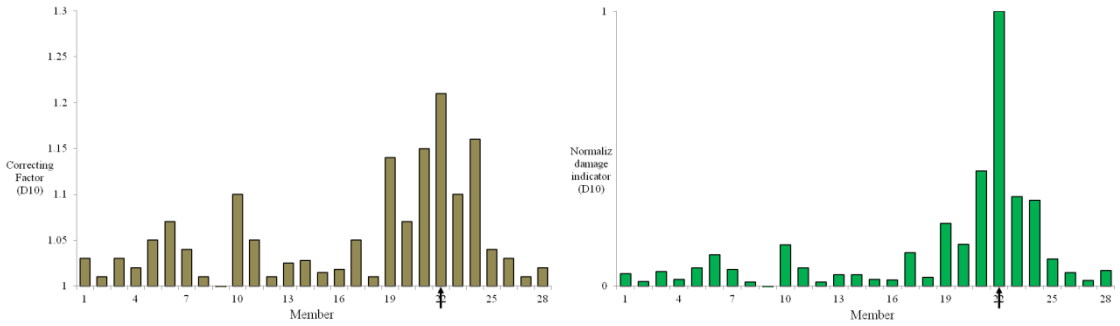

Figure 5.45: CMCM damage detection (left) and CMCM normalized by *WSI* (right) for D10

5.6 Damage Detection using Incomplete Measurements

5.6.1 "False positive" in DLV

False positive detection in DLV is one of the issues that is reported and discussed in a number of studies. This is when the method calculates zero or small stress for an undamaged member and identifies it as being damaged. False positive detection is not a drawback of the DLV method itself. It is the result of using DLV when the number of sensors is less than the number of DOFs i.e. incomplete measurement. In this case, the load vectors are not calculated for all degrees of freedom or nodes. In a frame or truss structure for example, this might cause zero stress for an intact member that is connected to a damaged member, simply because no other load vector is available between the two to balance the stress.

(Gao, 2005; Gao, et al., 2007) presented the experimental verification of DLV method. They tested a 5.6 m long, three-dimensional truss structure at University of Illinois. In both of their single damage scenarios, two intact members were falsely identified as damaged along with the damaged member. They explained that when the number of sensors is increased, the likelihood of false identification of damaged elements is significantly reduced. Briefly, their methodology was based on dividing the structure to different sections and using smart sensor network to measure the required DOFs.

Another study of this type is conducted by (An, et al., 2014). They tested an 8 m long, three-dimensional truss structure and used SDLV to detect damage scenarios under ambient vibration. Noting that their objectives and methodologies were different from those in this study, but they've also encountered and addressed DLV's false positive detection due to incomplete measurement. They've stated that "*when limited sensors of the detected structure or substructure are used to build the flexibility matrix, the SDLV method can only tell the damaged section which contains the damaged elements and false positives. Thus, if the exact damaged elements are required, the second step of damage detection should be conducted again in the damaged section with measured nodes from all nodes in this section*". In other word, in a structure with a big number of DOFs, test can be conducted in various stages. First a limited number of sensors can be used to approximate the location of damage and then a finer measurement setup is used to accurately locate the damaged member.

Although their solution is simple and practical, but it is based on the assumption that all the structure is potentially accessible and the reason for incomplete measurement is limited number of sensors or impracticality of a complete measurement. However in case of this study, the frame structure is not so large and so a complete measurement is practical. The assumed reason behind incomplete measurement is that certain part of the structure is difficult, expensive or even impossible to be measured. In this case, if the results of incomplete measurements are indicating that the damage is located in that section, it is not possible to redistribute the sensors in that area to further identify the damaged member. So at this part, the focus of this study is to find a way to rule out the false positive detections of DLV without redistributing the sensors.

5.6.2 Incomplete Measurements Results

To study the possibility of detecting damaged members when their corresponding DOFs are not measured, the data of the first 12 DOFs are eliminated in the analysis. These 12 DOFs are connected to columns C1 to C8 and beams B1 to B4 which means they effect the detection of damage in these members. Four damage scenarios D1, D2, D6 and D7 are involved with these unmeasured members and are selected to study the effect of incomplete measurements on DLV results.

As the first step, *WSI* index of all members are calculated for these 4 damage scenarios. As described before, damage locating vectors are load vectors that are applied to the location of sensors in a way that they cause zero or negligible stress on damage member. For example in case column 5 is damaged, the corresponding locating vectors of the two ends of the column i.e. nodes 5 and 9 are calculated in a way that they cancel each other and also the effect of any other force that is acting on the member. Now the question is that what if DOFs of one end of the member are not measured? For example in case of column C5, if the DOFs of node 5 are not measured it means no load vectors are calculated for one end of the member. So how the load vectors at node 9 can impose zero stress on C5 without the presence of counteracting load vectors at node 5? To answer this, it should be reminded that considering columns C1 and C5 as two different members is only valid if a node is defined between them. However since node 5 is not measured, in DLVs point of view columns 1 and 5 are not two separate members, instead it is one long element which is stretched between nodes 1 and 9. So damage in column 5 makes the load vectors at node 9 to be equal to its corresponding reaction force in node 1. In this case, the calculated *WSI* index is small not only for column 5, but also for column 1 which DLV sees it as part of the same member. This is what has been referred to as “false positive detection”, which in this case column 5 is the actual damaged member and column 1 is falsely detected by DLV.

Figure 5.46 is presenting the *WSI* index of four selected damage scenarios using incomplete measurements. As explained above, for damage scenario D1, although only column 5 is damaged, the *WSI* index of column 1 is also small. What can be concluded from this Figure is that if *WSI* index of two members that are in line with each other are small, considering that the connection of the two members are not measured, at least one of the two members are damaged. Another consideration in this Figure is that the *WSI* index of members 17 to 20 (beams B1 to B4) are also small. This could be easily described, considering that none of the DOFs of these members are measured and the small stress values of these members are in fact caused by the deformation of columns attached to them.

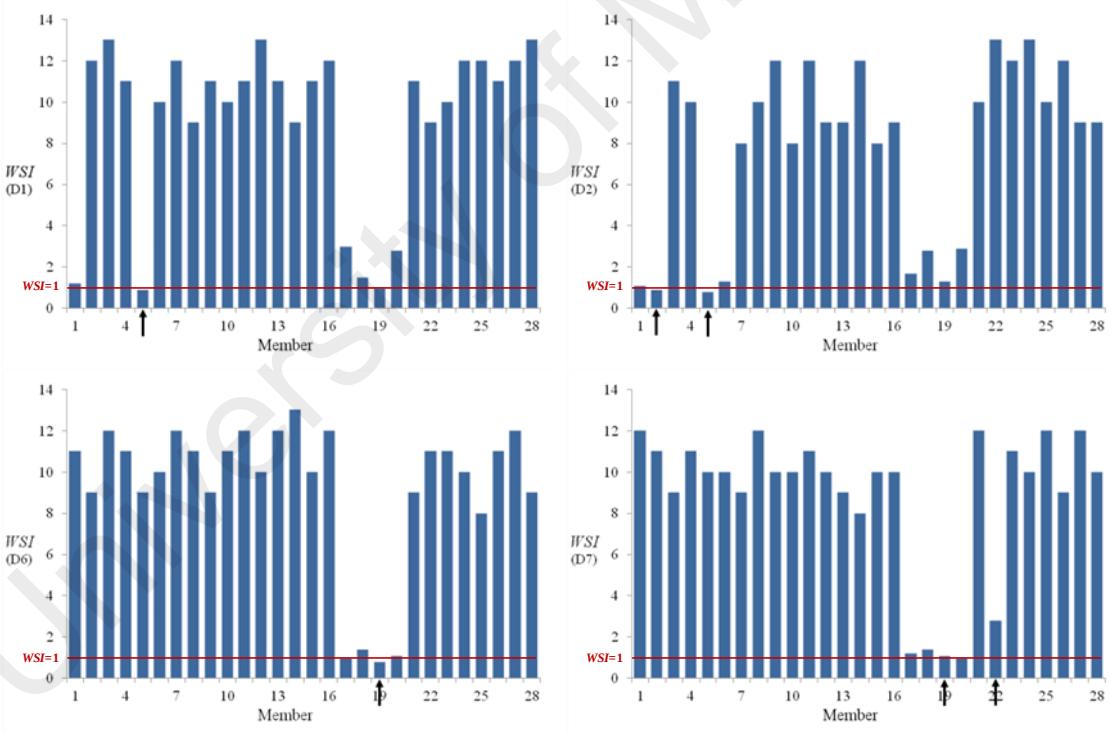

Figure 5.46: *WSI* index of D1, D2, D6 and D7 obtained using incomplete measurements

In case of D2 which columns C2 and C5 are damaged, the results are showing the same thing. Column C1 is below C5 and C6 is above C2. So existence of damage in columns C2 and C5 causes *WSI* index of C1 and C6 to be calculated low too i.e. false positive

detection of C1 and C6. In case of D6 which beam B3 (member 19) is damaged the *WSI* index of the beam is low. However noting can be concluded from this value since it is not really caused by damage in the member; instead it is caused by absence of load vectors at this member. It can be seen in this Figure that the *WSI* of all beams in that section are low and not just beam 3. The last damage scenario, D7, is the case which beam 6 (member 22) is damaged. Since it is known that both ends of this beam are measured, then the low value of *WSI* is an indication of damage in this beam.

The results of these four damage scenarios presented in Figure 5.46 shows that in case of incomplete measurements, DLV can in some cases approximate the damaged member. However even this approximation needs extra consideration on the geometry of the structure and the position of unmeasured DOFs. In case of columns, it is possible to detect the damaged leg in general, but not the actual damaged member. In case of unmeasured beams, DLV completely fails to locate damaged member. In case which damaged member is within the measured part of the structure, DLV works as usual.

5.6.3 Enhancing DLV using Frequency Shift Method

Obviously the main issue with incomplete measurements is that the mode shape vectors are not entirely available, however it does not affect the accuracy of estimated modal frequencies. In fact modal frequencies can be estimated using even a single sensor which is mounted in the right position. Consequently, the incomplete measurements only affect damage detection methods which are employing mode shapes, like it considerably affect the reliability of DLV. Considering this, a frequency based damage detection method should be a better choice in case of incomplete measurements. This is true; except that despite of complete or incomplete measurements, frequency based damage detection methods are not so reliable when it comes to damage location. However in case of incomplete measurements, pairing two or more detection methods

that are using different approaches can improve the accuracy of the final results i.e. enhancing the approximate predictions of DLV using a frequency based approach. In other word, the goal of the proposed frequency method is not to detect and locate damaged members throughout the structure. It only needs to rule out the false positive detections of DLV.

For this purpose, a complementary method is presented here that approximately indicates the damaged member using natural frequencies only. This method in general is based on categorizing the pattern of frequency shifts due to different damage scenarios and comparing them with the frequency shift that is estimated in the experiment. In order to generate sets of frequency shifts that are corresponding to the stiffness lost of unmeasured members, the finite element model of the frame structure should first be updated in respect to the experimental data. This condition indicates that although this method is using frequencies only, but it still relies on mode shapes and cannot be used independently. As it was mentioned above, it is more of a complementary method to increase the accuracy of the existing mode shape based method.

The results of model updating using incomplete measurements are presented in chapter 5.4.2. Different damage scenarios are then simulated using the updated finite element model. In this case, 8 columns and 4 beams are connected to the unmeasured nodes and need to be examined i.e. beams 1 to 4 and columns 1 to 8. In each scenario, the Young's Modulus of the member is reduced by 70% and new sets of natural frequencies are measured using FE dynamic analysis and ARTeMIS.

Table 5.3 is presenting the estimated frequencies of updated undamaged FE model for the first 9 modes. It is also presenting the percentage of frequency shift caused by each damage scenario in respect to the undamaged frequency. The results are also visualized

in Figure 5.47 and Figure 5.48. These graphs are demonstrating that each simulated damage scenario has a particular frequency shift pattern which is different from the others. However the level of this dissimilarity varies from case to case which can be measured by their correlations. It should be mentioned that beam B6 is included in this analysis although it is not among unmeasured members. It is because B6 is one of the two damaged members of damage scenario D7 and has been previously detected as possible damaged member using DLV.

Table 5.3: Frequency shifts caused by stiffness reduction in unmeasured members

	U (Hz)	Frequency shifts in respect to U (%)												
		B1	**B2**	**B3**	**B4**	**B6**	**C1**	**C2**	**C3**	**C4**	**C5**	**C6**	**C7**	**C8**
1	**4.68**	0.39	0.00	0.39	0.00	0.00	0.83	0.81	0.83	0.83	0.32	0.32	0.32	0.32
2	**5.68**	0.00	0.37	0.00	0.37	1.36	0.69	0.65	0.65	0.69	0.24	0.26	0.26	0.24
3	**9.47**	0.08	0.11	0.08	0.11	0.31	0.54	0.52	0.52	0.54	0.53	0.52	0.51	0.53
4	**30.82**	0.19	0.34	0.38	0.08	0.15	0.56	1.02	1.50	1.09	0.26	0.49	0.71	0.53
5	**32.56**	0.19	0.30	0.07	0.19	0.15	0.89	1.26	1.08	0.71	0.45	0.63	0.52	0.33
6	**40.87**	0.20	0.07	0.07	0.50	0.07	1.73	0.73	0.40	1.33	0.93	0.43	0.27	0.73
7	**62.95**	0.30	0.30	0.30	0.29	0.39	0.96	1.08	1.04	0.95	1.32	1.49	1.46	1.28
8	**73.45**	0.01	0.13	0.11	0.01	0.22	1.17	1.21	1.50	1.21	0.39	1.53	2.43	1.50
9	**85.72**	0.29	0.33	0.28	0.33	0.79	0.99	1.63	1.90	1.64	0.59	1.12	0.66	0.32

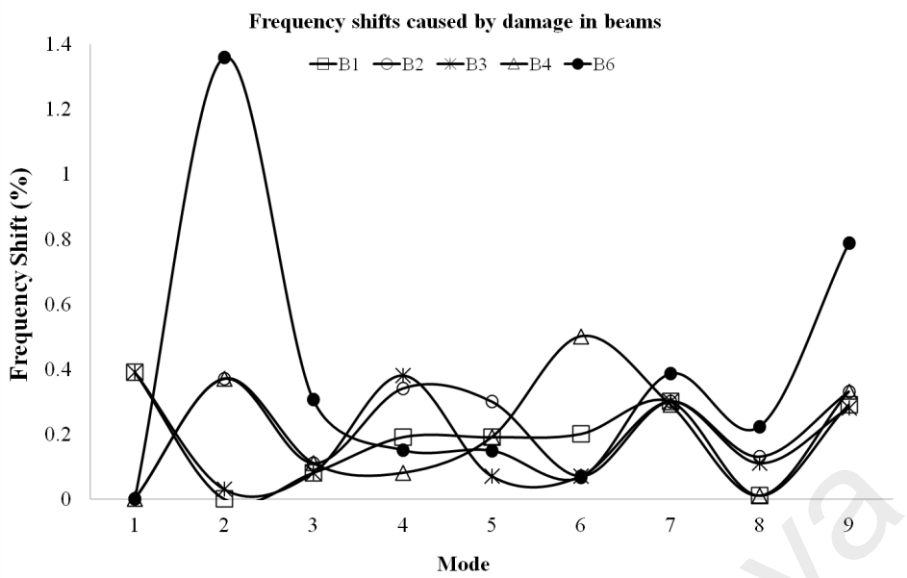

Figure 5.47: Frequency shifts caused by stiffness reduction in beams

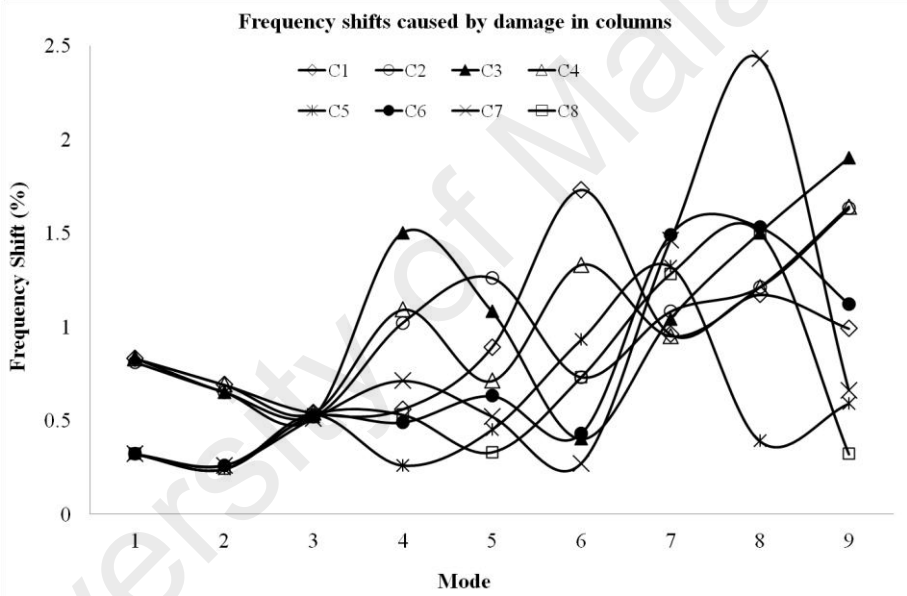

Figure 5.48: Frequency shifts caused by stiffness reduction in columns

Table 5.4 is presenting the cross correlation of frequency shifts of all members. For example, the correlation of columns C2 and C3 is 0.89, indicating that the frequency shifts caused by stiffness reduction in these two members are relatively similar. On the other hand, correlation of columns C2 and C5 is 0.08 which shows that the stiffness reduction in these two members cause different patterns of frequency shifts. Knowing the frequency shift cross correlations of all the members is particularly important, because if the experimental data are showing similar pattern with C2 and C3 for

instance, it is not likely that they are both responsible for that frequency shift. Instead, one of the two columns e.g. C2 is in fact the damaged member and C3 is correlated with the experimental data, only because it is correlated with C2. This issue is signifying that correlation alone is not a reliable damage indicator, because it is also possible for undamaged members to have significant correlation with the experimental data and this happens more than often.

To discriminate these two conditions, let's use the term "explain" instead of the general term "correlate". So in this case, the results of both C2 and C3 are correlated with the experimental data, but only C2 is in fact explaining it i.e. C2 is "explanatory variable" of experimental data. C3 is correlated with the experimental data, only because it is correlated with its explanatory variable. Let's be reminded that C2 and C3 are used here just as an example.

Table 5.4: Cross correlation of frequency shifts of unmeasured beams and columns

Corr.	B1	B2	B3	B4	B6	C1	C2	C3	C4	C5	C6	C7	C8
B1	1												
B2	-0.17	1											
B3	0.77	-0.01	1										
B4	-0.01	0.30	-0.41	1									
B6	-0.41	0.62	-0.36	0.44	1								
C1	0.12	-0.37	-0.24	0.53	-0.27	1							
C2	0.30	0.42	0.32	-0.02	0.00	0.15	1						
C3	0.16	0.45	0.48	-0.28	0.05	-0.14	0.89	1					
C4	0.26	0.07	0.28	0.32	-0.03	0.59	0.65	0.60	1				
C5	0.37	-0.02	0.07	0.51	-0.16	0.50	0.08	-0.16	0.23	1			
C6	0.03	0.16	0.15	-0.10	-0.05	0.23	0.63	0.58	0.43	0.49	1		
C7	-0.25	-0.01	0.06	-0.38	-0.15	0.15	0.40	0.48	0.25	0.18	0.87	1	
C8	-0.17	-0.18	0.01	-0.14	-0.29	0.38	0.14	0.15	0.22	0.50	0.79	0.89	1

5.6.3.1 Damage Scenario D1:

Figure 5.49 is illustrating the correlation of frequency shifts between all unmeasured members and experimental data of damage scenario D1 (Refer to Table 4.3). Two members are demonstrating high similarity with the experiment i.e. C5 and C6. However the correlations of B4, C1, C2 and C8 with D1 are also relatively high which could be sign of a multiple damage scenario.

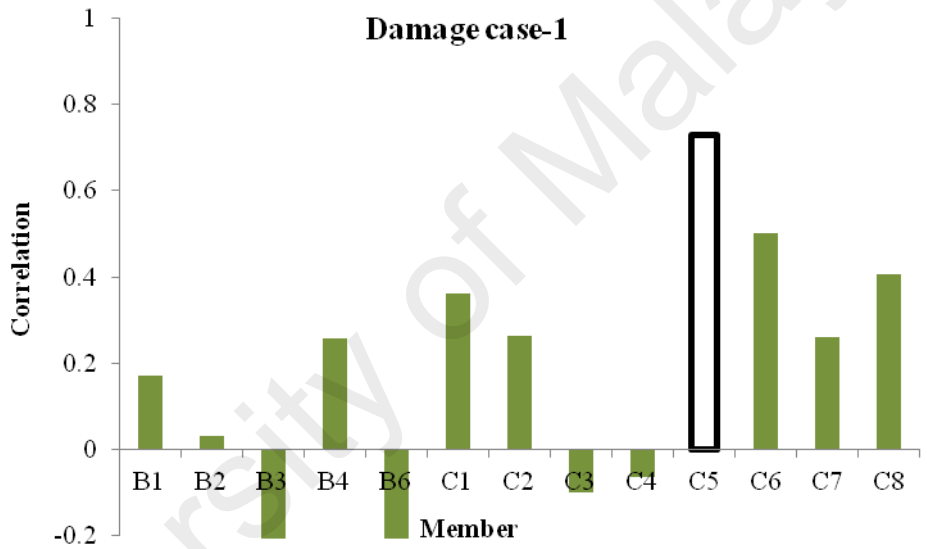

Figure 5.49: Correlation of frequency shifts between all unmeasured members and D1

To narrow down the number of possible damaged members, these results should be compared with the results of DLV in Figure 5.46. As described before, DLV is unable to identify damaged member in unmeasured part of the structure. However it is able to indicate the foot of the possible damaged column. In this case, the results of DLV are showing that among 8 unmeasured columns, C1 and C5 are the only possible damaged members. However based on DLV, any of the 4 unmeasured beams could also contribute to the damage scenario.

Referring to Table 5.4, the correlations of C6 and C8 with C5 (the possible damaged member) are around 50% which is relatively high. Assuming that C5 is the sole damaged member, this could explain the similarity between the frequency shifts of these two columns with experimental data. Figure 5.49 is showing that the similarity of C1 with experimental data is considerably lower than C5, which indicates that C5 is the likely damaged member. The high value of cross correlation between C1 and C5 (Table 5.4) also supports this scenario. However the other possibility is that both C1 and C5 are damaged, or perhaps the joint between the two columns is responsible for these results. Furthermore, any of the four beams, especially B1 and B4 are still possible cases which could contribute to this damage scenario.

As stated in APPENDIX 0, multiple regression analysis is also a reliable method to confirm whether C5 is the sole damaged member or not. As a reminder, if two sets of data are both correlated with the experiment, the results of multiple regression analysis can elucidate which one is in fact "explaining" the experimental data and which one is just correlated with the first one.

Figure 5.50 is showing the results of multiple regression analysis of columns C1 and C5. The top-left of this Figure is showing the relationship of C1 with the experimental data of damage scenario D1. The number on the line is called the regression coefficient of C1 and D1 which is 0.36, equal to their correlations which are presented in Figure 5.49. The number on the circle of D1 is called "R-squared" which is the coefficient of determination. In other word, it measures how much of D1 is predicted (or explained) by C1. In this case, the R2 of C1 on D1 is 0.13 (in the scale of 0 to 1) which shows D1 is not being considerably explained by C1.

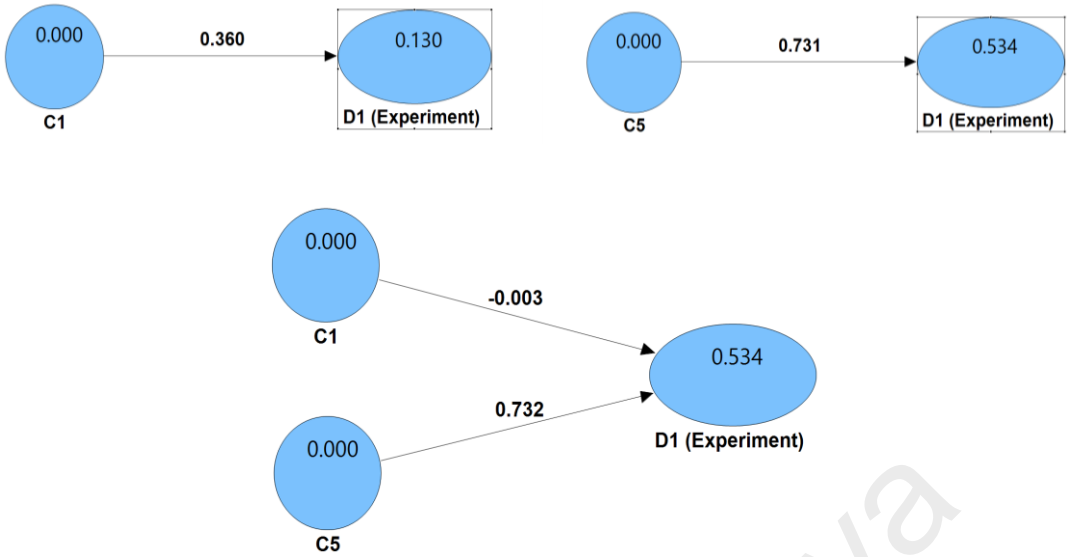

Figure 5.50: Regression coefficients of C1 and C5 with D1 in Smart PLS

The top-right of Figure 5.50 is showing the relationship of C5 with the experimental data of damage scenario D1. The regression coefficient of C5 on D1 is 0.73, also equal to their correlations shown in Figure 5.49. The R2 of C5 on D1 is 0.53 which is relatively high and shows that C5 is predicting D1 notably.

What if the relationships of C1 and C5 with D1 are determined at the same time in one model? The results of this model are presented in the bottom of Figure 5.50. It shows that when C1 and C5 are modelled together, the regression coefficient of C5 is still 0.73, but the regression coefficient of C1 is dropped from 0.36 to zero. It means the regression coefficient of C1 and D1 is entirely absorbed by C5 when it is presented in the model. This clearly indicates that C1 has no genuine relationship with D1 and in fact it is C5 that is fully responsible for the correlation of C1 and D1. In other word, C1 is 50% correlated with C5 (Table 5.4) and C5 is 73% correlated with D1. The result of multiply these two numbers is 0.36 which is exactly the correlation between C1 and D1. This again shows that C1 has no genuine relationship with D1 and it is correlated with D1, only because it is correlated with C5.

The same method can be used for all other members to see whether their relationship with D1 is real or it is through C5. Although the results of DLV are showing that no other column is involved in damage scenario D1, but they are also included. Table 5.5 is presenting the direct regression coefficient and also R^2 of all unmeasured members with D1. It also presents the Effect of C5 on the relationship of all members with D1. The results are showing that almost all the members (except for C6) have insignificant value of R^2 which indicates that D1 is not considerably being explained by them. In some cases, the presence of C5 in the model has dropped the regression coefficient to either zero or a small negative value. For B3 and C2, the regression coefficient is almost the same, with and without C5 being in the model and that is simply because they had no correlation with C5 in the first place. To sum up, either the low value of R^2 or the reduced regression coefficient are indicating that these members are not involved in this particular damage scenario.

However in case of C6, the R^2 is 0.25 which is noteworthy. Although 30% of the original 50% regression coefficient of C6 and D1 is absorbed by C5, but there is still 20% left which indicates a weak independent relationship between C6 and D1. So C6 could be seen as a possible damaged member besides C5. Although there is another factor which is against this possibility. The R^2 of C5 on D1 is 53%. If C6 is the other damaged member, the combination of C5 and C6 should probably have a higher R^2 on D1. However the R^2 of both C5 and C6 on D1 is 56% which is not significantly different. The word probably is used here because in certain conditions, it is mathematically possible that C6 is really damaged, but its presence does not increase the R^2 of C5 on D1. So based on these results, there is still a chance that C6 is damaged too, although not significant enough to doubt the results of DLV.

Table 5.5: Effect of C5 on the relationship of all members with D1

Member	Direct relationship with D1		Regression coefficient when modelled with C5
	Regression Coefficient	R^2	
B1	0.17	0.03	-0.12
B2	0.03	0.00	0.05
B3	-0.22	0.05	-0.28
B4	0.26	0.07	-0.16
C1	0.36	0.13	0.00
C2	0.26	0.07	0.20
C3	-0.10	0.01	0.02
C4	-0.06	0.00	-0.25
C6	0.50	0.25	0.19
C7	0.26	0.07	0.13
C8	0.41	0.16	0.06

5.6.3.2 Damage Scenario D2:

Figure 5.51 is illustrating the correlation of frequency shifts between all unmeasured members and experimental data of damage scenario D2 (Refer to Table 4.3). Three members are demonstrating high similarity with the experiment i.e. C2, C5 and C6. However the correlations of all other members (except for B6) with D1 are relatively high and close to 40%. This is expected since all these members have some level of correlation with either one of C2, C5 or C6, which means they probably have dependent relationship with D1. Unless they are actually the damaged member; which based on these numbers it is not likely the case. B6 is the only member which is not correlated with any of these three and consequently has no dependent relationship with D1.

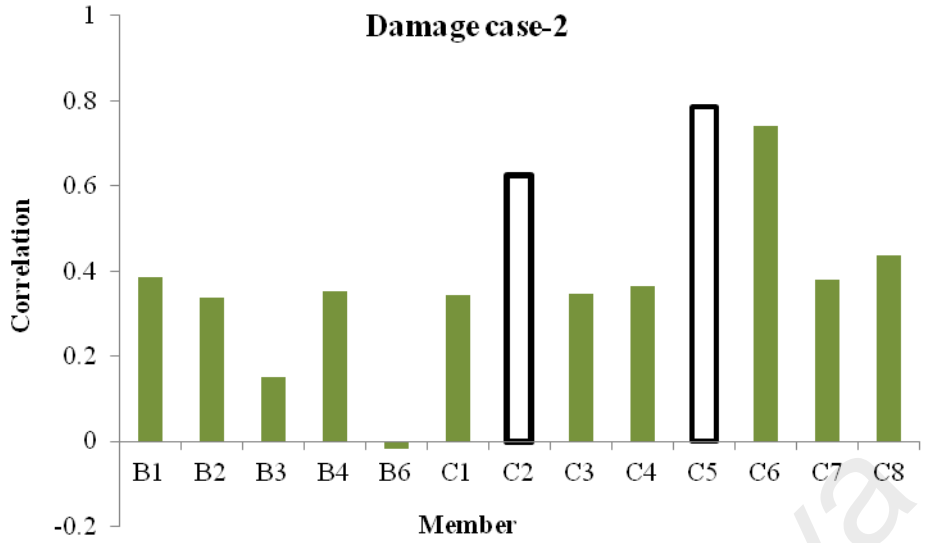

Figure 5.51: Correlation of frequency shifts between all unmeasured members and D2

The results of DLV (Figure 5.46) are showing that columns C3, C4, C7 and C8 are not among the possible damaged members. Furthermore they do not have a high correlation with D1, so these four columns are most probably not involved in this damage scenario. Based on this Figure and also the results of DLV (Figure 5.46), columns C2, C5 and C6 are most likely to be the damaged members. Although C1 does not seem to be able to explain D2 on its own, but it can be part of a multiple damage scenario. It is also possible for any of the beams to be involved in D2 if there is more than one damaged member. Since these results are proposing so many possibilities, regression analysis is the only way to confirm the damaged case.

Since C2, C5 and C6 are the most possible damaged members, first their direct relationship with D2 need to be examined. Figure 5.52 is presenting the regression coefficient and R^2 of these columns to D2. The results are showing that all three members have significant regression coefficient and R^2 in relation with D2. So there is a possibility that all three members are in fact damaged. However since C2 and C6 and also C5 and C6 are correlated, there are two other possibility that need to be examined.

The first is that either C6 has an indirect relationship with D2 through C2 or C5 or even both. The second possibility is that C2 or C5 or even both are in an indirect relationship through C6. C2 and C5 cannot have an indirect relationship through each other, because they are not correlated (Refer to Table 5.4).

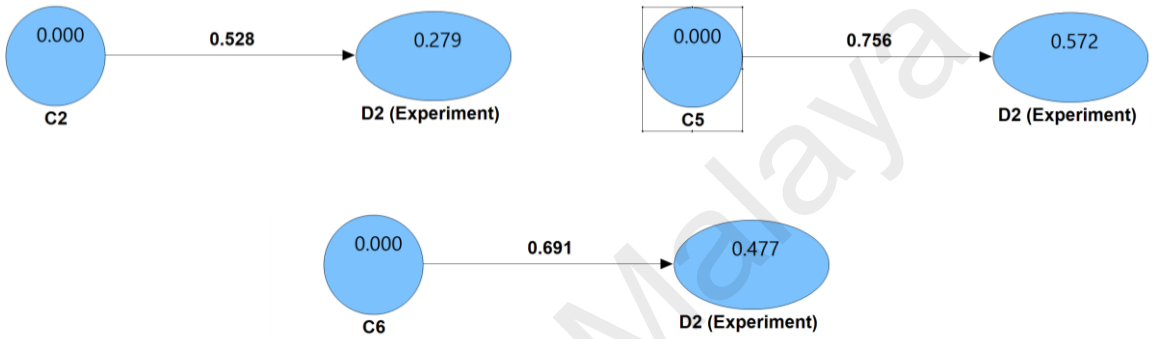

Figure 5.52: Direct relationship of C2, C5 and C6 with D2 in Smart PLS

Figure 5.53 is presenting the regression coefficient of C2, C5 and C6 with D2 in pairs. The results are showing that none of the direct regression coefficients are absorbed by the other column. It suggests that the relationship between these three members and D1 are not through each other. One way of describing this result is that all three members are explaining D2 independently, which means all three members are damaged. Although it is possible, but high values of R^2 is not in favour of this option. Because in case all three members are damaged, the R^2 of them together is expected to be around 0.6 to 0.8. So the R^2 of any two of them cannot be as large as that. In this case, the R^2 of C2 and C5 on D2 is 0.79, which is a very good prediction by itself. Therefore it does not seem to be any room for another variable in this model to determine D2 independently. The best way to answer this is to model all three columns in the same model to see their contribution on prediction of D2.

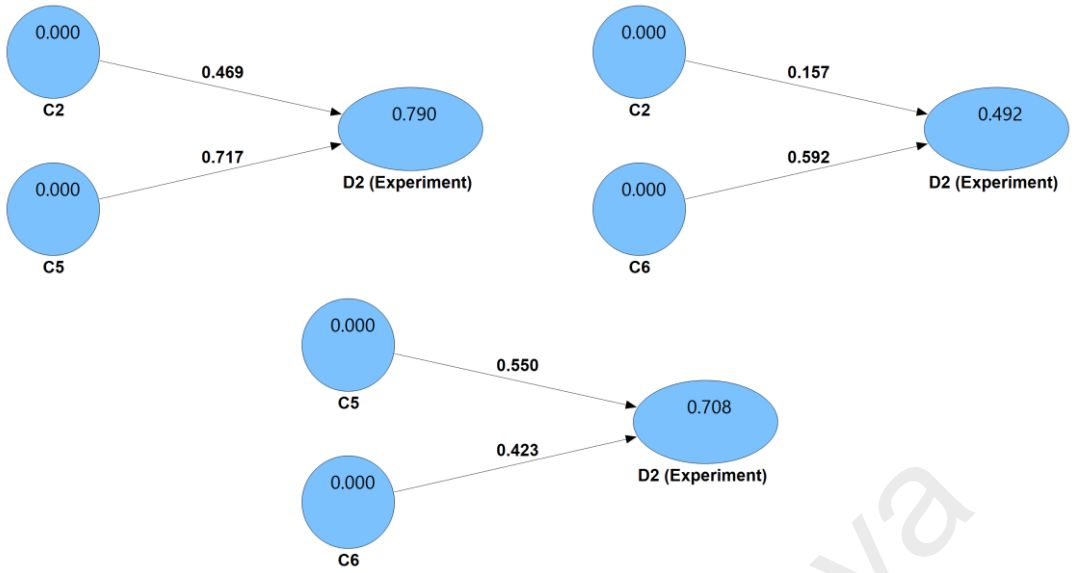

Figure 5.53: Regression coefficients of C2, C5 and C6 with D2 in Smart PLS

Figure 5.54 is presenting the results of regression analysis of all three suspected columns in the same model with D2. These results give a clearer picture of how these three columns are in relation with D2. As shown in this Figure, the regression coefficient of C2 and C5 to D2 are significant, but the relationship of C6 to D2 is disappeared. This indicates that C6 does not independently explain D2, therefore it is not damaged. Since C2 and C5 are not correlated, based on these results it can be most certainly concluded that they are both contributing on determining D2 and so they are both damaged.

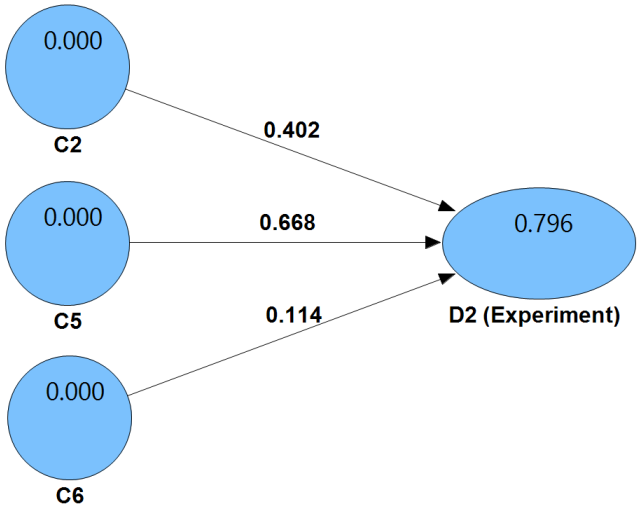

Figure 5.54: Regression coefficients of C2, C5 and C6 with D2 in Smart PLS (All in one model)

Now that two of the damaged members are identified, it is time to the next step and make sure no other member is contributing on determining D2 i.e. there is not any other damaged member. Before that, let's discuss the results of these three columns a bit further. The main question is, if C6 didn't have an independent relationship with D2, why C2 and C5 were not able to absorb its regression coefficient in Figure 5.53. To answer this, it should be noticed that D2 is at least a dual damage scenario (since other members are not being inspected yet). It means two damaged members are responsible for its frequency shifts. However the data sets that are provided by updated FE model only includes the frequency shifts of individual damaged members which requires 12 different FE analysis. So it is obviously not reasonable or even possible to include all the combinations of these 12 members. In case of this damage scenario, a damage scenario similar to D2 is not even available in FE data sets.

For example, if the frequency shifts caused by damage in column C2 and the frequency shifts caused by column C5 are correlated, it means the effects of these two columns on shifting the frequencies of the structure are similar. Therefore it is more probable that if these two members are damaged at the same time, the frequency shifts are more or less similar to their individual cases. However if C2 and C5 are shifting the frequency of the structure in different ways (no correlation) or in opposite ways (negative correlation), apparently when they are damaged simultaneously, the resulting frequency shifts are not similar to any of those individual cases. Referring to Figure 5.52, the direct regression coefficient of C2 and C5 on D2 are 0.53 and 0.76 respectively which are very significant. When they are separately modelled next to C6 (Figure 5.53), they are able to absorb a considerable part of the regression coefficient between C6 and D2. However since none of them are entirely determining D2, they are not able to absorb the entire regression coefficient between C6 and D2. When they are both placed in the model (Figure 5.54), they explain D2 completely and so when C6 is added to the model, it

does not exhibit any relationship with D2. In fact, if there was a single FE data set that represents the effect of damage of both C2 and C5 (let's name it C2+C5); it was able to absorb the regression coefficient of C6.

The accurate way of producing C2+C5 is by reducing the stiffness of both members in FE and calculating the frequency shifts. However it is also possible to reconstruct it using C2 and C5 data. This form of modelling is presented in Figure 5.55. There are a number of terminologies that are usually used in field of statistic and need to be described in order to discuss this Figure. The yellow rectangles are called "Items". Each item contains one of the data sets. The blue circles are called "variables" which are representing one or few items that are connected to them. A group of one variable and its corresponding items is called "measurement model" and finally a group of variables connected to each other is called the "structural model".

There are two types of measurement model i.e. reflective and formative. Since all the terms that are mentioned, including these two are originally from statistics and are generally used in the field of social science, their common definitions are usually sensible for social scientists. So instead of their original definition, a very simple explanation of reflective versus formative measurement is believed to be more useful in this case. In a reflective measurement model, the variable is calculated in a way that it is similar to all its items and reflects all of them. So apparently the important condition of a reflective measurement model is that all its items must represent the same thing and be highly correlated and similar. For example, imagine the modal testing of damage scenario D2 is repeated 5 times to increase its accuracy and the results are recorded in $D2_1$ to $D2_5$. Since these are five readings of the same damage scenario, they are expected to be very similar to each other and if one of them happened to be so different from the others (because of noise for instance), it should be eliminated from the

measurement model. In this case variable D2 should be constructed reflectively, since it represents the same thing as all its items.

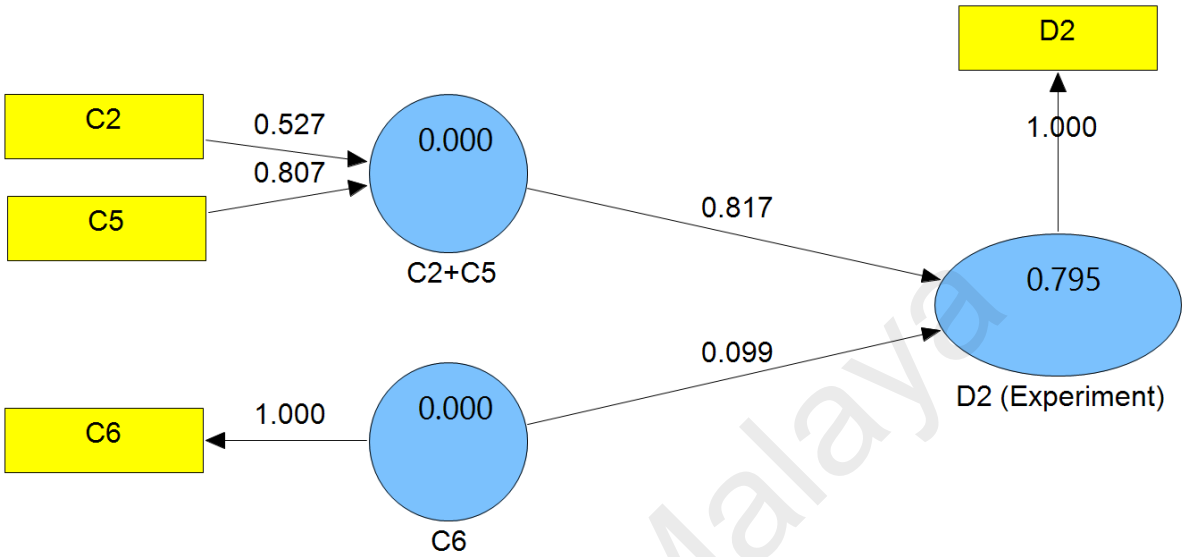

Figure 5.55: Formative measurement model of C2 and C5 in Smart PLS

On the other hand, in a formative measurement model the variable is formed by all its items, however it is representing a different phenomenon than them. A formative variable appreciates the differences between its items and the data of each item is contributing to shape a part of information in the resulting variable. So in a formative measurement model, the items are supposed to be not too similar to each other. The best example of a formative measurement model is C2+C5 in Figure 5.55. C2 and C5 are not expected to be similar. Depends on the condition, they can be very similar, totally different and even opposite each other. In this case, the C2+C5 variable should be measured formatively using C2 and C5. C2 and C5 are both influencing the new C2+C5 variable which could be totally different than each of them.

In statistical models, a reflective measurement model is indicated by arrows pointing from variable to the items, to show that the variable is reflecting each of its items, e.g. D2 in Figure 5.55. In this case the numbers on the arrows are showing how much the

reflective variable is similar to each of its items. A formative measurement model is indicated by the arrows pointing from the items to the variable, to show that the variable is being formed by all its items, e.g. C2+C5 in Figure 5.55. In this case, the numbers on the arrows are showing that how much each item has contributed to form the variable. If a measurement model has only one item, it cannot be called formative or reflective, because the variable is exactly the same as its item. In this case the direction of the arrow makes no difference. It should be noted that in the models shown previously, all the variables were measured using one item. So the items were purposely hidden to save space on the Figure, but they are all existed in the model.

Figure 5.55 is demonstrating that the new variable C2+C5 is predicting D2 completely and so C6 shows no relationship with D2 anymore. The effect of C2+C5 on the relationship of other members with D2 is calculated and presented in Table 5.6. The results are showing that none of the members have any independent relationship with D2 and so none of them are damaged. So D2 is correctly identified as a dual damage scenario of column 2 and column 5.

Table 5.6: Effect of C2+C5 on the relationship of all members with D2

Member	**Direct relationship with D2**		**Regression coefficient when modelled with C2+C5**
	Regression Coefficient	R^2	
B1	0.22	0.05	-0.24
B2	0.36	0.13	0.18
B3	-0.05	0.00	-0.27
B4	0.40	0.16	0.06
C1	0.24	0.06	-0.24
C3	0.25	0.06	-0.06
C4	0.24	0.06	-0.32
C6	0.69	0.48	0.10
C7	0.30	0.09	-0.02
C8	0.35	0.12	-0.10

5.6.3.3 Damage Scenario D6:

Figure 5.56 is illustrating the correlation of frequency shifts between all unmeasured members and experimental data of damage scenario D6. Five members are demonstrating high similarity with the experiment i.e. B1, B3, C2, C3 and C4. Referring to Table 5.4, the correlation of B1 and B3 and also the correlations of C2, C3 and C4 are relatively high which indicates that perhaps some of these members are having a dependant relationship with D6 through the yet unknown damaged member. The results of DLV (Figure 5.46) are predicting that none of the columns are damaged in this damage scenario. However three columns are demonstrating high relationship with D6. This could be due to their correlation with either B1 or B3. Although referring to Table 5.4, the correlation between beams and columns are not large enough to cause these results. So this should be investigated further using regression analysis.

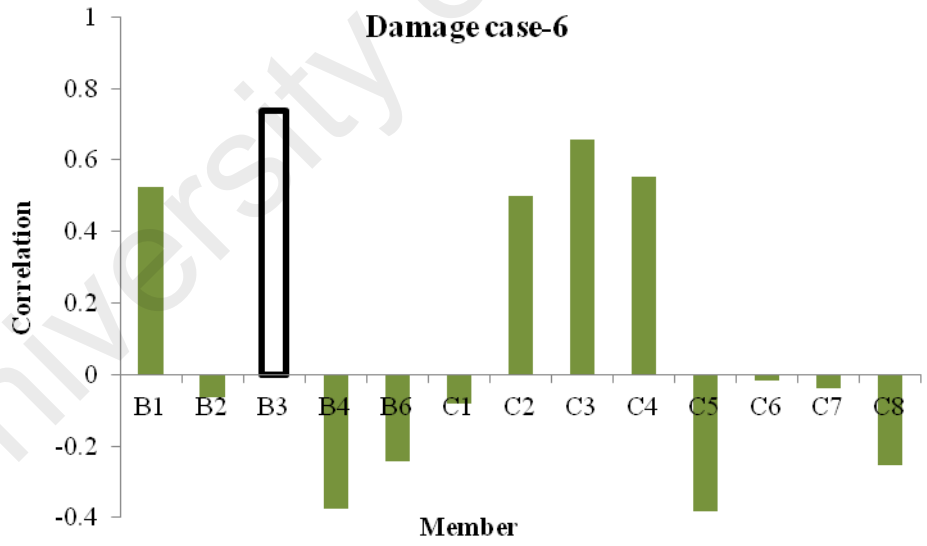

Figure 5.56: Correlation of frequency shifts between all unmeasured members and D6

Figure 5.57 is showing the direct regression coefficient and R^2 of the two beams and three columns with D6. All the R^2 are significant while B3 and C3 seem to have a better determination of D6.

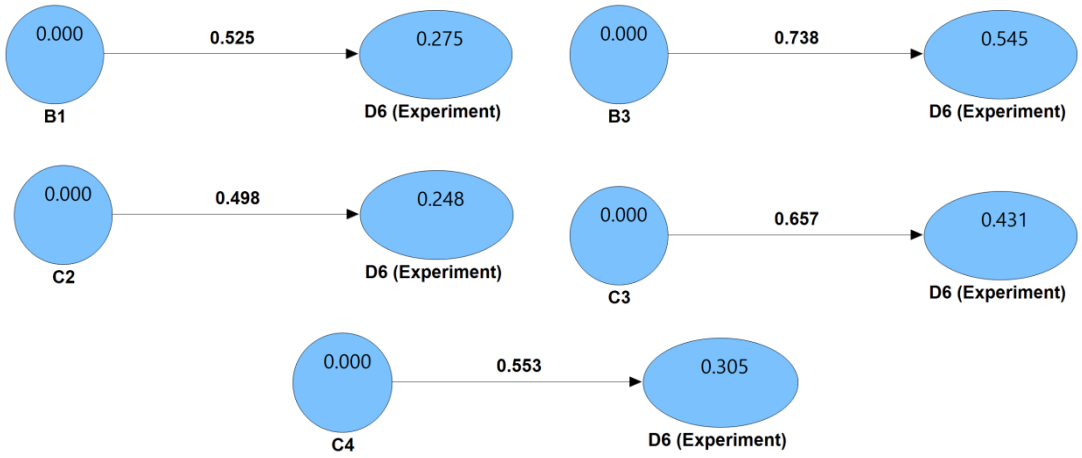

Figure 5.57: Regression coefficients of members with high correlation with D6 in Smart PLS (Direct relationship)

Figure 5.58 is showing the regression coefficient of these 5 members in pair. The regression coefficient of B1 and B3 is presented at top left of this Figure which shows that the relationship between B1 and D1 is not independent and goes through B3. So B1 is not the damaged member. Although other results are showing that B3 is not able to absorb the regression coefficient of none of the columns. So it suggests that at least one of these columns is in a multiple damage scenario with B3.

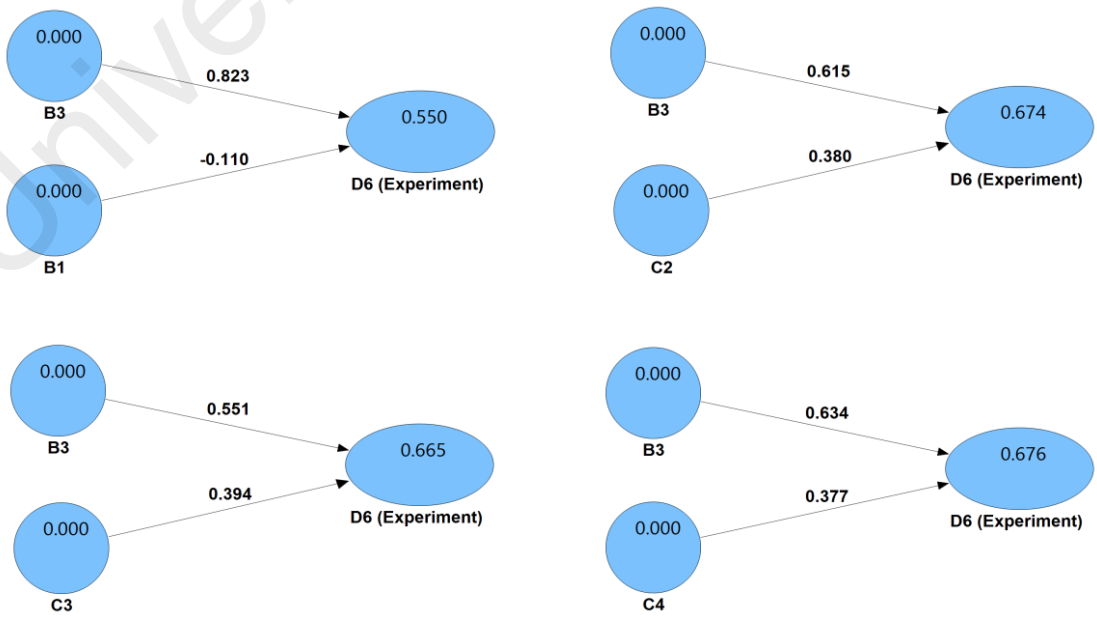

Figure 5.58: Effect of B3 on the relationship of B1, C2, C3 and C4 with D7 in Smart PLS

Figure 5.59 (left) is showing the regression coefficient of B3, C2 and C3 with D6 in one model. The results are showing that the regression coefficient of C2 is entirely absorbed by C3 and so C2 is not the damaged member. Figure 5.59 (right) is presenting the regression coefficient of B3, C3 and C4 to check if the relationship of C4 with D1 is through C3 or not. However the results are showing that the regression coefficients of both of them are reduced, but they are still meaningful. This is suggesting that B3, C3 and C4 are all might be damaged members.

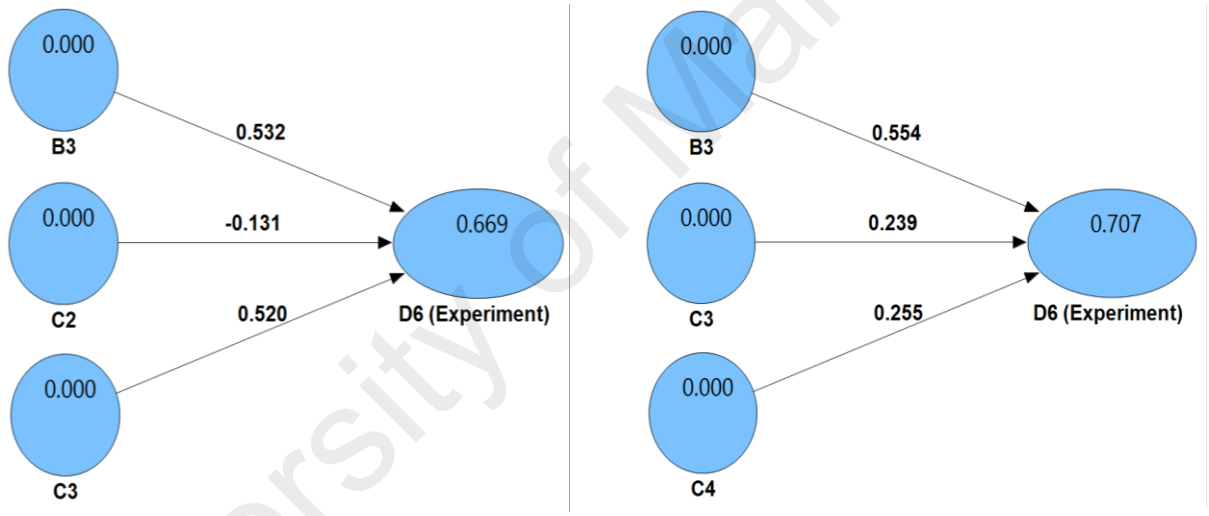

Figure 5.59: Regression coefficients of B3-C2-C3 and B3-C3-C4 in two models with D6 in Smart PLS

With the assumption of a multiple damage scenario, B3, C3 and C4 are used in a formative measurement model to create B3+C3+C4 variable that represents the multiple damage scenarios. This new variable is modelled with the remaining members to check if they have any effect of D6 (Table 5.7). The results do not show any independent relationship between the remaining members and D6.

Table 5.7: Effect of B3+C4+C4 on the relationship of all members with D6

Member	Direct relationship with D6		Regression coefficient when modelled with B3+C3+C4
	Regression Coefficient	R^2	
B1	0.52	0.27	-0.01
B2	-0.06	0.00	-0.19
B4	-0.37	0.14	-0.18
C1	-0.08	0.00	-0.07
C2	0.50	0.25	-0.01
C5	-0.38	0.14	-0.44
C6	-0.02	0.00	-0.41
C7	-0.04	0.00	-0.27
C8	-0.25	0.06	-0.35

Regression analysis has detected that damage scenario D6 is a multiple damage scenario with one beam and two columns being involved. This is in contrast with results of DLV that suggests no column is damaged. So either the results of DLV are false negative and it incorrectly gave pass to two damaged columns, or there is something wrong with the frequency shift data of D6 and the results of regression analysis. As mentioned earlier in this chapter, the error of DLV is always type II error i.e. giving false negative, which could be the case here. Considering the previous results of DLV, it typically makes wrong prediction on beams and never failed on the columns. So it is most likely that the results of DLV are correct and these two columns are not damaged. On the other hand, if it is assumed that the columns are not damaged, then it means that the regression analysis is suffering from a fault. It can be faulty experimental data or even a modelling error which caused these suspicious results. Therefore, even if it is assumed that the two columns are not damaged, it does not seem to be consistent to just ignoring the two columns and announcing beam B3 as the solo damaged member; although this is actually the case for damage scenario D6. So regression analysis has somehow failed to

reliably detect beam B3 as damaged member; however the results are meaningful enough to raise suspicions about this beam.

5.6.3.4 Damage Scenario D7:

Figure 5.60 is illustrating the correlation of frequency shifts between all unmeasured members and experimental data of damage scenario D7. B2 and B6 are having high correlations with D7 and so their regression coefficients are being examined. Referring to Table 5.4, the correlation of these two beams are 0.62 which indicates that perhaps one of these beams are having a dependent relationship with D7 through the other.

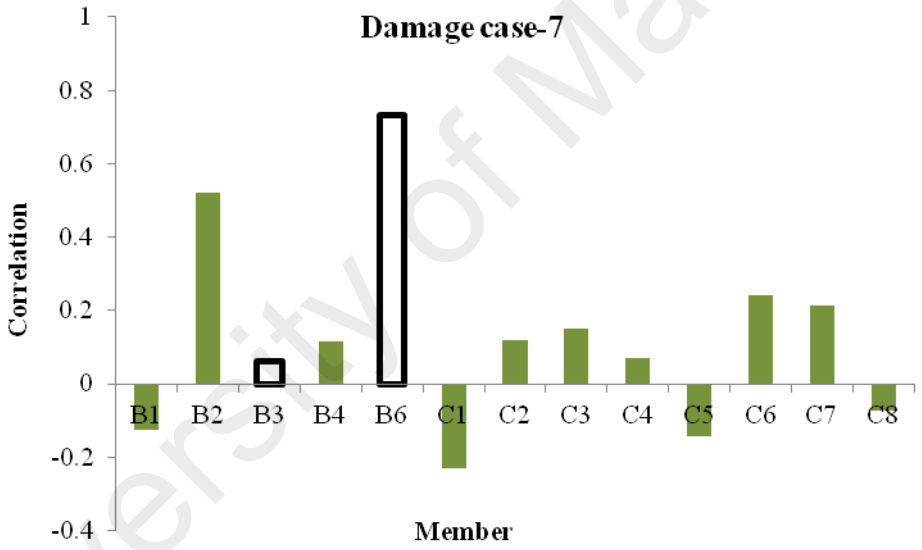

Figure 5.60: Correlation of frequency shifts between all unmeasured members and D7

Figure 5.61 is showing the direct regression coefficient and R^2 of B2 and B6 with D7. The R2 of B6 is very significant and much higher than the R^2 of B2. The results of DLV (Figure 5.46) are suggesting that B6 is damaged in damage scenario D7. In fact that is the reason why B6 is included in the regression analysis despite that it is a measured member. So knowing that B6 is damaged, the main task of regression analysis is to check whether other members are contributing in this damage scenario or not.

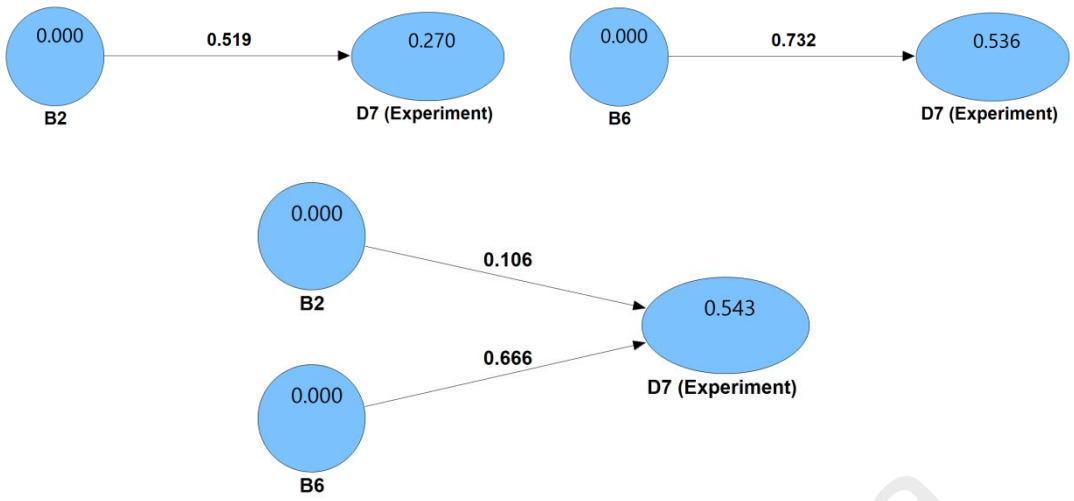

Figure 5.61: Regression coefficients of B2 and B6 with D7 in Smart PLS

Figure 5.61 is also demonstrating the regression coefficient of B2 and B6 with D7 in one model. The results are showing that the direct regression coefficient of B2 which is 0.52 is absorbed by B6 and is reduced to 0.11. This value is not significant enough for B2 to be identified as damaged member. Although the correlation of other members with D7 is very low (Figure 5.60), but they have to be checked in the same model with B6 to make sure no other member is contributing in this damage scenario.

Table 5.8 is presenting the Effect of B6 on the relationship of all members with D7. The results are showing that the direct regression coefficient and R^2 of beam B3 are zero, however when it is modelled with B6, its regression coefficient is increased significantly to 0.37. This is a perfect example to show that correlation is not a complete measure of contributory relationship between two variables; in this case between a damaged member and a damaged scenario which is partially caused by it.

The reason why B3 is not able to predict D7 directly is its correlation with B6. Referring to Table 5.4, the correlation of B3 and B6 is negative, indicating that they change the frequency of the structure not only differently, but in fact in opposite ways. Figure 5.47 is illustrating that how peaks and valleys of their frequency shift diagram

are opposite each other in the first five modes. It also shows that in general, the magnitude of the frequency shift of B6 is larger than B3. So consequently, the traces of the contribution of B3 on D7 are cancelling out by the opposite and dominant effect of B6. That is why when only B3 and D7 are in the picture (Figure 5.62), the model does not see any similarity between the two and so their regression coefficient is almost zero. It should be noted that the direct regression coefficient of zero does not imply anything in particular. Depending on the magnitude of D6 and also the correlation of D3 and D6, the direct regression coefficient of D3 under this circumstance could've been anything between a relatively low positive to a negative value, which in this case happened to be close to zero.

Table 5.8: Effect of B6 on the relationship of all members with D7

`Member	**Direct relationship with D7**		**Regression coefficient when modelled with B6**
	Regression Coefficient	R^2	
B1	-0.12	0.02	0.10
B2	0.52	0.27	0.11
B3	0.06	0.00	0.37
B4	0.11	0.01	-0.26
C1	-0.23	0.05	-0.04
C2	0.12	0.02	0.04
C3	0.15	0.08	-0.09
C4	0.07	0.00	-0.17
C5	-0.14	0.02	-0.03
C6	0.24	0.06	-0.07
C7	0.21	0.05	-0.14
C8	-0.07	0.00	-0.10

When B6 is presented in the model (Figure 5.62), its contribution to predict D7 is now determined by the model. As a result, the model realizes the differences between B6 and D7 and determines that these differences are 37% similar to B3.

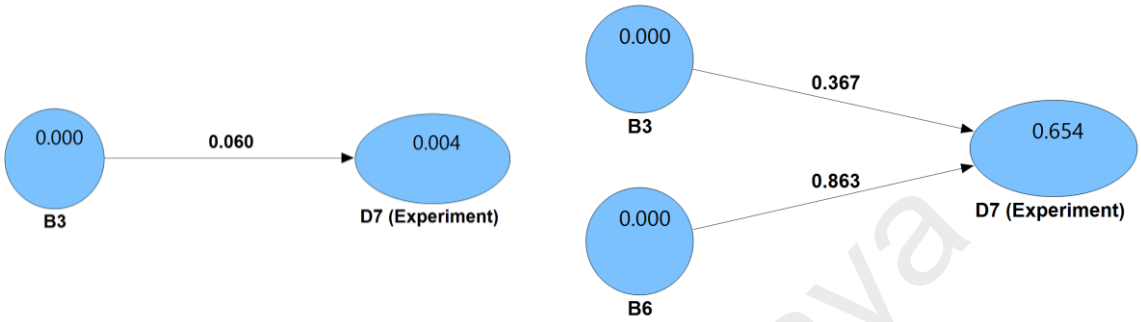

Figure 5.62: Regression coefficients of B3 and B6 with D7 in Smart PLS

B3 and B6 are both identified as contributing damaged members on D7. So a formative measurement model is used to create a new B3+B6 variable, using the data of B3 and B6 as shown in Figure 5.63. The results of regression analysis using the new model are showing that B3+B6 has direct regression coefficient of 0.81 to D7 and its R^2 on D7 is 0.65 which indicate that B3+B6 are determining D7 significantly. Once again, all the unmeasured members must be verified in the same model with B3+B6 to make sure there is no other contributor in this model. The results of this verification are presented in Table 5.9 which confirms there is no other damaged member in D7.

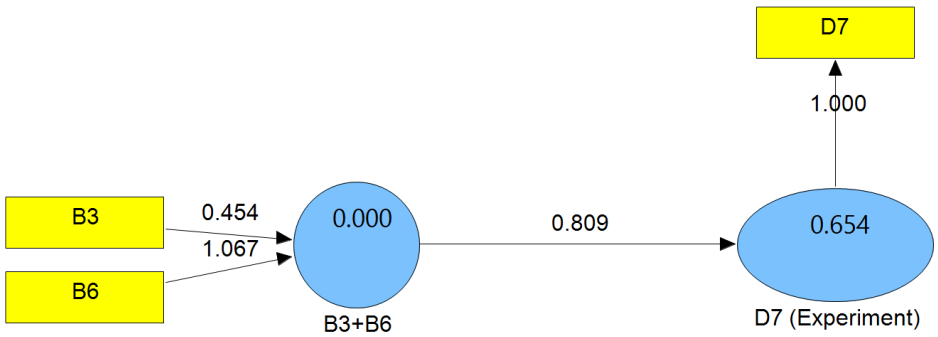

Figure 5.63: Formative measurement of B3 and B6 in Smart PLS

Table 5.9: Effect of B3+B6 on the relationship of all members with D7

`Member	Direct relationship with D7		Regression coefficient when modelled with B3+B6
	Regression Coefficient	R^2	
B1	-0.12	0.02	-0.06
B2	0.52	0.27	-0.02
B4	0.11	0.01	-0.13
C1	-0.23	0.05	0.10
C2	0.12	0.02	-0.07
C3	0.15	0.08	0.04
C4	0.07	0.00	-0.13
C5	-0.14	0.02	-0.03
C6	0.24	0.06	-0.03
C7	0.21	0.05	-0.21
C8	-0.07	0.00	0.06

Although this frequency based method was proposed to detect damage in unmeasured parts of the structure in case of incomplete measurement, but it can also be used for other damage scenarios to verify the results of the other methods. Even in case of complete measurement, it can be really helpful to verify the results of other methods that have been presented in this study. However since all aspects of implementing this method was discussed in these four damage scenarios, discussing the other damage scenarios do not add much to the content of this study and so are not reported. Although it should be reminded that this method is vastly relaying on model updating and the updating method that has been reported in this study is based on mode shapes. So unless any other updating method is used, this method cannot be seen as a standalone frequency based approach.

CHAPTER 6: CONCLUSION

This research and its primary goal was to perform modal based damage detection in a frame structure using operational data. This goal was perused by studying different aspects of this problem which are presented in the beginning of this thesis as four main objectives.

The first objective was employing operational modal testing on a lab-scaled frame structure in order to obtain reliable modal parameters for further steps of this study. This was pointed out as an individual objective, because the techniques of simulating operational modal analysis in the laboratory is not reported much in the literature. The main advantage of such experimental set up was that both EMA an OMA could be carried out on the model. So the results of experimental modal analysis were always available in all the cases to be used as benchmark to the findings of operational modal analysis.

The second objective was to mass normalize mode shapes obtained by OMA, which is in fact an ongoing subject in the literature. The concluding remarks of this objective are presented in Section 6.1

The third objective was to evaluate damage locating vector and its reliability when it uses the OMA identified and normalized modes as input. The concluding remarks of this objective are presented in Section 6.3

Finally, the main objective of this study was to propose a practical and effective method to detect damage using incomplete measurements which is concluded in sections 6.2 and 6.3.

6.1 Mass Normalization

Obtaining mass normalized mode shapes using operational modal analysis and in absence of the measured input force was one of the objectives of this study. The mass normalization method used in this study was based on changing the mass matrix of the structure and utilizing the extra information to scale the mode shapes. To do this, external weights were added to particular DOFs of the structure in different configurations and the scaling factors of each case were calculated. Either FE results or the results of EMA were used to evaluate the accuracy of the calculated scaling factor in each case.

Since input forces were measured in this case study, the calculated scaling factors had the privilege of being evaluated by a more reliable and accurate scaling method. This is obviously a deal breaker since the whole point of using such method is to be independent from measuring the input force; however, the measurement of input force was to verify the accuracy of the results. According to the results which are presented and discussed in chapter 5.3, the accuracy of this normalization method can be estimated and increased by taking few steps. The first and most important step is to find the best location, or a set of appropriate locations to add external weights. The most apparent principle is that the weights should not be added to the node of any of the modes, since it is not able to alter that particular mode. The best point to add mass is the point which is participating in all the mode shapes. If the number of modes is high, more than one location might be required to affect all the modes. This principle is good enough to approximate the possible locations to add weights. However the best way of evaluating them is FE modelling where the exact value of scaling factor is available.

The second contributing factor is the amount of mass added to the structure. This is also very important factor, because if the external weight is too small, it does not alter the

modes sufficiently and if it is too large, it completely changes the frequency and shape of the modes. This approximation is useful for the first estimation; however the optimum value of mass can be evaluated using FE analysis.

The first two steps help to narrow down different mass change scenarios in terms of position and amount of mass to be applied to the real structure. It is rational to select more than one mass scenario to be used in the experiment for more verification. It is particularly important, because the findings of FE analysis might not be perfectly applicable in the experiment. Hence the integrity of location and amount of added weights need to be evaluated for the experiment independently. As described in chapter 5.3, two parameters are suggested to indirectly evaluate the goodness of the findings, i.e. frequency shift and correlation of mode shapes. These two criterions can be used to accept or reject the calculated scaling factor of each individual mode or even the whole mass scenario. Using all these steps, mode shapes in OMA can be mass normalized with an acceptable level of accuracy.

One important concern about this normalization method is its implementation in real structures. While placing and moving external masses in a scaled model is not much of a concern, but its possibility and practicality must be assessed in real case scenarios. This dictates additional factors when the location and amount of masses are being selected. For example, if a number of concrete blocks are used as external weights, the best idea for different mass scenarios is to just move the blocks between different points in one floor (if possible) rather than moving them up and down the structure. Another simple and promising proposal is to use a number of light weight and high pressure plastic of polyethylene water tanks that can be easily moved all over the structure. The water can also be pumped to/from any point of the structure for almost no cost. Therefore there is no restriction when deciding on the location of weights. However due

to the low mass density of water, the amount of weight becomes a concern and the weight must be designed to be distributed in an area instead of being placed in one point.

6.2 Model Updating

The primary application of model updating in this study was matching the modes of FE and experiment so that they can be used in the frequency based damage detection to address incomplete measurements. Utilizing CMCM in this study and its results were pointing to the significant accuracy and reliability of this method. However this accuracy comes with a price i.e. the need for complete measurement of the structure and availability of all DOFs in mode shapes. This is in fact the disadvantage of this method since complete measurements are not always possible in real case problems. More importantly, it is in contrast with its application in this study i.e. being used to address incomplete measurement problem. There were two reasons why CMCM could still be used in this case. The first reason was that the number of missing DOFs was relatively low and the unmeasured and measured members were similar in size. So with some modifications to the original method, CMCM was still offering reasonable accuracy. The second reason was that the frequency based detection method is not very sensitive to the accuracy of model updating. Since the method relies on the relative frequency shifts and not the absolute values of frequencies, an approximate updating of the model is enough to provide concrete results.

6.3 Damage Identification

Three damage detection and localization methods were used in this study. These three methods were reported either individually or in conjunction with each other. Damage Locating Vectors was the core detection method that its locating ability was tested using

variety of damage scenarios i.e. single and multiple damage cases of beams and column. DLV has a number of advantages in compare to some other types of detection methods. One is its ability to locate damaged member regardless of the geometry of the structure. It is also capable of identifying individual damaged members in a multiple damage scenario.

The results of this study are showing that in case of incomplete measurements, DLV is still able to provide some useful information on the approximate location of damaged member. This particular feature of DLV is reported in a number of former studies, for example (An, et al., 2014; Gao, 2005; Gao, et al., 2007). In these studies, a few number of sensors are used to measure selected DOFs throughout the structure. So instead of locating the damaged member, DLV shows the area where the damaged member is located. Then they use a number of approaches to find the exact damaged member within that area, mainly based on increasing the resolution of measurement in the detected region. The important point is that in these cases, the reason behind incomplete measurement is to minimize the number of required sensors and the size of recorded data. However in case of this study, the reason of incomplete measurement is that a part of the structure is inaccessible. So unlike those studies, it is not possible to increase the measurement resolution in the detected region. That is why a frequency based approach is used in this study to locate the damaged member within the suspicious area detected by DLV.

The main weakness of the DLV approach used in this study is that it requires mass normalized mode shapes. This is a major concern of the method when it is being used in OMA. It should be emphasised that this weakness is not directly from DLV, but in fact

the way DLVs are obtained in this study i.e. modal flexibility matrix. There are other approaches to calculate DLVs which are in some extend addressing this issue (Bernal, 2006).

One particular issue that was encountered in this study, especially for beams, was the indistinct results of DLV i.e. the *WSI* index of damaged member being relatively or significantly lower than other members, but not lower than the threshold of 1. Part of this issue could be due to inaccuracies of modal identification and normalization, since the DLV results of FE and EMA are considerably more concrete. Another contributing factor is indeed the number of detected modes. This was also tested by reducing the number of modes to see its effect on accuracy of DLV results. It shows that the absence of higher and more local modes reduces the accuracy of the results considerably.

The second detection method that was modified and tested in this study was derived from CMCM model updating approach by employing the stiffness correcting factor as damage index. Similar to DLV, this method also required completely measured mode shapes, although in this case they could be arbitrary scaled. Similar to DLV, the results of this method were also correct, but indistinct. The interesting observation was that by combining the two methods, the consistency and accuracy of the results were significantly improved, as described in chapter 5.5.2.

The third detection method introduced in this study was relying solely on modal frequencies to address the incomplete measurement problem. It was based on producing frequency shift data of different damage scenarios using updated FE model and trying to predict the experimental frequency shifts using these data. In this study, this method were used to assess the unmeasured members only, whereas the measured members were still being assessed using DLV. As reported in former studies (An, et al., 2014;

Gao, 2005; Gao, et al., 2007), incomplete measurement causes false positive detection in DLV results. As mentioned earlier, in most of these studies, the false positive detection is resolved by increasing the measurement resolution in the suspected region and again using DLV to rule out the falsely detected members and locate the actual damaged member. This is not an option in this study, because in this case the unmeasured DOFs are assumed to be inaccessible. So the proposed frequency based method is in fact doing the same thing i.e. ruling out false positive detections, but using a different approach that does not require further measurements.

Furthermore, this method can be totally used stand alone to assess the entire structure, and since it only requires modal frequencies, it seems to be a much better solution than the other methods. However, it should be considered that although this method is entirely based on modal frequencies, but it requires FE model to be updated and most reliable updating methods including CMCM are based on mode shapes. The second point is that this method involves lots of tries and errors. The analyzing process of this method begins with a hand-full of members that are marked as damaged. They are then tested against each other, ruling out the intact members and identifying the damaged ones. This process becomes a lot more complicated and perhaps less reliable and accurate when the number of members are increased.

As an overall conclusion, there are varieties of damage detection approaches that are introduced in the literature and their reliability are tested using numerical simulations or in best case using controlled experimental data. However, all these methods are meant to be used in real full size structures in service with all the limits they impose. So it seems very realistic to single out a damage detection approach to be used in real case structures. The best strategy is to study different types of damage detection methods and

their abilities and weaknesses and to use a combination of them to find a solution for real structures. This was the perspective of this study.

6.4 Recommendations

There are a number of subjects that was not addressed in this thesis for various reasons, which are believed to be noteworthy for further studies. The frame structure reported in this thesis was a simple frame without horizontal or vertical braces, except for the third floor where amplifiers were located. However, the original proposal of this study was based on a frame with braces which was an approximate scale of a jacket platform in Persian Gulf. The effect of braces on process of damage detection can be further study.

The frequency based detection method that was introduced in this study was employed only for incomplete measurements. This method is relying on modal frequencies only, which makes it a perfect approach to be used in operational modal analysis. So it worth being modified to be used as a standalone detection method. This requires and updating method that is not based on availability of mode shapes.

REFERENCES

An, Y., Ou, J., Li, J., & Spencer, B. (2014). Stochastic DLV method for steel truss structures: simulation and experiment. *Smart Structures and Systems, 14*(2), 105-128.

Avitabile, P. (2001). Experimental modal analysis. *Sound and vibration, 35*(1), 20-31.

Bendat, J. S., & Piersol, A. G. (1980). Engineering applications of correlation and spectral analysis. *New York, Wiley-Interscience, 1980. 315 p., 1*.

Bernal, D. (2002). Load vectors for damage localization. *Journal of Engineering Mechanics, 128*(1), 7-14.

Bernal, D. (2006). Flexibility-based damage localization from stochastic realization results. *Journal of Engineering Mechanics, 132*(6), 651-658.

Bernal, D. (2007a). Damage localization from the null space of changes in the transfer matrix. *AIAA journal, 45*(2), 374-381.

Bernal, D. (2007b). *The stochastic dynamic damage locating vector approach.* Paper presented at the Proceedings of the 25th International Modal Analysis Conference.

Bernal, D. (2010). Load vectors for damage location in systems identified from operational loads. *Journal of Engineering Mechanics, 136*(1), 31-39.

Bernal, D., & Gunes, B. (2002). *Damage localization in output-only systems: A flexibility based approach.* Paper presented at the Proc. Of the International Modal Analysis Conference (IMAC) XX.

Bernal, D., & Gunes, B. (2004). Flexibility based approach for damage characterization: benchmark application. *Journal of Engineering Mechanics, 130*(1), 61-70.

Bernal, D., & Kunwar, A. (2016). Steady state shift damage localization. *Meccanica, 51*(11), 2861-2871.

Bjorck, A. (1996). *Numerical methods for least squares problems* (Vol. 103). Philadelphia: Society for Industrial and Applied Mathematics (Siam).

Boot, J., van de Molengraft, I. M., & Nuij, I. P. (2003). Frequency response measurement in closed loop: brushing up our knowledge. Eindhoven: Department of Mechanical Engineering, University of Technology Eindhoven

Bouzit, D., & Pierre, C. (1995). An experimental investigation of vibration localization in disordered multi-span beams. *Journal of Sound and Vibration, 187*(4), 649-670.

Brincker, R., & Andersen, P. (2003). *A way of getting scaled mode shapes in output only modal testing*. Paper presented at the Proc. 21st Int. Modal Analysis Conference, Kissimmee, FL.

Brincker, R., Rodrigues, J., & Andersen, P. (2004). *Scaling the mode shapes of a building model by mass changes*. Paper presented at the Proceeding of the 22nd IMAC.

Brincker, R., Zhang, L., & Andersen, P. (2000). *Modal identification from ambient responses using frequency domain decomposition*. Paper presented at the Proc. of the 18*'International Modal Analysis Conference (IMAC), San Antonio, Texas.

Brincker, R., Zhang, L., & Andersen, P. (2001). *Output-only modal analysis by frequency domain decomposition*. Paper presented at the The International Conference on Noise and Vibration Engineering.

Brownjohn, J. M., De Stefano, A., Xu, Y.-L., Wenzel, H., & Aktan, A. E. (2011). Vibration-based monitoring of civil infrastructure: challenges and successes. *Journal of Civil Structural Health Monitoring, 1*(3-4), 79-95.

Cavalieri, F., Imbimbo, M., Betti, R., & Brügger, A. (2009). *Damage detection of a steel frame subjected to ground motion*. Paper presented at the 3rd International Operational Modal Analysis Conference (IOMAC).

Cawley, P., & Adams, R. D. (1979). The Locations Of Defects In Structures From Measurements Of Natural Frequencies. *Journal of Strain Analysis, 14*(2), 49-57.

Chaudhari, T., & Maiti, S. (2000). A study of vibration of geometrically segmented beams with and without crack. *International Journal of Solids and Structures, 37*(5), 761-779.

Cheng, Y.-s., & Wang, Z. (2008). Detecting damage to offshore platform structures using the time-domain data. *Journal of Marine Science and Application, 7*, 7-14.

Coppotelli, G. (2009). On the estimate of the FRFs from operational data. *Mechanical Systems and Signal Processing, 23*(2), 288-299.

Cox, A. M., & Agnes, G. S. (1999). *A statistical analysis of space structure mode localization*. Paper presented at the Proceedings of the 1999 AIAA/ASME/ASCE/AHS/ASC Structures, Structural Dynamics, and Materials Conference and Exhibit.

Demmel, J. W. (1997). *Applied Numerical Linear Algebra*: Society for Industrial and Applied Mathematics (SIAM, 3600 Market Street, Floor 6, Philadelphia, PA 19104).

Der Kiureghian, A., & Ditlevsen, O. (2009). Aleatory or epistemic? Does it matter? *Structural Safety, 31*(2), 105-112.

Deraemaeker, A., & Worden, K. (2012). *New trends in vibration based structural health monitoring* (Vol. 520): Springer Science & Business Media.

Doebling, S. W., Farrar, C. R., & Goodman, R. S. (1997). *Effects of Measurement Statistics on the Detection of Damage in the Alamosa Canyon Bridge*. Paper presented at the 15th International Modal Analysis Conference, Orlando, FL,.

Doebling, S. W., Farrar, C. R., & Prime, M. B. (1998). A summary review of vibration-based damage identification methods. *Shock and vibration digest, 30*(2), 91-105.

Doebling, S. W., Farrar, C. R., Prime, M. B., & Shevitz, D. W. (1996). Damage identification and health monitoring of structural and mechanical systems from changes in their vibration characteristics: a literature review: Los Alamos National Lab., NM (United States).

Everitt, B. (1998). *Cambridge dictionary of statistics*: Cambridge University Press.

Ewins, D. J. (1984). *Modal testing: theory and practice* (Vol. 15): Research studies press Letchworth.

Farrar, C. R., & Jauregui, D. A. (1998a). Comparative study of damage identification algorithms applied to a bridge: I. Experiment. *Smart Materials & Structures, 7*(5), 704-719.

Farrar, C. R., & Jauregui, D. A. (1998b). Comparative study of damage identification algorithms applied to a bridge: II. Numerical study. *Smart Materials & Structures, 7*(5), 720-731.

Friswell, M., & Mottershead, J. E. (1995). *Finite element model updating in structural dynamics* (Vol. 38): Springer Science & Business Media.

Friswell, M. I. (2007). Damage identification using inverse methods. *Philosophical Transactions of the Royal Society a-Mathematical Physical and Engineering Sciences, 365*(1851), 393-410.

Friswell, M. I., Penny, J. E. T., & Wilson, D. A. L. (1994). Using Vibration Data and Statistical Measures to Locate Damage in Structures. *Modal Analysis-the International Journal of Analytical and Experimental Modal Analysis, 9*(4), 239-254.

Gao, Y. (2005). *Structural health monitoring strategies for smart sensor networks*. PhD Thesis, Graduate College of the University of Illinois at Urbana-Champaign, U.S.A.

Gao, Y., & Randall, R. (1996a). Determination of frequency response functions from response measurements—I. Extraction of poles and zeros from response cepstra. *Mechanical Systems and Signal Processing, 10*(3), 293-317.

Gao, Y., & Randall, R. (1996b). Determination of frequency response functions from response measurements—II. Regeneration of frequency response from poles and zeros. *Mechanical Systems and Signal Processing, 10*(3), 319-340.

Gao, Y., & Spencer, B. (2002). Damage localization under ambient vibration using changes in flexibility. *Earthquake Engineering and Engineering Vibration, 1*(1), 136-144.

Gao, Y., Spencer Jr, B., & Bernal, D. (2007). Experimental verification of the flexibility-based damage locating vector method. *Journal of Engineering Mechanics, 133*(10), 1043-1049.

Hair Jr, J. F., Hult, G. T. M., Ringle, C., & Sarstedt, M. (2016). *A primer on partial least squares structural equation modeling (PLS-SEM)* (2 ed.). Thousand Oaks, California: Sage Publications.

Hasan, W. M. (1995). Crack Detection from the Variation of the Eigenfrequencies of a Beam on Elastic-Foundation. *Engineering Fracture Mechanics, 52*(3), 409-421.

Heylen, W., & Sas, P. (2006). *Modal analysis theory and testing*: Katholieke Universteit Leuven, Departement Werktuigkunde.

Hout, B., & Avitabile, P. (2004). *Application of Operating Data Scaling Techniques using Multiple Approaches*. Paper presented at the 22nd IMAC, A Conference on Structural Dynamics, Detroit, Michigan,.

Hu, S.-L. J., & Li, H. (2007). Simultaneous mass, damping, and stiffness updating for dynamic systems. *AIAA journal, 45*(10), 2529-2537.

Hu, S.-L. J., Li, H., & Wang, S. (2007). Cross-model cross-mode method for model updating. *Mechanical Systems and Signal Processing, 21*(4), 1690-1703.

Hu, S.-L. J., & Liang, R. Y. (1993). An Integrated Approach to Detection of Cracks Using Vibration Characteristics. *Journal of the Franklin Institute-Engineering and Applied Mathematics, 330*(5), 841-853.

Huang, Q., Gardoni, P., & Hurlebaus, S. (2012). A probabilistic damage detection approach using vibration-based nondestructive testing. *Structural Safety, 38*, 11-21.

Ibsen, L. B., & Liingaard, M. (2006). Experimental modal analysis *DCE Technical Report No. 10*. Aalborg, Denmark Aalborg University.

Irvine, T. (2000). An introduction to frequency response functions. *Rapport, College of Engineering and Computer Science*.

Jacobsen, N.-J., Andersen, P., & Brincker, R. (2006). *Using enhanced frequency domain decomposition as a robust technique to harmonic excitation in*

operational modal analysis. Paper presented at the Proceedings of ISMA2006: international conference on noise & vibration engineering.

Juneja, V., Haftka, R. T., & Cudney, H. H. (1997). Damage detection and damage detectability - Analysis and experiments. *Journal of Aerospace Engineering, 10*(4), 135-142.

Kasper, D. G., Swanson, D. C., & Reichard, K. M. (2008). Higher-frequency wavenumber shift and frequency shift in a cracked, vibrating beam. *Journal of Sound and Vibration, 312*(1-2), 1-18.

Kennedy, M. C., & O'Hagan, A. (2001). Bayesian calibration of computer models. *Journal of the Royal Statistical Society: Series B (Statistical Methodology), 63*(3), 425-464.

Khatibi, M., Ashory, M., & Malekjafarian, A. (2009). *Scaling of mode shapes using mass-stiffness change method*. Paper presented at the Proceedings of the International Operational Modal Analysis Conference (IOMAC). Copenhagen, Denmark.

Kim, J.-T., & Stubbs, N. (1995). Damage detection in offshore jacket structures from limited modal information. *International Journal of Offshore and Polar Engineering, 5*(01).

Kim, J.-T., & Stubbs, N. (2003). Crack detection in beam-type structures using frequency data. *Journal of Sound and Vibration, 259*(1), 145-160.

Kranjc, T., Slavič, J., & Boltežar, M. (2013). The mass normalization of the displacement and strain mode shapes in a strain experimental modal analysis using the mass-change strategy. *Journal of Sound and Vibration, 332*(26), 6968-6981.

Li, H., Wang, J., & Hu, S.-L. J. (2008). Using incomplete modal data for damage detection in offshore jacket structures. *Ocean Engineering, 35*(17), 1793-1799.

Liang, R. Y., Choy, F. K., & Hu, J. (1991). Detection of cracks in beam structures using measurements of natural frequencies. *Journal of the Franklin Institute, 328*(4), 505-518.

Lifshitz, J. M., & Rotem, A. (1969). Determination of reinforcement unbonding of composites by a vibration technique. *Journal of Composite Materials, 3*(3), 412-423.

López Aenlle, M., Brincker, R., & Fernández Canteli, A. C. (2005). *Some methods to determine scaled mode shapes in natural input modal analysis*. Paper presented at the IMAC-XXIII: Conference & Exposition on Structural Dynamics - Structural Health Monitoring, Orlando, Florida, USA.

López Aenlle, M., Brincker, R., Fernández Canteli, A. C., & Villa García, L. M. (2005). *Scaling factor estimation by the mass change method.* Paper presented at the International Operational Modal Analysis Conferencee (IOMAC), Copenhagen, Denmark.

Maddalo, M., & Bernal, D. (2011). Truncation Effects on the Dynamic Damage Locating Vector (DDLV) Approach *Structural Dynamics, Volume 3* (pp. 349-356): Springer.

Maity, D., & Tripathy, R. R. (2005). Damage assessment of structures from changes in natural frequencies using genetic algorithm. *Structural Engineering and Mechanics, 19*(1), 21-42.

Mangal, L., Idichandy, V., & Ganapathy, C. (2001). Structural monitoring of offshore platforms using impulse and relaxation response. *Ocean Engineering, 28*(6), 689-705.

Messina, A., Williams, E., & Contursi, T. (1998). Structural damage detection by a sensitivity and statistical-based method. *Journal of Sound and Vibration, 216*(5), 791-808.

Mester, S., & Benaroya, H. (1994). Localization in near-periodic structures. *AIAA paper No*, 94-1503.

Morassi, A., & Rollo, M. (2001). Identification of two cracks in a simply supported beam from minimal frequency measurements. *Journal of Vibration and Control, 7*(5), 729-739.

Mottershead, J., & Friswell, M. (1993). Model updating in structural dynamics: a survey. *Journal of Sound and Vibration, 167*(2), 347-375.

Nandwana, B., & Maiti, S. (1997). Detection of the location and size of a crack in stepped cantilever beams based on measurements of natural frequencies. *Journal of Sound and Vibration, 203*(3), 435-446.

Nichols, J. (2003). Structural health monitoring of offshore structures using ambient excitation. *Applied Ocean Research, 25*(3), 101-114.

Noble, B., & Daniel, J. W. (1988). *Applied linear algebra* (Vol. 3): Prentice-Hall New Jersey.

Pandey, A., & Biswas, M. (1994). Damage detection in structures using changes in flexibility. *Journal of Sound and Vibration, 169*(1), 3-17.

Papadopoulos, L., & Garcia, E. (1998). Structural damage identification: a probabilistic approach. *AIAA journal, 36*(11), 2137-2145.

Parloo, E., Verboven, P., Guillaume, P., & Van Overmeire, M. (2002). Sensitivity-based operational mode shape normalisation. *Mechanical Systems and Signal Processing, 16*(5), 757-767.

Patil, D., & Maiti, S. (2003). Detection of multiple cracks using frequency measurements. *Engineering Fracture Mechanics, 70*(12), 1553-1572.

Qi, G., Xun, G., Xiaozhai, Q., Dong, W., & Chang, P. (2005). Local measurement for structural health monitoring. *Earthquake Engineering and Engineering Vibration, 4*(1), 165-172.

Salawu, O. S. (1997). Detection of structural damage through changes in frequency: A review. *Engineering Structures, 19*(9), 718-723.

Schwarz, B. J., & Richardson, M. H. (1999). Experimental modal analysis. *CSI Reliability week, 35*(1), 1-12.

Sekjær, C., Bull, T., Markvart, M. K., Johansen, R. J., Ulriksen, M. D., Tcherniak, D., et al. (2017). *Steady State Shift Damage Localization: a super-element approach.* Paper presented at the International Conference on Structural Engineering Dynamics ICEDyn 2017.

Shi, X., Li, H.-J., Yang, Y.-C., & Gong, C. (2008). A model experiment of damage detection for offshore jacket platforms based on partial measurement. *Structural Engineering and Mechanics, 29*(3), 311-325.

Shi, X., Matsui, T., Li, H. J., & Gong, C. (2007). *A Damage Detection Algorithm Based on Partial Measurement for Offshore Jacket Platforms.* Paper presented at the The Seventeenth International Offshore and Polar Engineering Conference.

Shi, Z., Law, S., & Zhang, L. (2002). Improved damage quantification from elemental modal strain energy change. *Journal of Engineering Mechanics, 128*(5), 521-529.

Shi, Z., Law, S., & Zhang, L. M. (2000). Structural damage detection from modal strain energy change. *Journal of Engineering Mechanics, 126*(12), 1216-1223.

Simoen, E., De Roeck, G., & Lombaert, G. (2015). Dealing with uncertainty in model updating for damage assessment: A review. *Mechanical Systems and Signal Processing, 56*, 123-149.

Stubbs, N., & Osegueda, R. (1990a). Global damage detection in solids- Experimental verification. *International Journal of Analytical and Experimental Modal Analysis, 5*, 81-97.

Stubbs, N., & Osegueda, R. (1990b). Global non-destructive damage evaluation in solids. *International Journal of Analytical and Experimental Modal Analysis, 5*, 67-79.

Ulriksen, M. D., Bernal, D., & Damkilde, L. (2017a). Shaped input distributions for structural damage localization. *Mechanical Systems and Signal Processing*.

Ulriksen, M. D., Bernal, D., Nielsen, M. E., & Damkilde, L. (2017b). Damage localization in offshore structures using shaped inputs. *Procedia Engineering, 199*, 2282-2287.

Walker, W. E., Harremoës, P., Rotmans, J., van der Sluijs, J. P., van Asselt, M. B., Janssen, P., et al. (2003). Defining uncertainty: a conceptual basis for uncertainty management in model-based decision support. *Integrated assessment, 4*(1), 5-17.

Wang, B.-T. (2001). *Determination of Mode Shapes from the Operational Deflection Shape*. Paper presented at the The 8th International Congress on Sound and Vibration.

Wang, S., Li, Y., & Li, H. (2015). Structural model updating of an offshore platform using the cross model cross mode method: An experimental study. *Ocean Engineering, 97*, 57-64.

Xia, Y., & Hao, H. (2003). Statistical damage identification of structures with frequency changes. *Journal of Sound and Vibration, 263*(4), 853-870.

Xu, Y., Qian, Y., Chen, J., & Song, G. (2015). Probability-based damage detection using model updating with efficient uncertainty propagation. *Mechanical Systems and Signal Processing, 60*, 958-970.

Yang, H., Li, H., & Hu, S.-L. (2004). *Damage localization for offshore structures by modal strain energy decomposition method*. Paper presented at the American Control Conference, 2004. Proceedings of the 2004.

Yeo, I., Shin, S., Lee, H. S., & Chang, S.-P. (2000). Statistical damage assessment of framed structures from static responses. *Journal of Engineering Mechanics, 126*(4), 414-421.

Yi, W.-J., Zhou, Y., Kunnath, S., & Xu, B. (2008). Identification of localized frame parameters using higher natural modes. *Engineering Structures, 30*(11), 3082-3094.

Zhang, L., & Brincker, R. (2005). *An overview of operational modal analysis: major development and issues*. Paper presented at the 1st international operational modal analysis conference.

Zhong, S., Oyadiji, S. O., & Ding, K. (2008). Response-only method for damage detection of beam-like structures using high accuracy frequencies with auxiliary mass spatial probing. *Journal of Sound and Vibration, 311*(3), 1075-1099.

LIST OF PUBLICATIONS AND PAPERS PRESENTED

Monajemi, H., Mazinani, I., Ong, Z. C., Khoo, S. Y., Kong, K. K., & Karim, R. (2015). Using local stiffness indicator to examine the effect of honeycombs on the flexural stiffness of reinforced concrete beams. *Measurement, 64*, 157-162.

Ravanfar, S. A., Razak, H. A., Ismail, Z., & Monajemi, H. (2015). An improved method of parameter identification and damage detection in beam structures under flexural vibration using wavelet multi-resolution analysis. *Sensors, 15*(9), 22750-22775.

Monajemi, H., Razak, H. A., & Ismail, Z. (2013). Damage detection in frame structures using damage locating vectors. *Measurement, 46*(9), 3541-3548.

Monajemi, H., Razak, H. A., & Ismail, Z. (2012). Reliability of Dynamically Measured Flexibility Matrix on Damage Detection of Frame Structures *Topics in Modal Analysis II, Volume 6* (pp. 369-376): Springer.